JRC Scientific and Technical Reports

NEW ANALYTICAL STRESS FORMULAE FOR ARBITRARY TIME DEPENDENT THERMAL LOADS IN PIPES

V. Radu, E. Paffumi, N. Taylor

EUR 22802 EN - 2007

JRC EUROPEAN COMMISSION

Institute for Energy

The Institute for Energy provides scientific and technical support for the conception, development, implementation and monitoring of community policies related to energy.
Special emphasis is given to the security of energy supply and to sustainable and safe energy production.

European Commission
Joint Research Centre
Institute for Energy

Contact information
Address: N. Taylor
E-mail: Nigel.taylor@ec.europa.eu
Tel.: +31-224-565202
Fax: +31-224-565641
http://ie.jrc.ec.europa.eu
http://www.jrc.ec.europa.eu

JRC PUBSY 7629

EUR 22802 EN
ISSN 1018-5593

Luxembourg: Office for Official Publications of the European Communities

Printed in The Netherlands

New analytical stress formulae for arbitrary time dependent thermal loads in pipes

V. Radu E. Paffumi N. Taylor

June 2007

Contents

Problem Definition

In some applications regarding thermal fatigue due to thermal transients (striping or turbulence) in mixing tees of class 1-2-3 piping systems of reactors, the temperature gradient within the pipe thickness must be considered time-dependent, as well as the thermal boundary conditions. In the present work the quasi-static thermoelasticity problem in a long hollow cylinder is solved analytically. This is the first step in a four-part JRC project studying thermal fatigue damage assessment, which consists of:

- new analytical stress formulae for arbitrary time dependent thermal loads in pipes;
- assessment of thermal fatigue crack growth;
- probabilistic and statistical approach to thermal fatigue;
- review and synthesis of thermal fatigue assessment methods from European and non-European Procedures

Time-dependent thermal boundary conditions are assumed to act on the inner surface of the cylinder. In the first step, the general relation for the temperature distribution is derived by means of the finite Hankel transform. In the second step, the analytical solution for temperature distribution in wall thickness of a hollow cylinder in the sinusoidal transient thermal loading case is developed. In third step the thermal stress components are extracted by means of the displacement technique applied to a one dimensional problem of cylindrical bodies. Specific solutions were determined for the case of a sinusoidal transient thermal loading case applied to a hollow cylinder. Finally the results are compared with those from a previous independent study which used finite element analyses to solve the problem. A further verification of the analytical predictions was performed with an in-house FE analysis using the ABAQUS program.

The results can be used in the assessment of the high cycle fatigue damage of mixing tees in the following parts of the draft European Procedure for Thermal Fatigue Analyses of Mixing Tees:

- level 2 - sinusoidal temperature fluctuation as boundary condition on inner surface of the pipe;
- level 3 - load spectrum fluctuation based on one-dimensional temperature and stress evaluation at each measured location;
- level 4 - fracture mechanics applied to thermal fatigue crack growth assessment based on evaluation of ΔJ or ΔK during a crack growth.

Nomenclature

r_i=a , r_e=b - inner and outer radii of the pipe;

θ - temperature change from the reference temperature;

T_o - reference temperature;

r - radial distance;

k - thermal diffusivity;

λ - thermal conductivity;

ρ - density;

c - specific heat coefficient;

F(t) - function of time representing the thermal boundary condition applied on the inner surface of the cylinder;

$J_\upsilon(z)$, $Y_\upsilon(z)$ - Bessel functions of first and second kind of order υ.

θ_0 - amplitude of temperature wave;

ω - wave frequency in rad/s;

t - time variable.

s_n - positive roots of the transcendental equation (kernel of finite Hankel transform);

ε_{rr} - radial strain;

$\varepsilon_{\theta\theta}$ - hoop strain;

ε_{zz} - axial strain;

σ_{rr} - radial stress;

$\sigma_{\theta\theta}$ - hoop stress;

σ_{zz} - axial stress;

χ, μ - Lamé elastic constants;

E - Young's modulus;

G= μ - shear modulus;

β - thermoelastic constant

α - coefficient of the linear thermal expansion

ν - Poisson's ratio

u - radial displacement.

1. Introduction

The development of thermal fatigue damage due to turbulent mixing or vortices in NPP piping systems is still not fully understood [1] and much effort continues to be devoted to experimental and analytical studies in this area [2,3]. As opposed to the relatively low number of cycles associated with thermal stratification, thermal striping[1] at vortices and in mixing areas is more of a high cycle nature [4]. Thermal gradients and turbulence in the coolant fluid can induce oscillating local stresses in the portion of the pipe near the inside surface if the flow rates are sufficiently high. These cyclical thermal stresses are caused by oscillations of the fluid temperature at the interface resulting from interfacial mixing of the hot and cold fluid layers. For example, the test results and theory [4] indicate that thermal striping is present when the local Richardson number[2] is less than 0.25. Numerical simulation of the type of thermal striping and high-cycle thermal fatigue that can occur at tee junctions of the LWR piping systems showed that the oscillation frequency of the temperature of the coolant is a key factor in the response of pipe wall temperature field and that the critical frequency range is 0.1 – 1Hz [5]. The amplitude of the metal temperature oscillations is smaller than the difference in the hot and cold coolant layers because the finite value of the heat transfer coefficient and the thermal inertia of the pipe. Therefore, the high-cycle fatigue damage caused by thermal stresses is initially limited to the pipe inner surface adjacent to the interface [5], and further crack growth depends on the thermal stress profile through the thickness of the pipe [6,7,8,9].

The current study addresses the development of the analytical solutions for the through-wall temperature response and thermal stress components in a hollow cylinder due to thermal transient in generals, and particularly for the sinusoidal transient thermal loading case.

[1] Thermal striping is defined as the effect of a rapid random oscillation of the surface temperature inducing a corresponding fluctuation of surface stresses and strains in the adjacent metal. It is characterized by large numbers of strain cycles having potential to add to any fatigue damage produced by strain cycles associated with other plant operation transients.

[2] The Richardson number is the ratio of the density gradient and horizontal velocity gradient [4]

2. Background on methods applied to solving thermoelasticity problems for thermal transients

Thermal stresses are defined [10,11,12,13] as self-balancing stresses produced by a non-uniform distribution of temperature or by differing coefficients of thermal expansion. These thermal stresses are developed in a solid body whenever any part is prevented from assuming the size and shape that it would freely assume under a change in temperature. In order to establish the allowable stresses, two types of thermal stress are defined. The first is a general thermal stress that develops with some distortion of the structure in which it occurs. When the level of this stress exceeds twice the yield strength of the material, successive thermal cycles may produce incremental distortion resulting in shakedown or, in extreme cases, ratcheting. Examples include the stress produced by an axial temperature distribution in a cylindrical shell or by the temperature difference between a nozzle and the shell to which it is attached, or the equivalent linear stress produced by a radial temperature distribution in a cylindrical shell. The second concerns the type of local thermal stress associated with almost complete suppression of differential thermal expansion and thus no significant global distortion of the body. Such stresses are considered only from the fatigue standpoint and are therefore classified as local stresses. Examples include the stress at a small hot spot on a vessel wall and the difference between the actual stress and equivalent linear stress resulting from a radial temperature distribution in a cylindrical shell.

In looking at the methods for analyzing thermal stress under thermal transients, we focus on those for hollow cylinders (pipes). A.E. Segal has studied [14] the transient response of a thick-walled pipe subjected to a generalized excitation of temperature on the internal surface using Duhamel's relationship. The generalization of the temperature excitation was achieved using a polynomial composed of integral-and half-order terms. To avoid the evaluation of recurring functions in the complex domain, Laplace transformation and a 10-term Gaver-Stehfest inversion formula were used to perform part of the necessary integrations. In the reference [15] Lee and Yoo have applied a numerical approach using the Green's function method (GFM) for analysis of crack propagation under thermal transient loads. They have shown that GFM can be used to efficiently evaluate thermal stresses for fatigue damage analysis or SIFs for crack propagation

analyses. The same authors reported [16] an evaluation procedure of thermal striping damage on secondary piping of liquid metal fast reactors (LMFR) using GFM and standard FEM. A.S. Shahani and S.M. Nabavi solved the quasi-static thermoelasticity problem in a thick-walled cylinder analytical using the finite Hankel transform for the differential equations of both temperature and displacements [17]. S. Marie proposed [18] an extension of the analytical solution for the temperature and stresses in the event of a thermal shock in a pipe containing a fluid by a simple solution for any variation of the temperature in the fluid. The approach consists of breaking down the fluid temperature variation into a succession of linear shocks. The paper reported analytical expressions for the elastic thermal stresses, based on temperature fields calculated by the finite element method. N. Noda and K.-S. Kim used a Green's function approach based on the laminate theory to solve the two-dimensional unsteady temperature field and associated thermal stresses in an infinite hollow circular cylinder [19]. The unsteady heat conduction equation has been formulated as an eigenvalue problem by making use of the eigenfunction expansion theory and laminate theory. The associated thermoelastic field was analyzed using the thermoelastic displacement potential function and Michell's function.

In the scope of the present work we were specifically interested in an analytic formulation which could applied to a wide range or pipe geometries and temperature conditions relevant to coolant piping systems. None of the above approaches were available found to be fully suitable: in some cases the geometry boundary conditions were inappropriate, in others the published information was insufficient to allow direct implementation. As a result, it was decided to develop an new solution to meet our requirements; this is presented in the following sections.

3. Development of an analytical solution for temperature distribution

The calculation of the temperature distribution in a piping subsystem must be distinguished from that in components with more complex geometries. Pipes can be represented as hollow cylinders and with such a simple geometry it becomes possible to use analytical tools to get the time-dependent temperature profile through wall thickness. Hence a pipe wall model subject to a sinusoidal fluctuation of fluid temperature can be used for assessment of thermal stripping damage phenomenon. A suitable analytical solution of time-dependence temperature in pipes provides a basis for obtaining solutions for the associated thermal stress components and their profile through the wall thickness.

This approach facilities extraction of stress intensity ranges for computing cumulative usage factors (CUFs) and also for crack growth analysis in areas of piping affected by turbulent mixing.

3.1 The finite Hankel transform method

Laplace, Fourier, Hankel and Mellin transforms have been applied to the solution of boundary-value problems in mathematical physics [20]. The application of such transforms reduces a partial differential equation in *n* independent variables to one in *n-1* variables and it is often possible, by successive operations of this type, to reduce the problem to the solution of an ordinary differential equation. In applying the method of integral transforms to problems formulated in finite domains it is necessary to introduce finite intervals on the transform integral. Transforms of this nature are called finite transforms. Sneddon [21] considered a Bessel function as a kernel of a finite integral which he defined as a Hankel transform and showed its usefulness for solving certain boundary value problems. The Hankel transform arises naturally in problems posed in cylindrical coordinates which are solved using the technique of separation of variables, involving Bessel functions [22]. This transform is more appropriate for solving differential equations with boundary conditions in which there is an axial symmetry.

Consider a hollow cylinder of the inner and outer radii r_i=a and r_e=b, respectively. Also, consider that the cylinder is made of a homogeneous isotropic material. The one-dimensional heat diffusion equation in cylindrical coordinates is [11,12]:

$$\frac{\partial^2\theta}{\partial r^2}+\frac{1}{r}\cdot\frac{\partial\theta}{\partial r}=\frac{1}{k}\cdot\frac{\partial\theta}{\partial t} \tag{1}$$

where:

$$\theta = T(r,t)-T_o \tag{2}$$

is the temperature change from the reference temperature (where the reference temperature T_o is the temperature of the body in the unstrained state or the ambient temperature before changing of temperature);

r - radial distance;

k - the thermal diffusivity which is defined as:

$$k=\frac{\lambda}{\rho c} \tag{3}$$

λ – the thermal conductivity;

ρ - the density;

c – the specific heat coefficient;

The thermal boundary condition (Dirichlet conditions) for a hollow cylinder are:

$$\theta(a,t) = F(t) \tag{4}$$

$$\theta(b,t) = 0 \text{ (adiabatic condition hypothesis)} \tag{5}$$

and the initial condition is

$$\theta(r,0) = 0 \tag{6}$$

The function *F(t)* is a known function of time representing the thermal boundary condition applied on the inner surface of the cylinder. Later on this function will be adapted for sinusoidal transient thermal loading.

The differential equation (1) contains a linear operator L, applied to a function f, in the general form

$$Lf = \frac{1}{r}\left\{\frac{d}{dr}\left(r\frac{df}{dr}\right)\right\} - \frac{v^2}{r^2}f \tag{7}$$

The problem may be solved using the finite Hankel transform[17,20,22], defined by the following relation:

$$\overline{F}(s_n,t) = H[f(r,t);s_n] = \int_a^b r \cdot f(r,t) \cdot K(r,s_n)dr \tag{8}$$

where:

s_n is the transform parameter;

$K(r,s_n)$ is the kernel of the transformation

The inverse transform of (8) is defined as

$$f(r,t) = H^{-1}[\overline{F}(s_n,t);r] = \sum_{n=1}^{\infty} a_n \cdot \overline{F}(s_n,t) \cdot K(r,s_n) \tag{9}$$

The a_n parameter should be inferred using the orthogonality of solutions of the Sturm-Liouville differential equation that correspond to the linear operator from Eqn.(7) as

$$a_n = \frac{1}{\int_a^b r \cdot [K(r,s_n)]^2 dr} \tag{10}$$

The proper form of the kernel $K(r,s_n)$ depends on the form of the governing differential equation and also on the boundary condition applied. Taking into account the form of

linear operator given in Eqn.(7), the kernel of the transformation can be chosen [17,20,22] as

$$K(r,s_n) = A \cdot J_\upsilon(s_n \cdot r) + B \cdot Y_\upsilon(s_n \cdot r) \tag{11}$$

where $J_\upsilon(z)$ and $Y_\upsilon(z)$ are the Bessel functions of first and second kind of order υ.

The boundary conditions of the problem are defined by the linear operators M and N as follows:

$$Mf = m_1 \cdot f(a) + m_2 \cdot \frac{\partial f(a)}{\partial r} \tag{12}$$

$$Nf = n_1 \cdot f(b) + n_2 \cdot \frac{\partial f(b)}{\partial r} \tag{13}$$

The values of the characteristic roots, s_n, and constants A and B in Eqn. (11) may be obtained from the following equations

$$MK(a,s_n) = 0 \tag{14}$$

$$NK(b,s_n) = 0 \tag{15}$$

If we apply the finite Hankel transform (8) to the linear operator (7) and integrate twice , we obtain:

$$\begin{aligned} H[Lf;s_n] = a \cdot \left[\frac{dK(a,s_n)}{dr} \cdot f(a,t) - K(a,s_n) \cdot \frac{\partial f(a,t)}{\partial r} \right] - \\ - b \cdot \left[\frac{dK(b,s_n)}{dr} \cdot f(b,t) - K(b,s_n) \cdot \frac{\partial f(b,t)}{\partial r} \right] - s_n^2 \overline{F}(s_n,t) \end{aligned} \tag{16}$$

3.2 Solution for 1-D heat diffusion equation for a hollow cylinder

By comparison of the derivative operator with respect to *r* from Eq. (1) with operator (7), it can be seen that $\upsilon = 0$. From Eqs. (4), (5) with (12) ,(13), for the present problem Eqs. (14) and (15) can be written as

$$K(a,s_n) = 0 \tag{17}$$

$$K(b,s_n) = 0 \tag{18}$$

The corresponding kernel of the Hankel transform may be obtained [16], using Eqs. (11) and (17, 18) as follows:

$$K(r,s_n) = Y_o(s_n \cdot a) \cdot J_o(s_n \cdot r) - J_o(s_n \cdot a) \cdot Y_o(s_n \cdot r) \tag{19}$$

The s_n terms are the positive roots of the transcendental equation:

$$Y_o(s_n \cdot a) \cdot J_o(s_n \cdot b) - J_o(s_n \cdot a) \cdot Y_o(s_n \cdot b) = 0 \tag{20}$$

As consequence, with the kernel (19) and applying the Hankel transform from Eq. (8) to Eq.(1), using Eq. (16), boundary conditions Eqs.(4,6) and also Eqs. (17,18), the result is

$$\frac{1}{k}\cdot\frac{d\bar{\theta}}{dt}+s_n^2\cdot\bar{\theta}=a\cdot F(t)\cdot\frac{dK(a,s_n)}{dr} \tag{21}$$

where

$$\bar{\theta}(r,s_n)=H[\theta(r,t)] \tag{22}$$

Using the properties of the Bessel functions (Appendix 1) on kernel (19) we obtain:

$$\frac{dK(r,s_n)}{dr}=-s_n\cdot Y_o(s_n\cdot a)\cdot J_1(s_n\cdot r)+s_n\cdot J_o(s_n\cdot a)\cdot Y_1(s_n\cdot r) \tag{23}$$

Another property of Bessel functions is:

$$J_{\nu+1}(z)\cdot Y_\nu(z)-J_\nu(z)\cdot Y_{\nu+1}(z)=\frac{2}{\pi\cdot z} \tag{24}$$

With Eq.(24) we obtain:

$$\frac{dK(a,s_n)}{dr}=-\frac{2}{\pi\cdot a} \tag{25}$$

Substituting Eq. (25) in (21) gives:

$$\frac{1}{k}\cdot\frac{d\bar{\theta}}{dt}+s_n^2\cdot\bar{\theta}=-\frac{2}{\pi}F(t) \tag{26}$$

Eq. (26) can be re-written in the form

$$\frac{d\bar{\theta}}{dt}+k\cdot s_n^2\cdot\bar{\theta}=-\frac{2\cdot k}{\pi}F(t) \tag{27}$$

With the initial condition from Eq.(6), the solution is:

$$\bar{\theta}(s_n,t)=\frac{-2\cdot k}{\pi}\cdot e^{-k\cdot s_n^2\cdot t}\int_0^t e^{k\cdot s_n^2\cdot\tau}\cdot F(\tau)d\tau \tag{28}$$

From Eq.(10) the coefficients a_n are obtained using the orthogonality of the solutions of Sturm-Liouville differential equation and kernel (19) as

$$a_n=\frac{\pi^2}{2}\cdot\frac{s_n^2\cdot J_0^2(s_n\cdot b)}{J_0^2(s_n\cdot a)-J_0^2(s_n\cdot b)} \tag{29}$$

Finally, the temperature distribution in the thickness of the hollow cylinder may be obtained substituting Eqs. (19, 28, 29) into Eq.(9) as follows

$$\theta(r,t) = k \cdot \pi \cdot \sum_{n=1}^{\infty} \frac{s_n^2 \cdot J_0^2(s_n \cdot b)}{J_0^2(s_n \cdot b) - J_0^2(s_n \cdot a)} \left[Y_o(s_n \cdot a) \cdot J_o(s_n \cdot r) - J_o(s_n \cdot a) \cdot Y_o(s_n \cdot r) \right] \times \times \left[e^{-k \cdot s_n^2 \cdot t} \int_0^t e^{k \cdot s_n^2 \cdot \tau} F(\tau) d\tau \right] \quad (30)$$

where s_n are the positive roots of the transcendental equation

$$Y_o(s_n \cdot a) \cdot J_o(s_n \cdot b) - J_o(s_n \cdot a) \cdot Y_o(s_n \cdot b) = 0 \quad (20')$$

The main advantage of expressing the temperature distribution in the form of Eq.(30) is that the temperature field can be analyzed for various boundary conditions on inner surface expressed by means of function F(t). As example, for sinusoidal thermal loading or for thermal shock (expressed as a polynomial function of time) the integral from Eq. (30) can be relatively easy solved and, finally the thermal response in the body of the specimen can be obtained for the above initial and boundary conditions.

3.3 Temperature distribution in a hollow cylinder subjected to sinusoidal thermal transient loading

The solution for the temperature distribution during a thermal transient for a hollow cylinder as given in (30), can be written as follows:

$$\theta(r,t) = k \cdot \pi \cdot \sum_{n=1}^{\infty} \theta_1(a,b,s_n) \cdot \theta_2(a,r,s_n) \cdot \theta_3(t,s_n) \quad (31)$$

where

$$\theta_1(a,b,s_n) = \frac{s_n^2 \cdot J_0^2(s_n \cdot b)}{J_0^2(s_n \cdot b) - J_0^2(s_n \cdot a)} \quad (32)$$

$$\theta_2(a,r,s_n) = Y_o(s_n \cdot a) \cdot J_o(s_n r) - J_o(s_n \cdot a) \cdot Y_o(s_n \cdot r) \quad (33)$$

$$\theta_3(t,s_n) = e^{-k \cdot s_n^2 \cdot t} \int_0^t e^{k \cdot s_n^2 \cdot \tau} F(\tau) d\tau \quad (34)$$

For the time-dependent term $\theta_3(t,s_n)$, the boundary condition for thermal loading on inner surface of hollow cylinder is expressed as:

$$F(t) = \theta_0 \cdot \sin(\omega \cdot t) = \theta_0 \cdot \sin(2\pi \cdot f \cdot t) \quad (35)$$

where

θ_0 – amplitude of temperature wave and ω *and f* correspond to the wave frequency in rad/s and cycles/sec respectively;

t – time variable.

By substituting Eq. 35 into Eq. 34 and integrating gives:

$$\theta_3(\omega,t,s_n)=\theta_0\cdot\frac{\omega\cdot e^{-k\cdot s_n^2\cdot t}+(k\cdot s_n^2)\cdot\sin(\omega\cdot t)-\omega\cdot\cos(\omega\cdot t)}{(k\cdot s_n^2)^2+\omega^2} \tag{36}$$

Therefore, the complete formula for temperature distribution in the thickness of hollow circular cylinder for sinusoidal thermal loading on the inner surface is:

$$\theta(r,\omega,t)=k\cdot\pi\cdot\sum_{n=1}^{\infty}\frac{s_n^2\cdot J_0^2(s_n\cdot b)}{J_0^2(s_n\cdot b)-J_0^2(s_n\cdot a)}\left[Y_o(s_n\cdot a)\cdot J_o(s_n r)-J_o(s_n\cdot a)\cdot Y_o(s_n\cdot r)\right]\times$$
$$\times\left[\theta_0\cdot\frac{\omega\cdot e^{-k\cdot s_n^2\cdot t}+(k\cdot s_n^2)\cdot\sin(\omega\cdot t)-\omega\cdot\cos(\omega\cdot t)}{(k\cdot s_n^2)^2+\omega^2}\right] \tag{37}$$

A similar approach can be used to obtain a through-wall thermal distribution for other boundary conditions on the inner surface. If we use a time-dependent proper function *F(t)* applied as a thermal boundary condition on inner surface of the hollow cylinder in Eq. (34), for instance modeling a constant temperature, thermal shock, linear or exponential decay, etc., then the result will be a similar expression to Eq. (37).

4. Development of analytical solution for thermal stress components

4.1 Stress components for a cylindrical body

The constitutive equations, following the generalized Hook's law, for a homogeneous isotropic body in a cylindrical coordinate system are [11,12,13]:

$$\varepsilon_{rr}=\frac{1}{E}\left[\sigma_{rr}-\nu\cdot(\sigma_{\theta\theta}+\sigma_{zz})\right]+\alpha\cdot\theta=\frac{1}{2G}\left(\sigma_{rr}-\frac{\nu}{1+\nu}\Theta\right)+\alpha\cdot\theta \tag{38}$$

$$\varepsilon_{\theta\theta}=\frac{1}{E}\left[\sigma_{\theta\theta}-\nu\cdot(\sigma_{rr}+\sigma_{zz})\right]+\alpha\cdot\theta=\frac{1}{2G}\left(\sigma_{\theta\theta}-\frac{\nu}{1+\nu}\Theta\right)+\alpha\cdot\theta \tag{39}$$

$$\varepsilon_{zz}=\frac{1}{E}\left[\sigma_{zz}-\nu\cdot(\sigma_{rr}+\sigma_{\theta\theta})\right]+\alpha\cdot\theta=\frac{1}{2G}\left(\sigma_{zz}-\frac{\nu}{1+\nu}\Theta\right)+\alpha\cdot\theta \tag{40}$$

and

$$\varepsilon_{r\theta}=\frac{\sigma_{r\theta}}{2G};\ \varepsilon_{\theta z}=\frac{\sigma_{\theta z}}{2G};\varepsilon_{zr}=\frac{\sigma_{zr}}{2G} \tag{41}$$

with $\Theta = \sigma_{rr} + \sigma_{\theta\theta} + \sigma_{zz}$ (42)

The alternative forms are

$$\sigma_{rr} = 2\mu \cdot \varepsilon_{rr} + \chi \cdot e - \beta \cdot \theta \quad (43)$$

$$\sigma_{\theta\theta} = 2\mu \cdot \varepsilon_{\theta\theta} + \chi \cdot e - \beta \cdot \theta \quad (44)$$

$$\sigma_{zz} = 2\mu \cdot \varepsilon_{zz} + \chi \cdot e - \beta \cdot \theta \quad (45)$$

where

χ, μ – the Lamé elastic constants

$$\chi = \frac{2\nu \cdot G}{1 - 2\nu} \quad (46)$$

E – Young's modulus

G= μ – shear modulus

$$G = \frac{E}{2(1+\nu)} \quad (47)$$

$\theta = T(r,t) - T_o$ is the temperature change from the reference temperature T_o (where the reference temperature can be the temperature of the body in the unstrained state or the ambient temperature before a change of temperature)

β - the thermoelastic constant

$$\beta = \frac{\alpha \cdot E}{1 - 2\nu} \quad (48)$$

α – the coefficient of the linear thermal expansion

ν – the Poisson's ratio

The one-dimensional equilibrium equation in the radial direction is:

$$\frac{d\sigma_{rr}}{dr} + \frac{\sigma_{rr} - \sigma_{\theta\theta}}{r} = 0 \quad (49)$$

The displacement technique is also be applied to the solution of one-dimensional problems of hollow cylinder. The generalized Hooke's law for problems [12] (plane stress and plane strain) in a cylindrical coordinate system is

$$\varepsilon_{rr} = \frac{1}{E'}\left(\sigma_{rr} - \nu' \cdot \sigma_{\theta\theta}\right) + \alpha' \cdot \theta - c' \quad (50)$$

$$\varepsilon_{\theta\theta} = \frac{1}{E'}\left(\sigma_{\theta\theta} - \nu' \cdot \sigma_{rr}\right) + \alpha' \cdot \theta - c' \quad (51)$$

$$\varepsilon_{r\theta} = \frac{1}{2G} \cdot \sigma_{r\theta} \quad (52)$$

where

$$E' = \begin{cases} \dfrac{E}{1-\nu^2} \\ E \end{cases} \quad \text{for plane strain, and plane stress respectively} \tag{53}$$

$$\nu' = \begin{cases} \dfrac{\nu}{1-\nu} \\ \nu \end{cases} \quad \text{for plane strain and plane stress respectively} \tag{54}$$

$$\alpha' = \begin{cases} (1+\nu)\alpha \\ \alpha \end{cases} \quad \text{for plane strain and plane stress respectively} \tag{55}$$

$$c' = \begin{cases} \nu\varepsilon_0 \\ 0 \end{cases} \quad \text{for plane strain and plane stress respectively} \tag{56}$$

The axial stress is zero (σ_{zz}=0) for plane stress, and a constant axial strain (ε_{zz}= ε_0) may occur for a plane strain condition.

For plane strain a normal stress σ_{zz} acts on cross-sections of the long cylinder and is necessary to maintain the body in the state of plane strain. Therefore, the normal stress σ_{zz} is dependent on the normal stresses σ_{rr} and $\sigma_{\theta\theta}$. From Eq. (40) it follows that:

$$\varepsilon_0 = \frac{1}{E'}\left[\sigma_{zz} - \nu'\cdot\left(\sigma_{rr} + \sigma_{\theta\theta}\right)\right] + \alpha'\cdot\theta \tag{57}$$

and finally for plane strain state the relationship for σ_{zz} is

$$\sigma_{zz} = \frac{\nu}{1+\nu}\left(\sigma_{rr} + \sigma_{\theta\theta}\right) - (1+\nu)\cdot\alpha\cdot\theta\frac{E}{1-\nu^2} + \frac{E}{1-\nu^2}\varepsilon_0 \tag{58}$$

When all strains and stresses are only functions of radial distance *r*, the strain-displacement relations are:

$$\varepsilon_{rr} = \frac{du}{dr} \tag{59}$$

$$\varepsilon_{\theta\theta} = \frac{u}{r} \tag{60}$$

$$\varepsilon_{r\theta} = 0 \tag{61}$$

where *u* is the radial displacement.

By use of Eqs. (59, 60, 61) in Eqs. (50, 51, 52) the components of stress in cylindrical coordinates can be expressed as:

$$\sigma_{rr} = \frac{E'}{1-\nu'^2}\left[\frac{du}{dr} + \nu'\cdot\frac{u}{r} - (1+\nu')\cdot\alpha'\cdot\theta + (1+\nu')\cdot c'\right] \tag{62}$$

$$\sigma_{\theta\theta} = \frac{E'}{1-\nu'^2}\left[\nu'\cdot\frac{du}{dr} + \frac{u}{r} - (1+\nu')\cdot\alpha'\cdot\theta + (1+\nu')\cdot c'\right] \tag{63}$$

$$\sigma_{r\theta} = 0 \tag{64}$$

The substitution of Eqs. (62, 63) in Eq. 49 yields

$$\frac{d}{dr}\left[\frac{1}{r}\cdot\frac{d(r\cdot u)}{dr}\right] = (1+\nu')\cdot\alpha'\cdot\frac{d\theta(r,t)}{dr} \tag{65}$$

The general solution of Eq. (65) is

$$u = (1+\nu')\cdot\alpha'\cdot\frac{1}{r}\int_r \theta(r,t)\cdot r\cdot dr + C_1\cdot r + \frac{C_2}{r} \tag{66}$$

The integration constants C_1 and C_2 may be determined from the boundary conditions. By use of Eq. (66) and Eqs. (62, 63, 64) the stress components in cylindrical coordinates for a cylindrical body are

$$\sigma_{rr} = -\frac{\alpha'.\cdot E'}{r^2}\int_r \theta(r,t)\cdot r\cdot dr + \frac{E'}{1-\nu'}\cdot C_1 - \frac{E'}{1+\nu'}\cdot\frac{C_2}{r^2} + \frac{E'}{1-\nu'}\cdot c' \tag{67}$$

$$\sigma_{\theta\theta} = \frac{\alpha'.\cdot E'}{r^2}\int_r \theta(r,t)\cdot r\cdot dr - \alpha'\cdot E'\cdot\theta(r,t) + \frac{E'}{1-\nu'}C_1 + \frac{E'}{1+\nu'}\cdot\frac{C_2}{r^2} + \frac{E'}{1-\nu'}\cdot c' \tag{68}$$

$$\sigma_{r\theta} = 0 \tag{69}$$

4.2 Stress components for a hollow cylinder

The analytical solution for stress components will be specified for a hollow circular cylinder (or a cylinder with a concentric circular hole, as defined in [13]) with appropriate boundary conditions.

We consider that the hollow cylinder is made of a homogeneous isotropic material. The solutions for plane stress and plane strain will first be stated. Thereafter the hollow cylinder is considered to be sufficiently long in axial direction to apply the hypothesis of plain strain and an analytical solution for thermal stress components during thermal transients will be specified. It is assumed that the thermomechanical properties do not change during a thermal transient and that the strain rates due to the thermal loading are small, so both the inertia and thermo mechanical coupling terms in the thermoelasticity governing equations can be neglected.

Let us consider the radii a and b for hollow cylinder

$$\begin{aligned} r_i &= a \\ r_e &= b \end{aligned} \tag{70}$$

The boundary conditions for traction free surfaces are:

$$\sigma_{rr} = 0 \qquad \text{at } r_i = a, r_e = b \tag{71}$$

Substituting Eq. (71) in Eqs. (67, 68) the integration constants C_1 and C_2 may be determined as follows

$$C_1 = \alpha' \cdot (1-\nu') \cdot \frac{1}{b^2 - a^2} \cdot \int_a^b \theta(r,t) \cdot r \cdot dr - c' \tag{72}$$

$$C_2 = \alpha' \cdot (1+\nu') \cdot \frac{a^2}{b^2 - a^2} \cdot \int_a^b \theta(r,t) \cdot r \cdot dr \tag{73}$$

Thus the stress components for a hollow cylinder are:

$$\sigma_{rr} = \alpha' \cdot E' \left[-\frac{1}{r^2} \cdot \int_a^r \theta(r,t) \cdot r \cdot dr + \frac{r^2 - a^2}{r^2 \cdot (b^2 - a^2)} \int_a^b \theta(r,t) \cdot r \cdot dr \right] \tag{74}$$

$$\sigma_{\theta\theta} = \alpha' \cdot E' \left[\frac{1}{r^2} \cdot \int_a^r \theta(r,t) \cdot r \cdot dr + \frac{r^2 + a^2}{r^2 \cdot (b^2 - a^2)} \int_a^b \theta(r,t) \cdot r \cdot dr - \theta(r,t) \right] \tag{75}$$

with

$$\sigma_{zz} = 0 \quad \text{for plane stress} \tag{76}$$

$$\sigma_{zz} = \frac{\alpha \cdot E}{1-\nu} \left(\frac{2\nu}{b^2 - a^2} \int_a^b \theta(r,t) \cdot r \cdot dr - \theta(r,t) \right) + E \cdot \varepsilon_0 \qquad \text{for plane strain} \tag{77}$$

Also, the radial displacement is

$$u = (1+\nu') \cdot \alpha' \cdot \left[\frac{1}{r} \int_a^r \theta(r,t) \cdot r \cdot dr + \left(\frac{1-\nu'}{1+\nu'} r + \frac{a^2}{r} \right) \cdot \frac{1}{b^2 - a^2} \int_a^b \theta(r,t) \cdot r \cdot dr \right] - c' \cdot r \tag{78}$$

The constant axial strain ε_0 for plain strain can be determined from the condition that the axial force is zero

$$2\pi \int_a^b \sigma_{zz} \cdot r \cdot dr = 0 \tag{79}$$

Substituting Eq. (77) in Eq. (79), the constant axial strain ε_0 is given by

$$\varepsilon_0 = \frac{2\alpha}{b^2 - a^2} \int_a^b \theta(r,t) \cdot r \cdot dr \tag{80}$$

The axial stress and the radial displacement for plain strain with a constant axial strain are:

$$\sigma_{zz} = \frac{\alpha \cdot E}{1-\nu}\left(\frac{2}{b^2-a^2}\int_a^b \theta(r,t)\cdot r \cdot dr - \theta(r,t) \right) \tag{81}$$

$$u = (\frac{1+\nu}{1-\nu})\cdot \alpha \cdot \left[\frac{1}{r}\int_a^r \theta(r,t)\cdot r\cdot dr + \left(\frac{1-3\nu}{1+\nu} r + \frac{a^2}{r} \right) \cdot \frac{1}{b^2-a^2}\int_a^b \theta(r,t)\cdot r\cdot dr \right] \tag{82}$$

In conclusion, the stress components and the radial displacement for a hollow circular cylinder are given in the following relationships:

Plane stress

$$u = (1+\nu)\cdot \alpha \cdot \left[\frac{1}{r}\int_a^r \theta(r,t)\cdot r\cdot dr + \left(\frac{1-\nu}{1+\nu} r + \frac{a^2}{r} \right) \cdot \frac{1}{b^2-a^2}\int_a^b \theta(r,t)\cdot r\cdot dr \right] \tag{83}$$

$$\sigma_{rr} = \alpha \cdot E\left[-\frac{1}{r^2}\cdot \int_a^r \theta(r,t)\cdot r\cdot dr + \frac{r^2-a^2}{r^2\cdot(b^2-a^2)}\int_a^b \theta(r,t)\cdot r\cdot dr \right] \tag{84}$$

$$\sigma_{\theta\theta} = \alpha \cdot E\left[\frac{1}{r^2}\cdot \int_a^r \theta(r,t)\cdot r\cdot dr + \frac{r^2+a^2}{r^2\cdot(b^2-a^2)}\int_a^b \theta(r,t)\cdot r\cdot dr - \theta(r,t) \right] \tag{85}$$

Plane strain (long hollow circular cylinder)

$$u = (\frac{1+\nu}{1-\nu})\cdot \alpha \cdot \left[\frac{1}{r}\int_a^r \theta(r,t)\cdot r\cdot dr + \left((1-2\nu)\cdot r + \frac{a^2}{r} \right) \cdot \frac{1}{b^2-a^2}\int_a^b \theta(r,t)\cdot r\cdot dr \right] \tag{86}$$

for $\varepsilon_{zz}=0$

$$u = (\frac{1+\nu}{1-\nu})\cdot \alpha \cdot \left[\frac{1}{r}\int_a^r \theta(r,t)\cdot r\cdot dr + \left(\frac{1-3\nu}{1+\nu} r + \frac{a^2}{r} \right) \cdot \frac{1}{b^2-a^2}\int_a^b \theta(r,t)\cdot r\cdot dr \right] \tag{87}$$

for $\varepsilon_{zz}=\varepsilon_0$

$$\sigma_{rr} = \frac{\alpha \cdot E}{1-\nu}\left[-\frac{1}{r^2}\cdot \int_a^r \theta(r,t)\cdot r\cdot dr + \frac{r^2-a^2}{r^2\cdot(b^2-a^2)}\int_a^b \theta(r,t)\cdot r\cdot dr \right] \tag{88}$$

$$\sigma_{\theta\theta} = \frac{\alpha \cdot E}{1-\nu}\left[\frac{1}{r^2}\cdot \int_a^r \theta(r,t)\cdot r\cdot dr + \frac{r^2+a^2}{r^2\cdot(b^2-a^2)}\int_a^b \theta(r,t)\cdot r\cdot dr - \theta(r,t) \right] \tag{89}$$

$$\sigma_{zz} = \frac{\alpha \cdot E}{1-\nu}\left(\frac{2\nu}{b^2-a^2}\int_a^b \theta(r,t)\cdot r \cdot dr - \theta(r,t) \right) \qquad \text{for } \varepsilon_{zz}=0 \tag{90}$$

$$\sigma_{zz} = \frac{\alpha \cdot E}{1-\nu}\left(\frac{2}{b^2 - a^2}\int_a^b \theta(r,t)\cdot r \cdot dr - \theta(r,t) \right) \qquad \text{for } \varepsilon_{zz}=\varepsilon_0 \tag{91}$$

$$\sigma_{r\theta} = 0 \tag{92}$$

The above solutions for stress components are independent of the temperature field [12] and are valid for both steady and transient conditions.

4.3 Thermal stress components in a long hollow cylinder subject to sinusoidal transient thermal loading

Eqs.(88, 89, 90, 91) have been utilized to develop general solutions for the thermal stress components for any thermal transient case. In the next step these are made specific to the sinusoidal thermal boundary condition case.

In Chapter 3 we developed the following equation for the temperature distribution in the thickness of a hollow cylinder under sinusoidal transient thermal loading:

$$\theta(r,\omega,t) = k\cdot\pi\cdot\sum_{n=1}^{\infty}\frac{s_n^2\cdot J_0^2(s_n\cdot b)}{J_0^2(s_n\cdot b)-J_0^2(s_n\cdot a)}\left[Y_o(s_n\cdot a)\cdot J_o(s_n r) - J_o(s_n\cdot a)\cdot Y_o(s_n\cdot r)\right]\times$$
$$\times\left[\theta_0\cdot\frac{\omega\cdot e^{-k\cdot s_n^2\cdot t} + (k\cdot s_n^2)\cdot\sin(\omega\cdot t) - \omega\cdot\cos(\omega\cdot t)}{(k\cdot s_n^2)^2+\omega^2}\right] \tag{37'}$$

for known inner and outer radii *a and b respectively*. As already suggested, Eq. (37') can be represented in condensed form as:

$$\theta(r,\omega,t) = k\cdot\pi\cdot\sum_{n=1}^{\infty}\theta_1(a,b,s_n)\cdot\theta_2(a,r,s_n)\cdot\theta_3(\omega,t,s_n) \tag{93}$$

with

$$\theta_1(a,b,s_n) = \frac{s_n^2\cdot J_0^2(s_n\cdot b)}{J_0^2(s_n\cdot b)-J_0^2(s_n\cdot a)} \tag{94}$$

$$\theta_2(a,r,s_n) = Y_o(s_n\cdot a)\cdot J_o(s_n r) - J_o(s_n\cdot a)\cdot Y_o(s_n\cdot r) \tag{95}$$

$$\theta_3(\omega,t,s_n) = \theta_0\cdot\frac{\omega\cdot e^{-k\cdot s_n^2\cdot t} + (k\cdot s_n^2)\cdot\sin(\omega\cdot t) - \omega\cdot\cos(\omega\cdot t)}{(k\cdot s_n^2)^2+\omega^2} \tag{96}$$

In Eqs. (88, 89, 90, 91) for the stress components there are two kinds of integral, in the following forms:

$$I_1(r,\omega,t) = \int_a^r \theta(r,t)\cdot r\cdot dr \tag{97}$$

$$I_2(\omega,t) = \int_a^b \theta(r,t)\cdot r\cdot dr \tag{98}$$

From the general form of temperature distribution (Eq.93) the radial dependence of temperature arises just in the second term as:

$$\theta_2(a,r,s_n) = Y_o(s_n \cdot a) \cdot J_o(s_n r) - J_o(s_n \cdot a) \cdot Y_o(s_n \cdot r) \tag{95'}$$

Performing the integrals from Eqs. (97) and (98) on $\theta_2(a,r,s_n)$ from Eq. (95') and based on the Bessel function properties, the results are

$$\int_a^r \theta_2(a,r,s_n) r dr = \frac{1}{s_n}\left\{Y_o(s_n \cdot a) \cdot \left[r \cdot J_1(s_n \cdot r) - a \cdot J_1(s_n \cdot a)\right] - J_o(s_n \cdot a) \cdot \left[r \cdot Y_1(s_n \cdot r) - a \cdot Y_1(s_n \cdot a)\right]\right\} \tag{99}$$

$$\int_a^b \theta_2(a,r,s_n) r dr = \frac{1}{s_n}\left\{Y_o(s_n \cdot a) \cdot \left[b \cdot J_1(s_n \cdot b) - a \cdot J_1(s_n \cdot a)\right] - J_o(s_n \cdot a) \cdot \left[b \cdot Y_1(s_n \cdot b) - a \cdot Y_1(s_n \cdot a)\right]\right\} \tag{100}$$

Eqs. (99) and (100) can be substituted into Eqs. (97) and (98) so that the complete results of integrals I_1 and I_2 for sinusoidal case are

$$I_1(r,\omega,t) = \int_a^r \theta(r,t) \cdot r \cdot dr = k \cdot \pi \cdot \sum_{n=1}^{\infty} \frac{s_n^2 \cdot J_0^2(s_n \cdot b)}{J_0^2(s_n \cdot b) - J_0^2(s_n \cdot a)} \times$$
$$\times \left[\frac{1}{s_n}\left\{Y_o(s_n \cdot a) \cdot \left[r \cdot J_1(s_n \cdot r) - a \cdot J_1(s_n \cdot a)\right] - J_o(s_n \cdot a) \cdot \left[r \cdot Y_1(s_n \cdot r) - a \cdot Y_1(s_n \cdot a)\right]\right\}\right] \times \tag{101}$$
$$\times \left[\theta_0 \cdot \frac{\omega \cdot e^{-k \cdot s_n^2 \cdot t} + (k \cdot s_n^2) \cdot \sin(\omega \cdot t) - \omega \cdot \cos(\omega \cdot t)}{(k \cdot s_n^2)^2 + \omega^2}\right]$$

$$I_2(\omega,t) = \int_a^b \theta(r,t) \cdot r \cdot dr = k \cdot \pi \cdot \sum_{n=1}^{\infty} \frac{s_n^2 \cdot J_0^2(s_n \cdot b)}{J_0^2(s_n \cdot b) - J_0^2(s_n \cdot a)} \times$$
$$\times \left[\frac{1}{s_n}\left\{Y_o(s_n \cdot a) \cdot \left[b \cdot J_1(s_n \cdot b) - a \cdot J_1(s_n \cdot a)\right] - J_o(s_n \cdot a) \cdot \left[b \cdot Y_1(s_n \cdot b) - a \cdot Y_1(s_n \cdot a)\right]\right\}\right] \times \tag{102}$$
$$\times \left[\theta_0 \cdot \frac{\omega \cdot e^{-k \cdot s_n^2 \cdot t} + (k \cdot s_n^2) \cdot \sin(\omega \cdot t) - \omega \cdot \cos(\omega \cdot t)}{(k \cdot s_n^2)^2 + \omega^2}\right]$$

with s_n being the positive roots of the transcendental equation

$$Y_o(s_n \cdot a) \cdot J_o(s_n \cdot b) - J_o(s_n \cdot a) \cdot Y_o(s_n \cdot b) = 0 \tag{20''}$$

The displacement and stress responses for any temperature field were obtained for plane strain conditions (long hollow cylinder) in Eqs. (86-91). With Eqs.(101) and (102) we obtain the complete formulae for thermal stress components in a long hollow circular cylinder in the case of sinusoidal transient thermal loading on inner surface.

The radial thermal stress component:

$$\sigma_{rr}(r,\omega,t)=\frac{\alpha\cdot E}{1-\nu}\times\left\{\left(-\frac{1}{r^2}\right)k\cdot\pi\cdot\sum_{n=1}^{\infty}\frac{s_n^2\cdot J_0^2(s_n\cdot b)}{J_0^2(s_n\cdot b)-J_0^2(s_n\cdot a)}\times\right.$$
$$\times\left[\frac{1}{s_n}\left\{Y_o(s_n\cdot a)\cdot\left[r\cdot J_1(s_n\cdot r)-a\cdot J_1(s_n\cdot a)\right]-J_o(s_n\cdot a)\cdot\left[r\cdot Y_1(s_n\cdot r)-a\cdot Y_1(s_n\cdot a)\right]\right\}\right]\times$$
$$\times\left[\theta_0\cdot\frac{\omega\cdot e^{-k\cdot s_n^2\cdot t}+(k\cdot s_n^2)\cdot\sin(\omega\cdot t)-\omega\cdot\cos(\omega\cdot t)}{(k\cdot s_n^2)^2+\omega^2}\right]+\frac{r^2-a^2}{r^2(b^2-a^2)}\times$$
$$\times k\cdot\pi\cdot\sum_{n=1}^{\infty}\frac{s_n^2\cdot J_0^2(s_n\cdot b)}{J_0^2(s_n\cdot b)-J_0^2(s_n\cdot a)}\times \qquad (103)$$
$$\times\left[\frac{1}{s_n}\left\{Y_o(s_n\cdot a)\cdot\left[b\cdot J_1(s_n\cdot b)-a\cdot J_1(s_n\cdot a)\right]-J_o(s_n\cdot a)\cdot\left[b\cdot Y_1(s_n\cdot b)-a\cdot Y_1(s_n\cdot a)\right]\right\}\right]\times$$
$$\left.\times\left[\theta_0\cdot\frac{\omega\cdot e^{-k\cdot s_n^2\cdot t}+(k\cdot s_n^2)\cdot\sin(\omega\cdot t)-\omega\cdot\cos(\omega\cdot t)}{(k\cdot s_n^2)^2+\omega^2}\right]\right\}$$

The hoop thermal stress component

$$\sigma_{\theta\theta}(r,\omega,t)=\frac{\alpha\cdot E}{1-\nu}\times\left\{\left(\frac{1}{r^2}\right)k\cdot\pi\cdot\sum_{n=1}^{\infty}\frac{s_n^2\cdot J_0^2(s_n\cdot b)}{J_0^2(s_n\cdot b)-J_0^2(s_n\cdot a)}\times\right.$$
$$\times\left[\frac{1}{s_n}\left\{Y_o(s_n\cdot a)\cdot\left[r\cdot J_1(s_n\cdot r)-a\cdot J_1(s_n\cdot a)\right]-J_o(s_n\cdot a)\cdot\left[r\cdot Y_1(s_n\cdot r)-a\cdot Y_1(s_n\cdot a)\right]\right\}\right]\times$$
$$\times\left[\theta_0\cdot\frac{\omega\cdot e^{-k\cdot s_n^2\cdot t}+(k\cdot s_n^2)\cdot\sin(\omega\cdot t)-\omega\cdot\cos(\omega\cdot t)}{(k\cdot s_n^2)^2+\omega^2}\right]+\frac{r^2+a^2}{r^2(b^2-a^2)}\times$$
$$\times k\cdot\pi\cdot\sum_{n=1}^{\infty}\frac{s_n^2\cdot J_0^2(s_n\cdot b)}{J_0^2(s_n\cdot b)-J_0^2(s_n\cdot a)}\times$$
$$\times\left[\frac{1}{s_n}\left\{Y_o(s_n\cdot a)\cdot\left[b\cdot J_1(s_n\cdot b)-a\cdot J_1(s_n\cdot a)\right]-J_o(s_n\cdot a)\cdot\left[b\cdot Y_1(s_n\cdot b)-a\cdot Y_1(s_n\cdot a)\right]\right\}\right]\times$$
$$\times\left[\theta_0\cdot\frac{\omega\cdot e^{-k\cdot s_n^2\cdot t}+(k\cdot s_n^2)\cdot\sin(\omega\cdot t)-\omega\cdot\cos(\omega\cdot t)}{(k\cdot s_n^2)^2+\omega^2}\right]-$$
$$-k\cdot\pi\cdot\sum_{n=1}^{\infty}\frac{s_n^2\cdot J_0^2(s_n\cdot b)}{J_0^2(s_n\cdot b)-J_0^2(s_n\cdot a)}\left[Y_o(s_n\cdot a)\cdot J_o(s_n r)-J_o(s_n\cdot a)\cdot Y_o(s_n\cdot r)\right]\times$$
$$\left.\times\left[\theta_0\cdot\frac{\omega\cdot e^{-k\cdot s_n^2\cdot t}+(k\cdot s_n^2)\cdot\sin(\omega\cdot t)-\omega\cdot\cos(\omega\cdot t)}{(k\cdot s_n^2)^2+\omega^2}\right]\right\} \qquad (104)$$

The axial thermal stress component

$$\sigma_{zz}(r,\omega,t)=\frac{\alpha\cdot E}{1-\nu}\left\{\frac{2\nu}{b^2-a^2}\times k\cdot\pi\cdot\sum_{n=1}^{\infty}\frac{s_n^2\cdot J_0^2(s_n\cdot b)}{J_0^2(s_n\cdot b)-J_0^2(s_n\cdot a)}\times\right.$$
$$\times\left[\frac{1}{s_n}\left\{Y_o(s_n\cdot a)\cdot\left[b\cdot J_1(s_n\cdot b)-a\cdot J_1(s_n\cdot a)\right]-J_o(s_n\cdot a)\cdot\left[b\cdot Y_1(s_n\cdot b)-a\cdot Y_1(s_n\cdot a)\right]\right\}\right]\cdot$$
$$\cdot\left[\theta_0\cdot\frac{\omega\cdot e^{-k\cdot s_n^2\cdot t}+(k\cdot s_n^2)\cdot\sin(\omega\cdot t)-\omega\cdot\cos(\omega\cdot t)}{(k\cdot s_n^2)^2+\omega^2}\right]- \qquad (105)$$
$$-k\cdot\pi\cdot\sum_{n=1}^{\infty}\frac{s_n^2\cdot J_0^2(s_n\cdot b)}{J_0^2(s_n\cdot b)-J_0^2(s_n\cdot a)}\left[Y_o(s_n\cdot a)\cdot J_o(s_n r)-J_o(s_n\cdot a)\cdot Y_o(s_n\cdot r)\right]\times$$
$$\left.\times\left[\theta_0\cdot\frac{\omega\cdot e^{-k\cdot s_n^2\cdot t}+(k\cdot s_n^2)\cdot\sin(\omega\cdot t)-\omega\cdot\cos(\omega\cdot t)}{(k\cdot s_n^2)^2+\omega^2}\right]\right\}$$

for $\varepsilon_{zz}=0$

$$\sigma_{zz}(r,\omega,t)=\frac{\alpha\cdot E}{1-\nu}\left\{\frac{2}{b^2-a^2}\times k\cdot\pi\cdot\sum_{n=1}^{\infty}\frac{s_n^2\cdot J_0^2(s_n\cdot b)}{J_0^2(s_n\cdot b)-J_0^2(s_n\cdot a)}\times\right.$$
$$\times\left[\frac{1}{s_n}\left\{Y_o(s_n\cdot a)\cdot\left[b\cdot J_1(s_n\cdot b)-a\cdot J_1(s_n\cdot a)\right]-J_o(s_n\cdot a)\cdot\left[b\cdot Y_1(s_n\cdot b)-a\cdot Y_1(s_n\cdot a)\right]\right\}\right]\times$$
$$\times\left[\theta_0\cdot\frac{\omega\cdot e^{-k\cdot s_n^2\cdot t}+(k\cdot s_n^2)\cdot\sin(\omega\cdot t)-\omega\cdot\cos(\omega\cdot t)}{(k\cdot s_n^2)^2+\omega^2}\right]- \qquad (106)$$
$$-k\cdot\pi\cdot\sum_{n=1}^{\infty}\frac{s_n^2\cdot J_0^2(s_n\cdot b)}{J_0^2(s_n\cdot b)-J_0^2(s_n\cdot a)}\left[Y_o(s_n\cdot a)\cdot J_o(s_n r)-J_o(s_n\cdot a)\cdot Y_o(s_n\cdot r)\right]\times$$
$$\left.\times\left[\theta_0\cdot\frac{\omega\cdot e^{-k\cdot s_n^2\cdot t}+(k\cdot s_n^2)\cdot\sin(\omega\cdot t)-\omega\cdot\cos(\omega\cdot t)}{(k\cdot s_n^2)^2+\omega^2}\right]\right\}$$

for $\varepsilon_{zz}=\varepsilon_0$

In "condensed forms" the above equations are

$$\sigma_{rr}(r,\omega,t)=\frac{\alpha\cdot E}{1-\nu}\left[-\frac{1}{r^2}\cdot I_1(r,\omega,t)+\frac{r^2-a^2}{r^2\cdot(b^2-a^2)}\cdot I_2(\omega,t)\right] \qquad (107)$$

$$\sigma_{\theta\theta}(r,\omega,t)=\frac{\alpha\cdot E}{1-\nu}\left[\frac{1}{r^2}\cdot I_1(r,\omega,t)+\frac{r^2+a^2}{r^2\cdot(b^2-a^2)}\cdot I_2(\omega,t)-\theta(r,\omega,t)\right] \qquad (108)$$

$$\sigma_{zz}(r,\omega,t)=\frac{\alpha\cdot E}{1-\nu}\left(\frac{2\nu}{b^2-a^2}\cdot I_2(\omega,t)-\theta(r,\omega,t)\right) \quad \text{for } \varepsilon_{zz}=0 \quad (109)$$

$$\sigma_{zz}(r,\omega,t)=\frac{\alpha\cdot E}{1-\nu}\left(\frac{2}{b^2-a^2}\cdot I_2(\omega,t)-\theta(r,\omega,t)\right) \quad \text{for } \varepsilon_{zz}=\varepsilon_0 \quad (110)$$

5. Application to a Benchmark Case and Discussion

In order to validate the predictive capability of the analytical solutions developed in this study, the benchmark case of thermal striping at a FBR secondary circuit tee junction [23] was chosen. This relates to a thermomechanical and fracture mechanics assessment performed in the 1990's in the framework of the European Commission's Working Group on Codes and Standards by the following participants: NNC Ltd. (lead), Framatome (Novatome), AEA Technology and Leicester University. Also, an independent Korean study performed on the same benchmark was reported in [16]. The benchmark is posed as a thermoelastic problem, and although the application of the present work is foreseen for LWR reactors, it provides the best available data for checking the analytical solutions described in the previous chapters.

The problem is based on operational experience with the secondary circuit of the French PHENIX reactor. The input data was obtained (by Framatome) from the actual characteristics of the reactor coolant circuit and because of its complexity, it was simplified where possible. PHENIX is a 250 MWe demonstration plant, with three secondary loops, modular steam generators and integrated primary circuit. During normal operation, sodium at 340 ºC flows in the main pipe of the secondary circuit. A small pipe, connected by a tee junction to the main pipe, discharges sodium at 430 ºC into the main pipe. The mixing of the two flows (ΔT= 90ºC) produced a thermal striping phenomenon.. The main features of the circuit in the tee junction area are shown in Figure 1. The main pipe in the junction area consists in a horizontal straight part, an elbow, and vertical straight part where the tee junction is connected.

In the straight parts the main pipe has the following characteristics: inner diameter: Φ_i= 494 mm and wall thickness: t= 7 mm. Both pipes are made of AISI 304 stainless, steel grade: Z5 CN 18.10 In the present work the following material properties values at 400 ºC were used [23]:

- steel density: ρ=7803 kg/m^3;

- specific heat coefficient: c=550 j/kg.K;
- thermal conductivity: λ=19.39 W/m.K;
- mean thermal expansion: $\alpha_m=17.9\cdot10^{-6}$ K^{-1};
- Young's modulus: E= $161\cdot10^3$ MPa;
- yield Stress: σ_y = 161 MPa
- thermal diffusivity: $k=\frac{\lambda}{c\cdot\rho}=4.5\cdot10^{-6}$ m^2/s.

The results of the calculations performed in the 1990s by NNC and Framatome reported in [23] and those of the Korean study reported in [16] have been used for comparison of the predictive capability of the analytical solutions developed in the present study. Also, a new FE simulation has now been performed using ABAQUS commercial software. The comparison of these results with the analytic predictions is discussed in section 5.2 below.

The results from NNC calculations include a fatigue assessment, using a version of the UK thermal striping method applied to austenitic steel, performed on the basis of AEA's thermo hydraulic analysis of the TC01A signal. For thermal analyses an axisymmetric ABAQUS finite element model of a slice through the large pipe wall was used. For the stress calculations an analytic approach was adopted. The formulations for the stress components (similar to Eqs.88, 89 and 91) were applied to the output of the ABAQUS temperature calculations (FIL. file) with a Fortran post processor to determine the stress components at each node for each the temperature solutions. For calculation of the axial stress the $\varepsilon_{zz}=\varepsilon_0$ condition was used as the mechanical boundary condition.

The Framatome calculations were performed using in-house methods applied to the AEA thermal hydraulic output TC01A and assuming sinusoidal fluctuations as an approximation to the signal. For tee junction area the frequencies 0.5 Hz and 1 Hz were used because they induce the maximum stresses in the wall [23]. To determine the load arising from the sinusoidal temperature fluctuations a computer code (SYSTUS release 233) was used. For calculation of the axial stress the $\varepsilon_{zz}=0$ condition was used as the mechanical boundary condition.

The Korean study used FEM (ABAQUS version 5.7) for the heat transfer, thermal stress and fracture mechanics analyses. In addition, Fortran programs were developed for the thermal stress and fracture analyses using Green's function method and ASME section III, subsection NH for fatigue damage evaluation.

In present analyses we apply sinusoidal thermal loading with similar characteristics to that used by Framatome:

- temperature fluctuation range: ΔT=85 ºC;
- the reference temperature : T_o= 385 ºC;
- the frequencies: f=0.5 Hz and f= 1 Hz

For the sinusoidal function described in Eq.(35), this implies that the amplitude $\theta_0 = \Delta T/2$ = 42.5°C, about a mean value of 385°C.

For temperature profiles in the wall thickness for both sinusoidal signal of 0.5 Hz and 1 Hz the following relationship, which was developed in the present study, is used:

$$\theta(r,\omega,t) = k\cdot\pi\cdot\sum_{n=1}^{\infty}\frac{s_n^2\cdot J_0^2(s_n\cdot b)}{J_0^2(s_n\cdot b)-J_0^2(s_n\cdot a)}\left[Y_o(s_n\cdot a)\cdot J_o(s_n r)-J_o(s_n\cdot a)\cdot Y_o(s_n\cdot r)\right]\times$$
$$\times\left[\theta_0\cdot\frac{\omega\cdot e^{-k\cdot s_n^2\cdot t}+(k\cdot s_n^2)\cdot\sin(\omega\cdot t)-\omega\cdot\cos(\omega\cdot t)}{(k\cdot s_n^2)^2+\omega^2}\right] \qquad (37'')$$

with s_n being the positive roots of the transcendental equation

$$Y_o(s_n\cdot a)\cdot J_o(s_n\cdot b)-J_o(s_n\cdot a)\cdot Y_o(s_n\cdot b)=0 \qquad (20''')$$

$J_0(z)$ and $Y_0(z)$ are Bessel functions of first and second kind of order 0. The through-wall thermal stress components for the sinusoidal signal at both 0.5 Hz and 1 Hz are obtained from the following relationships, developed in section 4 above: 103, 104. 105 and 106.

For fatigue assessment (Appendix 2) of components subject to multiaxial stress states, the various codes and standards [1,10,24] require the use of parameters such as "*Effective stress intensity range"* based on maximum shear stress yield criterion (Tresca) or maximum distortion energy yield criterion (von Mises). Based on the last mentioned one, the following additional scalar stress values are evaluated:

- *Von Mises equivalent stress*:

$$\sigma_{VM}=\sqrt{\frac{(\sigma_{rr}-\sigma_{\theta\theta})^2+(\sigma_{zz}-\sigma_{\theta\theta})^2+(\sigma_{rr}-\sigma_{zz})^2}{2}} \qquad (111)$$

- *Effective equivalent stress intensity range* (for using with Maximum Distortion Energy Yield Criterion in fatigue crack initiation):

$$\Delta S_{range} = \sqrt{\frac{\left(\Delta\sigma_{rr} - \Delta\sigma_{\theta\theta}\right)^2 + \left(\Delta\sigma_{zz} - \Delta\sigma_{\theta\theta}\right)^2 + \left(\Delta\sigma_{rr} - \Delta\sigma_{zz}\right)^2}{2}} \quad (112)$$

The Framatome [23] fatigue analyses used the methodology from the RCC-MR code (Design and Construction Rules for Mechanical Components of FBR Nuclear Islands), and the plasticity effects were taken into account by means of K_υ and K_ε factors (respectively triaxiality and local plastic stress concentration effects):

$$\Delta\varepsilon_{TOT} = \left(K_\upsilon + K_\varepsilon - 1\right) \cdot \frac{2(1+\nu)}{3E} \cdot \Delta S_{range} \quad (113)$$

Some comments are necessary before discussing the comparison between various methods. The analytical solutions for the temperature distribution (Eq. 37'') and the associated thermal stress components (Eqs. 103', 104', 105', 106') were implemented by means of specially written routines implemented in the MATLAB software package (MATLAB 7.3 version, with Symbolic Math Toolbox). A first task was to establish the number of roots needed from transcendental equation (20''') because the response of the solutions become more stabile as the number of roots is increased. We used one hundred roots and note that further increasing the number gives negligible improvement in the predictions. This means that an equal number of the evaluations of the above equations must be performed. Also, due to Bessel function properties, the accuracy of the analytical solutions for both the temperature and the stress response is strongly dependent on the size of the incremental steps in the *"r"* variable (radial distance through wall thickness). An investigation was made to optimize this and it was concluded that several hundred are required. Taking into account the complex mathematical series expansions used for the analytical solutions for temperature distribution and thermal stress components through the wall thickness of hollow cylinder, the solutions show some point-to-point variability and therefore we applied a smoothing technique based on the polynomial fitting of analytical distributions. This technique is widely applied [1,6,7,8] to facilitate the calculation of stress intensity factors based on the thermal stresses profile [9], which are used for crack growth assessment.

5.1 Comparison with independent studies on predicted temperature and stress distribution

The temperature profile distributions through wall-thickness of hollow cylinder have been obtained using Eq. (37'') for sinusoidal signal frequencies of f=0.5 Hz and f= 1Hz.

In Figure 2, for f=0.5 Hz, the temperature profiles are shown for different time: t1= 0.5 sec and t2=1.5 sec (corresponding to instants of maximum deviation of the fluid temperature from the mean or reference value) and t3=1 sec and t4= 2 sec, (minimum, i.e. zero, deviation from the reference temperature). As can be observed, at the times of maximum deviation, the resulting temperature field decays significantly through of pipe wall thickness, reaching negligible values after 3 mm deep. The temperature distributions are identical with those obtained in the Korean study [16] (see Figure 4) and by Framatome [23] (see Figure 5). Figure 3 shows the time-dependence of temperature at selected locations through the pipe thickness. The thermal reponse of the material has a sinusoidal form but with a decreased amplitude corresponding to the depth in the pipe wall. The temperature distributions calculated by NNC (Figure 6) display the same characteristics , but in relation to 300 °C as reference temperature.

Figures 7 and 8 show the through-thickness and time dependence of the temperature profiles for f=1 Hz. As expected, the penetration depth of the temperature fluctuations are smaller (about 2 cm) than for f=0.5 Hz. Again the results are in good agreement with temperature distributions obtained by Framatome for the f=1 Hz case (Figure 9).

Calculations of the hoop, axial and radial thermal stress components have been made for the same frequencies (f=0.5 Hz and f=1 Hz) as in the thermal analyses. The distribution of the thermal stresses over the thickness of the wall is analyzed for a period of 2 sec in case of f=0.5 Hz and for sec for f=1Hz. In first half of each time period the stresses are compressive at the inner surface, switching then to tensile for the second half.

Figure 10 shows the limiting hoop stress distributions for f=0.5 Hz. On inner surface the maximum values are: $\sigma_{\theta comp}$= -169.5 MPa (in compression), $\sigma_{\theta tensile}$= 171.5MPa (in tension), giving a range value of $\Delta\sigma_{\theta\theta}$=341 MPa . For f=1 Hz (Figure 11) the respective values are: $\sigma_{\theta comp}$ = -160 MPa, $\sigma_{\theta tensile}$ =160 MPa, $\Delta\sigma_{\theta\theta}$= 320MPa . As expected, $\Delta\sigma_{\theta\theta}$ (1 Hz) < $\Delta\sigma_{\theta\theta}$ (0.5Hz). A comparison could be made with the NNC calculation [23], see Figure 12,

For axial thermal stress component two evaluations were performed: for ε_{zz}= ε_0 (as used by NNC) and ε_{zz}= 0 (Framatome). In the first case (Figures 13 and 14) we obtain the following maximum values: σ_{zcomp}= -137 MPa, $\sigma_{ztensile}$= 156MPa , $\Delta\sigma_{zz}$ =293 MPa for f=0.5 Hz and σ_{zcomp}= -137MPa, $\sigma_{ztensile}$= 151 MPa , $\Delta\sigma_{zz}$ =288 MPa for f=1 Hz. In the ε_{zz}= 0 case the results are: σ_{zcomp}= -160MPa, $\sigma_{ztensile}$= 167MPa, $\Delta\sigma_{zz}$=327 MPa and σ_{zcomp}= -153 MPa, $\sigma_{ztensile}$= 157 MPa, $\Delta\sigma_{zz}$ = 310 MPa for f =0.5Hz and f=1 Hz respectively (Figures 15 and

16). Using the Framatome predictions for f=0.5Hz (Figures 17 and 18), a direct comparison with the results from the present work is made in Figure 19 (ε_{zz}= 0). For f=1 Hz the comparison used the corresponding Framatome results given in Figures 20 and 21, and Figure 22 shows the two sets of axial thermal stress predictions for ε_{zz}= 0. The agreement is considered good for f=0.5Hz and very good at f=1Hz.

No predictions of radial thermal stress are reported in the NCC or Framatome studies. In any case the present work for f=0.5 Hz and f=1Hz show that the values are too small to have an impact on thermal fatigue assessment.

The von Mises equivalent stress profiles are displayed in Figures 25 and 26 for f=0.5 Hz in the ε_{zz}= ε_0 and ε_{zz}= 0 cases respectively. Two instants of time were chosen: t=0.5 sec (for maximum values) and t=4 sec (for minimum values). Comparing the Framatome calculations (Figure 27) and those of the present work, very good agreement is obtained, as shown in Figure 28. A similar comparison for f=1 Hz was performed based on Figures 29 and 30 (present work) and Figure 31 (Framatome calculations). The von Mises equivalent stress profiles are in very closely agreement as can be seen in Figure 32. From the Korean study [16] a stress intensity profile (Tresca definition) is shown in Figure 33, with a similar profile through the wall thickness.

The effective equivalent stress intensity range profile distribution has been evaluated for both frequencies and the ε_{zz}= ε_0 and ε_{zz}= 0 cases. For f=0.5 Hz (Figures 34 and 35) the results for $\Delta S_{range.max}$ are 307 and 328 MPa, respectively. The results for f=1 Hz are displayed in Figures 36 and 37 and the corresponding maximum $\Delta S_{range.max}$ values are 275.7 and 293.4 MPa. These results confirm the frequency f=0.5 Hz is more critical than f=1Hz from thermal fatigue point of view. Tables 1 and 2 summarise the main results from the present work and from other reported analyses of this benchmark.

Table 1 Results for thermal stress components at f=0.5 Hz

Thermal stress components	Present work	Framatome[23]	NNC[23]	Ref. [16]
Hoop stress range (MPa)	$\Delta\sigma_{\theta\theta}$= 341	$\Delta\sigma_{\theta\theta}$= 310	-	186.6
Axial stress range (MPa)				
ε_{zz}= ε_0	$\Delta\sigma_{zz}$= 293	-	-	211
ε_{zz}=0	$\Delta\sigma_{zz}$= 327	$\Delta\sigma_{\theta\theta}$= 310	-	
Radial stress range (MPa)	$\Delta\sigma_{rr}$= 1	-	-	42.6
Von Mises equivalent stress (MPa)				
ε_{zz}= ε_0	σ_{VMmax}=152	-	-	
ε_{zz}= 0	σ_{VMmax}=163	- σ_{VMmax}=154	-	

Effective stress intensity range (MPa)				
$\varepsilon_{zz}= \varepsilon_0$	$\Delta S_{rangemax}$=307	-	-	
$\varepsilon_{zz}= 0$	$\Delta S_{rangemax}$=328	$\Delta S_{rangemax}$=310	$\Delta S_{rangemax}$=315	292.7

Table 2 Results for thermal stress components at f=1 Hz

Thermal stress components	Present work	Framatome[23]	NNC[23]	Ref. [16]
Hoop stress range (MPa)	$\Delta\sigma_{\theta\theta}$= 320	-	-	-
Axial stress range (MPa)				
$\varepsilon_{zz}= \varepsilon_0$	$\Delta\sigma_{zz}$= 288	-	-	-
ε_{zz}=0	$\Delta\sigma_{zz}$= 310	- $\Delta\sigma_{zz}$= 280	-	
Radial stress range (MPa)	$\Delta\sigma_{rr}$= 0.8	-	-	-
Von Mises equivalent stress (MPa)				
$\varepsilon_{zz}= \varepsilon_0$	σ_{VMmax}=141	-	-	
$\varepsilon_{zz}= 0$	σ_{VMmax}=153	- σ_{VMmax}=154	-	
Effective stress intensity range (MPa)				
$\varepsilon_{zz}= \varepsilon_0$	$\Delta S_{rangemax}$=275.7	-	-	
$\varepsilon_{zz}= 0$	$\Delta S_{rangemax}$=293.4	$\Delta S_{rangemax}$=320	-	-

Overall the comparisons have demonstrated good agreement between predictions from the analytical solutions for thermal stresses developed in the present work with those obtained from finite element models in refs. [16] and [23].

5.2 Comparison with JRC finite element simulations

The prediction of analytical solutions for thermal response and associated thermal stresses developed in the pipe were additionally compared with finite element analyses results performed in a simple elastic model. This was intended to provide a basis for future benchmarking of different scenarios and for assessing the relative merits of the different approaches. The commercial code ABAQUS was used to perform a standard un-coupled finite element calculation i.e. first the thermal analysis of the sinusoidal thermal load and second a mechanical analysis, when the resulting temperature fields are applied to determine the elastic thermal stresses.

The finite element model used axi-symmetric 8-nodes elements (Figure 38 a). Axisymmetry was assumed and the length of the cylinder segment was chosen to more than twice the wall thickness. Auxiliary software routines were used to automatically generate finite element meshes with a progressive mesh refinement towards the inner pipe surface to capture the large strain variations induced by the thermal loads.

Two different boundary conditions were considered:

- top edge of the sample free to expand in the axial direction, Figure 38b;
- top edge of the sample fixed in the axial direction, Figure 38c.

N.B. The model is restrained in the radial direction at the top outer edge, but this has virtually no influence on stress distributions in the bottom radial plane, which are used for comparison with the analytical solutions. The material properties used for elastic analyses are mentioned in previous chapter.

The characteristic thermal sinusoidal signals applied during this analyse were similar to those used in the analytical calculation. The reference temperature of the sample is T_0=385˚C, the temperature fluctuation range is ΔT=85˚C and the frequencies considered are v=0.5Hz and v=1Hz.

The thermal sinusoidal loads have been applied at time zero at the inner wall of the sample uniformly heated at 385˚C for t<0sec. The load was applied for 9 sec and the temperature and stress/strain variations across the wall thickness in function of time have been monitored.

To apply the sinusoidal load in the FE analysis the easiest option was to use the standard Fourier series routine by means of the *AMPLITUDE keyword and its periodic option. The amplitude, *Amp*, defined in this way results in:

$$Amp = A_0 + \sum_{n=1}^{N}\left[A_n \cos n\varpi\left(t - t_0\right) + B_n \sin n\varpi(t - t_0)\right] \qquad \text{for } t \geq t_0 \qquad (114)$$

$$Amp = A_0 \qquad \text{for } t < t_0 \qquad (115)$$

where *N* is the number of terms in the Fourier series, *ω* is the radial frequency in rad/sec, t_0 is the starting time, A_0 is the constant term in the Fourier series, $A_{n=1,2...}$ are the first, second, etc. coefficients of the cosine terms and $B_{n=1,2...}$ are the first, second, etc. coefficients of the sine terms. In our case: N=1, $A_0=T_0$, A_1=0, B_1=42.5 ˚C.

Plots of the temperature field at several instants of time, during of temperature wave propagation across the wall thickness are shown in Figure 39 for f=0.5 Hz and Figure 40 for f=1 Hz. As can be seen the temperature wave front is non-homogenous due to the rapid fluctuation of the thermal load at the inner boundary of model.

Figures 41 and 42 show the von Mises iso-stress plots at a frequency f= 1Hz corresponding to the point-to-point temperature fluctuations in the body of pipe, for free

and fixed boundary conditions respectively. The visible distortion (strongly magnified for better visualization) in the latter is due to the radial constraint at the top of the model.

Before graphically comparing the results from analytical and finite element analyses it is important to mention that in the following, the instants of time for calculating the temperature and corresponding elastic stress components have been chosen to comply with the time steps used in the FE analysis.

The predicted temperature profiles across the wall-thickness are shown in Figures 43 and 44 for frequencies of f=0.5 Hz and f= 1Hz. The analytical predictions fit quite well to those from the FEA at the same instants of time.

Figures 45 and 46 show the maximum and minimum hoop thermal stresses for both frequencies. These values correspond to a fixed edge boundary condition. In the case of axial stress the comparison has been made for both the boundary condition cases: fixed and free axial strains. Figures 47 to 50 confirm the good agreement between the predicted and FE axial stress values across the wall thickness of the pipe for both the boundary conditions. The von Mises equivalent stress comparisons are depicted in Figures 51-54. Even though the FE stress gradients for the free axial displacement boundary condition ($\varepsilon_{zz}=\varepsilon_0$) are a bit higher for the analytical solutions, still the maximum values very close to those obtained by FEA. For the fixed boundary condition both the axial stress maximum values and the gradients are in good agreement with the FE results. The effective equivalent stress intensity range is a very important parameter in relation to the fatigue curves used to obtain the cumulative usage factors for fatigue crack initiation assessment. The agreement between analytical and FEA calculations is rather good for maximum values as well as for the stress gradient through the wall-thickness, can be seen in Figures 55-58. Table 3 summarizes the results of the above comparisons. The agreement between analytical and FEA predictions provides verification of the analytical model developed during this work.

Table 3 Comparison between analytical and FEA calculation for thermal stresses due to sinusoidal thermal loading

	f=0.5 Hz		f= 1 Hz	
Stress component	Analytical MPa	FEA MPa	Analytical MPa	FEA MPa
Hoop stress	300	280	325	308
Axial stress				
$\varepsilon_{zz}=0$	290	285	310	312
$\varepsilon_{zz}=\varepsilon_0$	265	240	312	313

Von Mises stress				
$\varepsilon_{zz}=0$	163	159	153	156
$\varepsilon_{zz}=\varepsilon_0$	135	138	142	141
ΔS_{range}				
$\varepsilon_{zz}=0$	280	279	304	307
$\varepsilon_{zz}=\varepsilon_0$	263	263	283	288

6. Conclusions

Analytical solutions with several new features have been developed for temperature and elastic thermal stress distributions for a hollow circular cylinder under sinusoidal thermal transient loading at the inner surface. The approach uses a finite Hankel transform in a general form for any transient thermal loading for a hollow cylinder. Using the properties of Bessel functions, an analytical solution for temperature distribution through wall thickness was derived for a special case of sinusoidal transient thermal loading on inner pipe surface. The solutions for associated thermal stress components were developed by means of the displacement technique. To the authors' knowledge, this is first time a complete set of such analytical expressions has been openly published.

The solution method has been implemented using the MATLAB software package. Several practical issues have been resolved, for instance it is found that typically 100 roots of the transcendental equation are required to obtain a stable response and that the number of radial steps through the wall thickness needs to be of the order of many hundred, since the accuracy for both temperature and stresses is strong dependent on this variable

The predictions made using the solution method have been successfully benchmarked by comparison with results of independent studies on a FBR secondary circuit tee-junction, which used a combination of finite element methods for temperature distributions and analytical methods for stresses.

The analytical solution predictions for the FBR benchmark were additionally checked against results of a new finite element analysis with commercial software ABAQUS on elastic 2-D axisymmetric model.

The new analytic solution scheme can be used to support several elements of the proposed European Thermal Fatigue Procedure for high cycle fatigue damage assessment of mixing tees, including:

- level 2 – for analyses assuming a sinusoidal temperature fluctuation as boundary condition on inner surface of the pipe;

- level 3 – for load spectrum analysis based on one-dimension temperature and stress evaluations at each measured location;
- level 4 – providing through-thickness stress profiles for thermal fatigue crack growth assessment.

Further work will address the integration of the solution scheme into an overall process for determining thermal fatigue usage factors, considering also aspects as plasticity effects and selection of fatigue life curves.

References

1. S. Chapuliot, C. Gourdin, T. Payen, J.P.Magnaud, A.Monavon, Hydro-thermal-mechanical analysis of thermal fatigue in a mixing tee, Nuclear Engineering and Design 235 (2005) 575-596
2. NEA/CSNI/R (2005) 8, Thermal cycling in LWR components in OECD-NEA member countries, JT001879565
3. NEA/CSNI/R(2005)2, FAD3D –An OECD/NEA benchmark on thermal fatigue in fluid mixing areas, JT00188033
4. IAEA-TECDOC-1361, Assessment and management of ageing of major nuclear power plant components important to safety-primary piping in PWRs, IAEA, July 2003
5. Lin-Wen Hu, Jeongik Lee, Pradip Saha, M.S.Kazimi, Numerical Simulation study of high thermal fatigue caused by thermal stripping, Third International Conference on Fatigue of Reactor Components, Seville, Spain 3-6 October 2004, NEA/CSNI/R(2004)21
6. Brian B. Kerezsi, John W.H. Price, Using the ASME and BSI codes to predict crack growth due to repeated thermal shock, International Journal of Pressure Vessels and Piping 79 (2002) 361-371
7. C. Faidy RSE-M. A general presentation of the French codified flaw evaluation procedure, International Journal of Pressure Vessel and Piping 77 (2000) 919-927
8. T. Wakai, M. Horikiri, C. Poussard, B. Drubay A comparison between Japanese and French A 16 defect assessment procedures for thermal fatigue crack growth, Nuclear Engineering and Design 235 (2005) 937-944
9. A.R. Shahani, S.M. Nabavi, Transient thermal stress intensity factors for an internal longitudinal semi-elliptical crack in a thick-walled cylinder, Engineering Fracture Mechanics (2007), doi:101016/j.engfrachmech.2006.11.018
10. API 579 Fitness-for-Service-API Recommended Practice 579, First Edition, January 2000, American Petroleum Institute
11. B.A. Boley, J. Weiner, Theory of Thermal Stresses, John Wiley & Sons, 1960
12. N. Noda, R.B. Hetnarski, Y. Tanigawa, Thermal Stresses, 2nd Ed., Taylor & Francis, 2003

13. S.P. Timoshenko, J.N. Goodier, Theory of Elasticity, McGraw-Hill, New York, (1987)
14. A.E. Segal, Transient analysis of thick-walled piping under polynomial thermal loading, Nuclear Engineering and Design 226 (2003) 183-191
15. H.-Y. Lee, J.-B. Kim, B. Yoo Green's function approach for crack propagation problem subjected to high cycle thermal fatigue loading, International Journal of Pressure Vessel and Piping 76 (1999) 487-494
16. H.-Y.Lee, J.-B. Kim, B. Yoo Tee-Junction of LMFR secondary circuit involving thermal, thermomechanical and fracture mechanics assessment on a stripping phenomenon, IAEA-TECDOC-1318, "Validation of fast reactor thermomechanical and thermohydraulic codes", Final report of a coordinated research project 1996-1999 (1999)
17. A.R. Shahani, S.M. Nabavi, Analytical solution of the quasi-static thermoelasticity problem in a pressurized thick-walled cylinder subjected to transient thermal loading, Applied Mathematical Modelling (2006), doi:10.1016/j.apm.2006.06.008
18. S. Marie, Analytical expression of the thermal stresses in a vessel or pipe with cladding submitted to any thermal transient, International Journal of Pressure Vessel and Piping 81 (2004) 303-312
19. K.-S. Kim , N. Noda, Green's function approach to unsteady thermal stresses in an infinite hollow cylinder of functionally graded material, Acta Mechanica 156, 145-161 (2000)
20. N.T. Eldabe, M. El-Shahed, M. Shawkey , An extension of the finite Hankel transform, Applied Mathematics and Computations 151 (2004) 713-717
21. I.N. Sneddon, The Use of Integral Transforms, McGraw-Hill, New York, (1993)
22. M. Garg, A.Rao, S.L. Kalla, On a generalized finite Hankel transform, Applied Mathematics and Computation (2007), doi:10.1016/j.amc.2007.01.076
23. D. Buckthorpe, O. Gelineau, M.W.J. Lewis, A. Ponter, Final report on CEC study on thermal stripping benchmark –thermo mechanical and fracture calculation, Project C5077/TR/001, NNC Limited 1988
24. O.K. Chopra, W.J. Shack, Effect of LWR Coolant Environments on the fatigue Life of reactor Materials, Draft report for Comment, NUREG/CR-6909, ANL 06/08, July 2006, U.S. Nuclear Regulatory Commission , Office of Nuclear Regulatory Research, Washington, DC

FIGURES

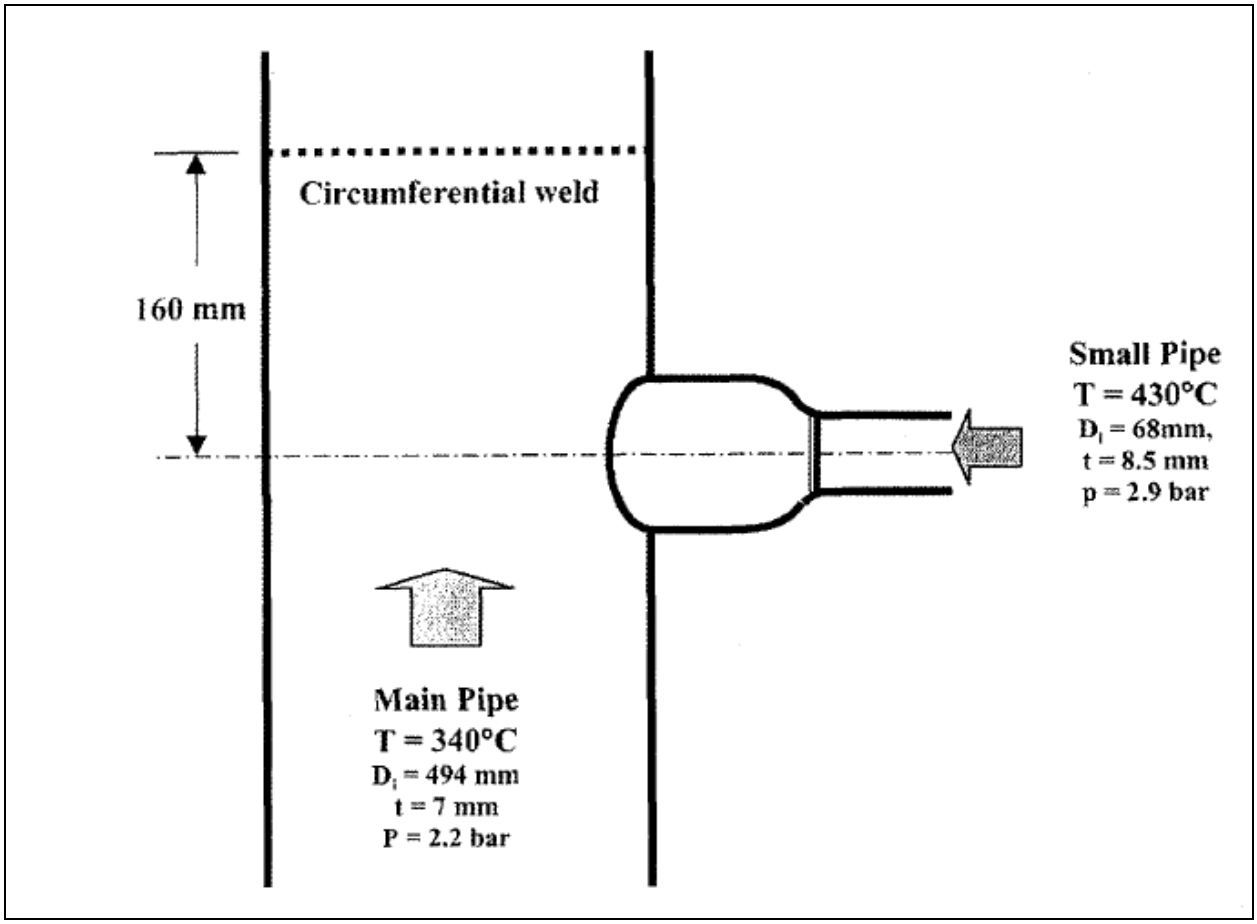

Figure 1. Geometrical characteristics of the components in the tee junction area

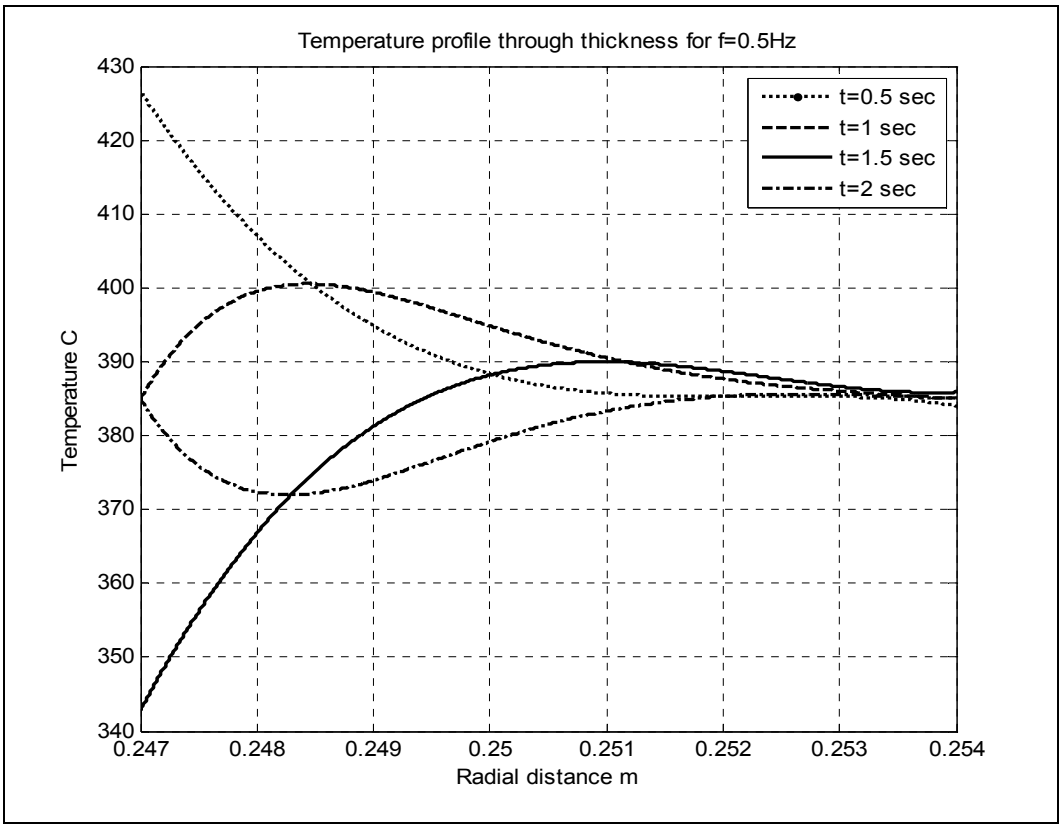

Figure 2 Temperature profile distribution through wall-thickness of hollow cylinder at various moments of time, f=0.5 Hz

NB: r_i=0.247 m, inner surface of pipe; r_e=0.247 m, outer surface of pipe

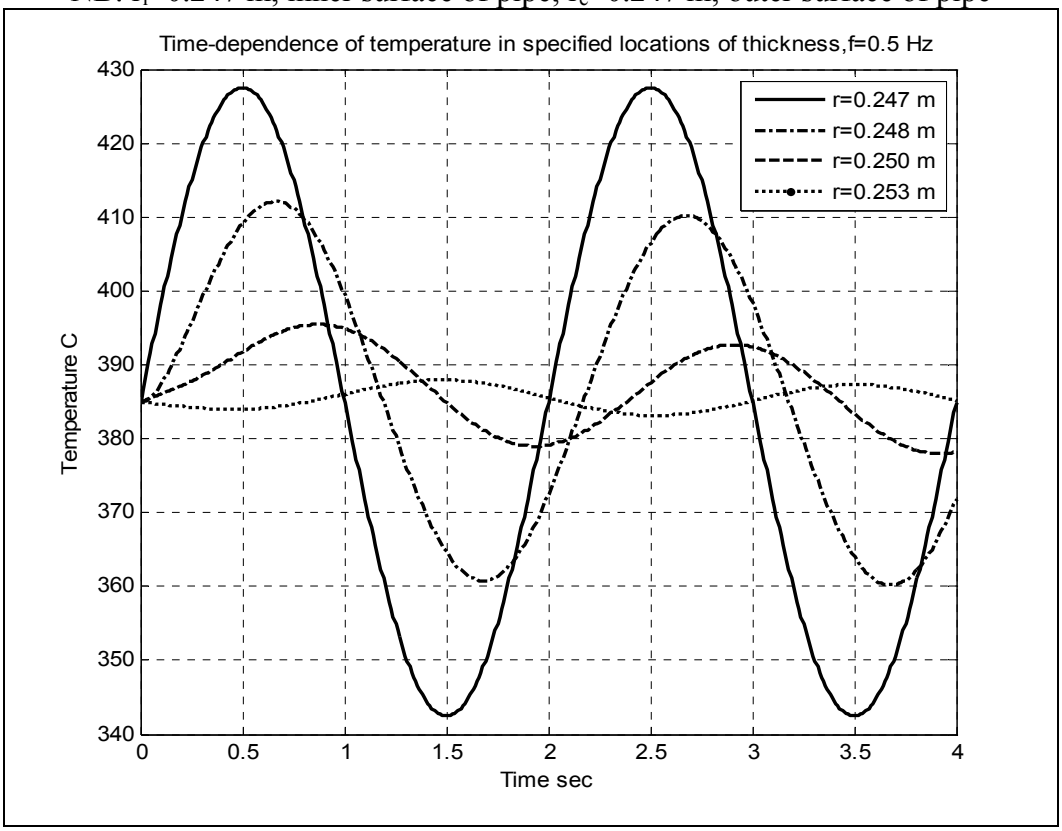

Figure 3 Time-dependence of temperature in some locations of wall-thickness for frequency f=0.5 Hz

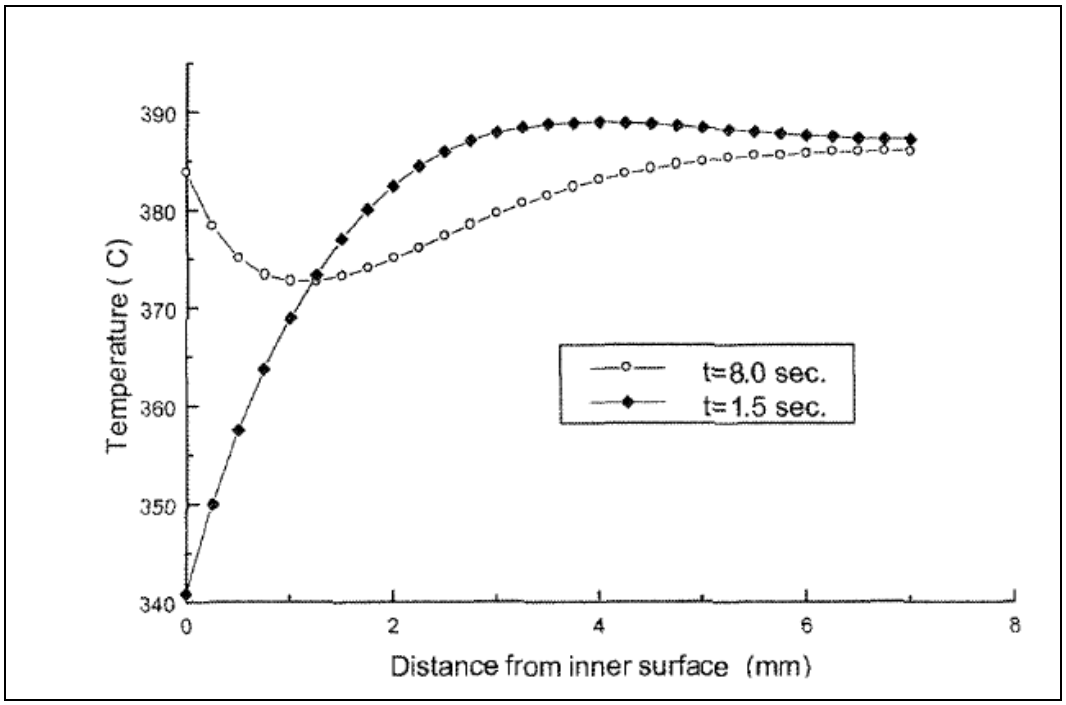

Figure 4. Temperature profile along the thickness direction for sinusoidal loading, f= 0.5 Hz [16]

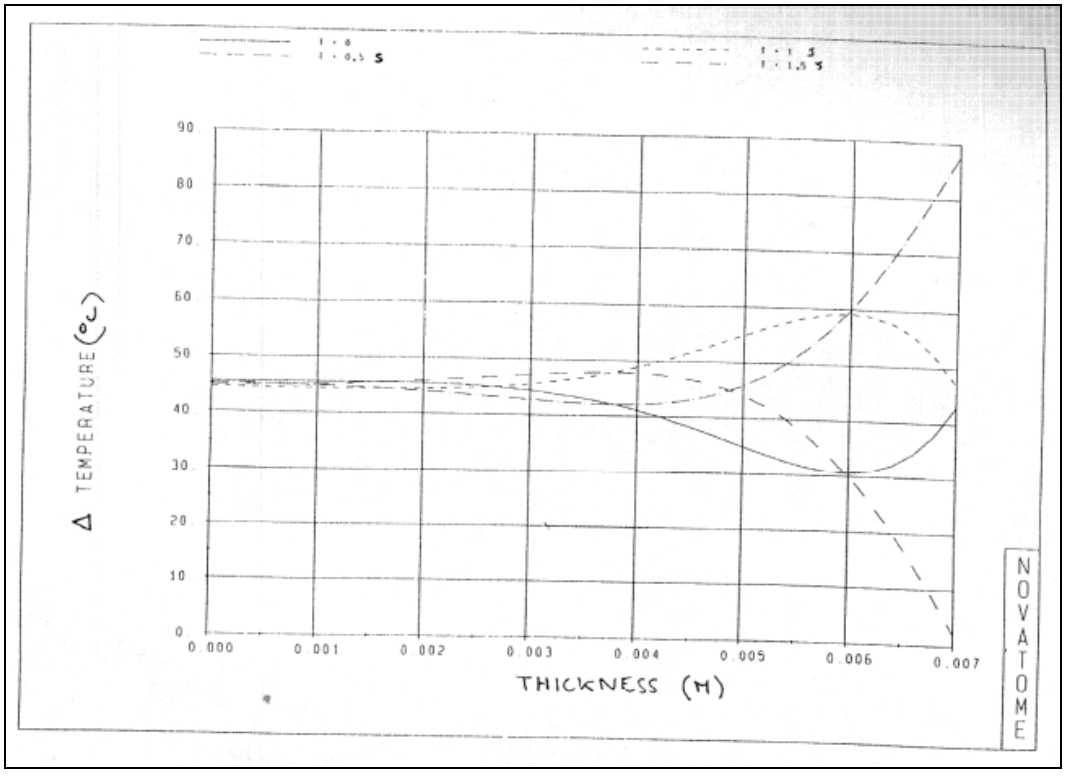

Figure 5. Framatome calculations: Temperature profile for f= 0.5 Hz sinusoidal signal [23]

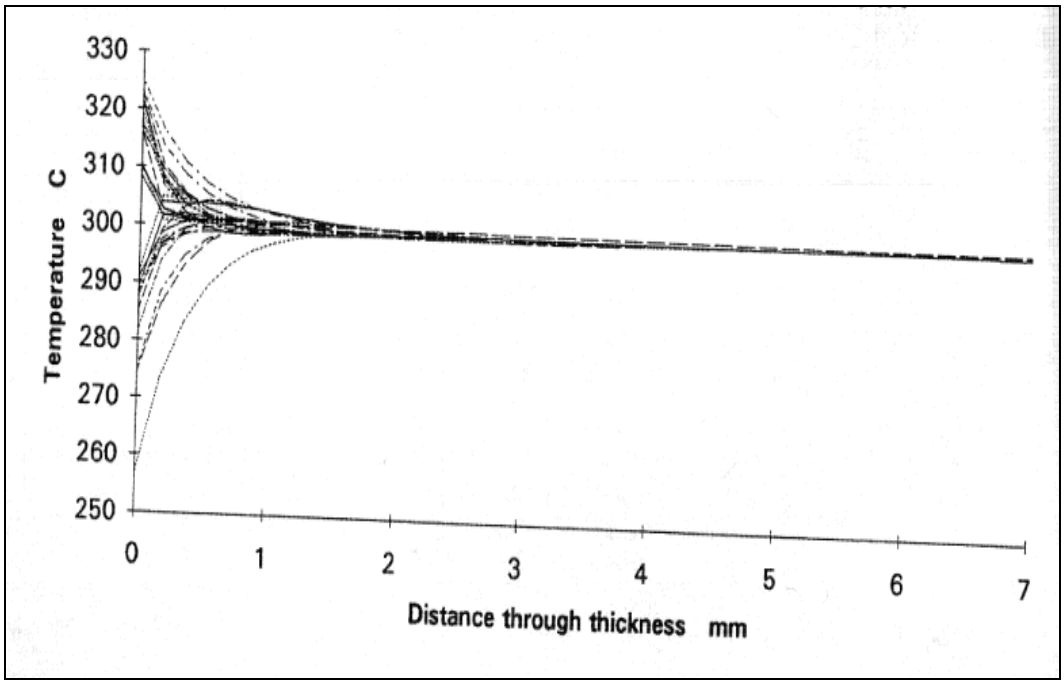

Figure 6. NNC calculations: Typical temperature results using filtered AEA TC01A data - Temperature variation through thickness over time period 20.2 s to 20.9 sec [23]

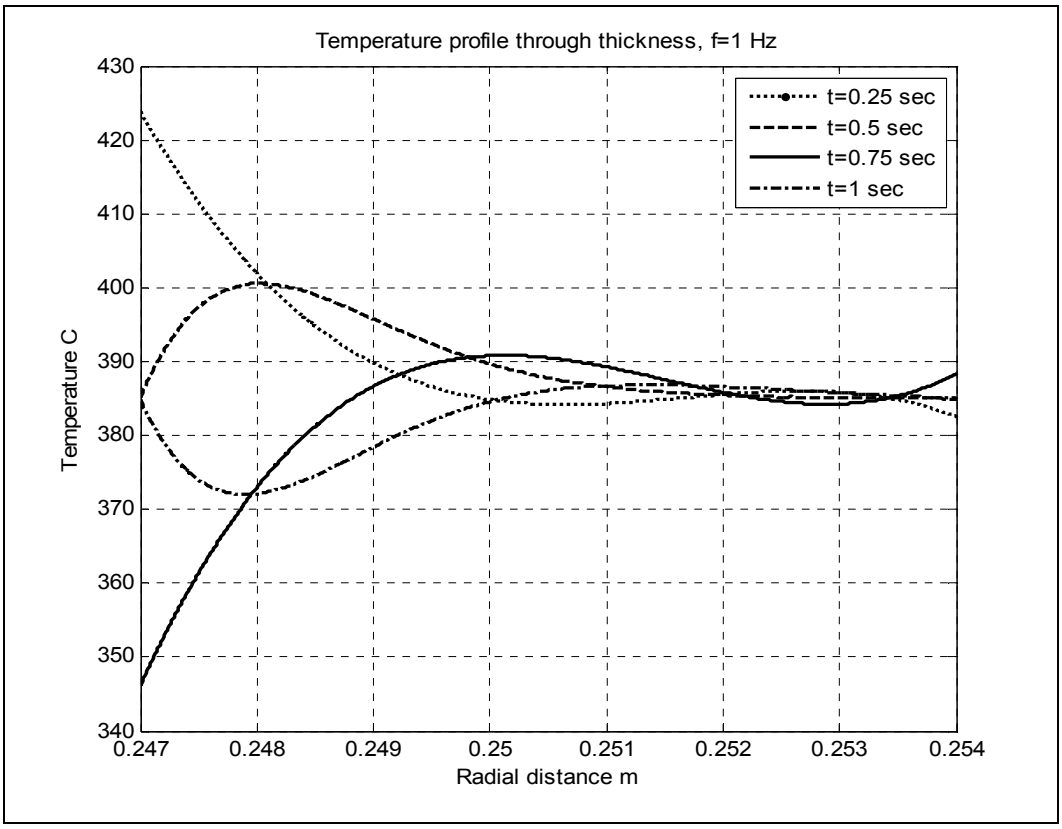

Figure 7. Temperature profile distribution through wall-thickness of hollow cylinder at various moments of time for frequency f=1 Hz

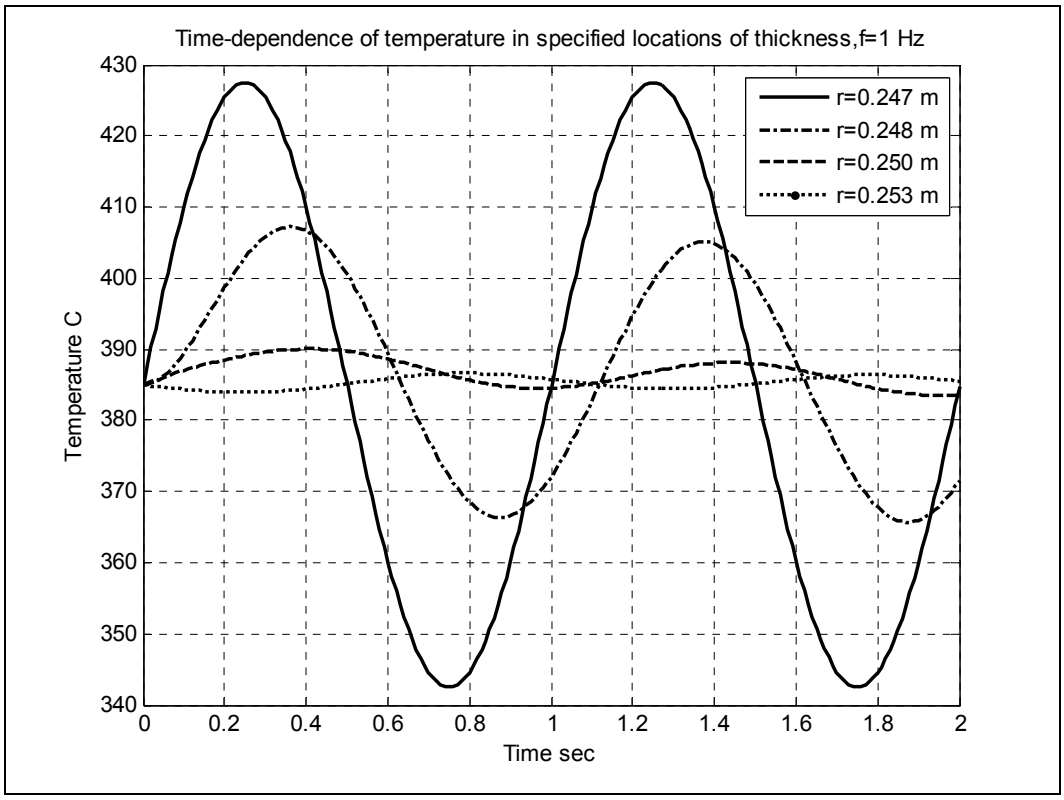

Figure 8. Time-dependence of temperature in some locations of wall-thickness for frequency f=1 Hz

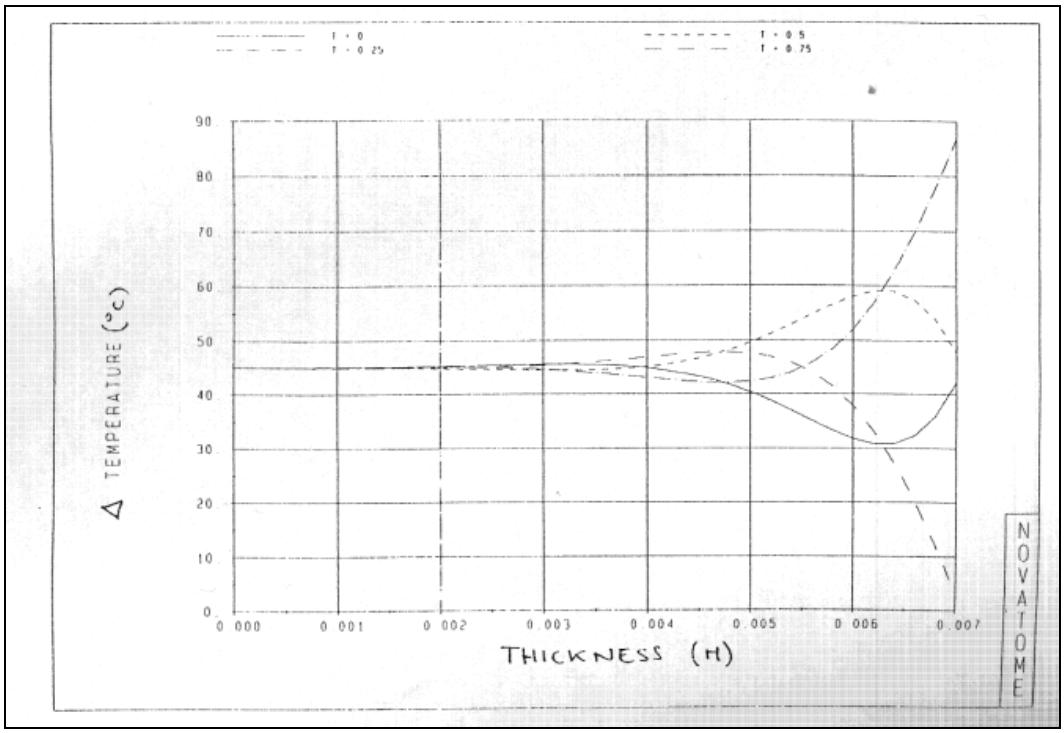

Figure 9. Framatome calculations: Temperature profile for f= 1 Hz sinusoidal signal [23]

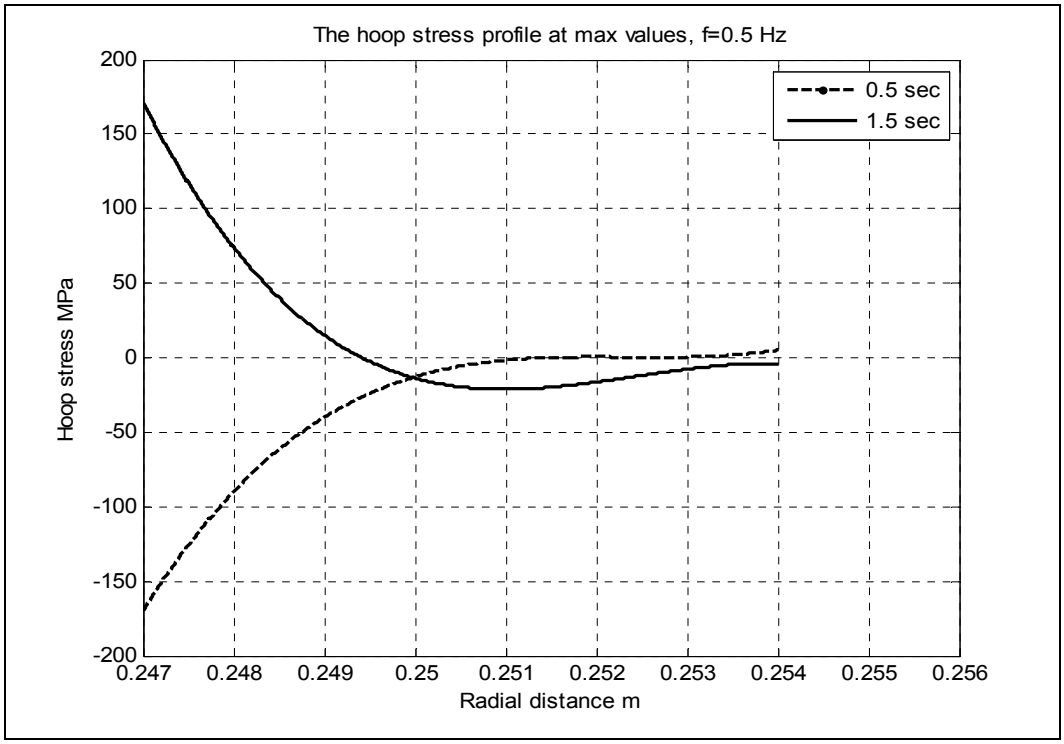

Figure 10. The hoop stress profile distributions through wall thickness of hollow cylinder for instants with extreme values, for f=0.5 Hz (σ_{comp}= -169.5 MPa, $\sigma_{tensile}$= 171.5MPa, $\Delta\sigma_{\theta\theta}$=341 MPa)

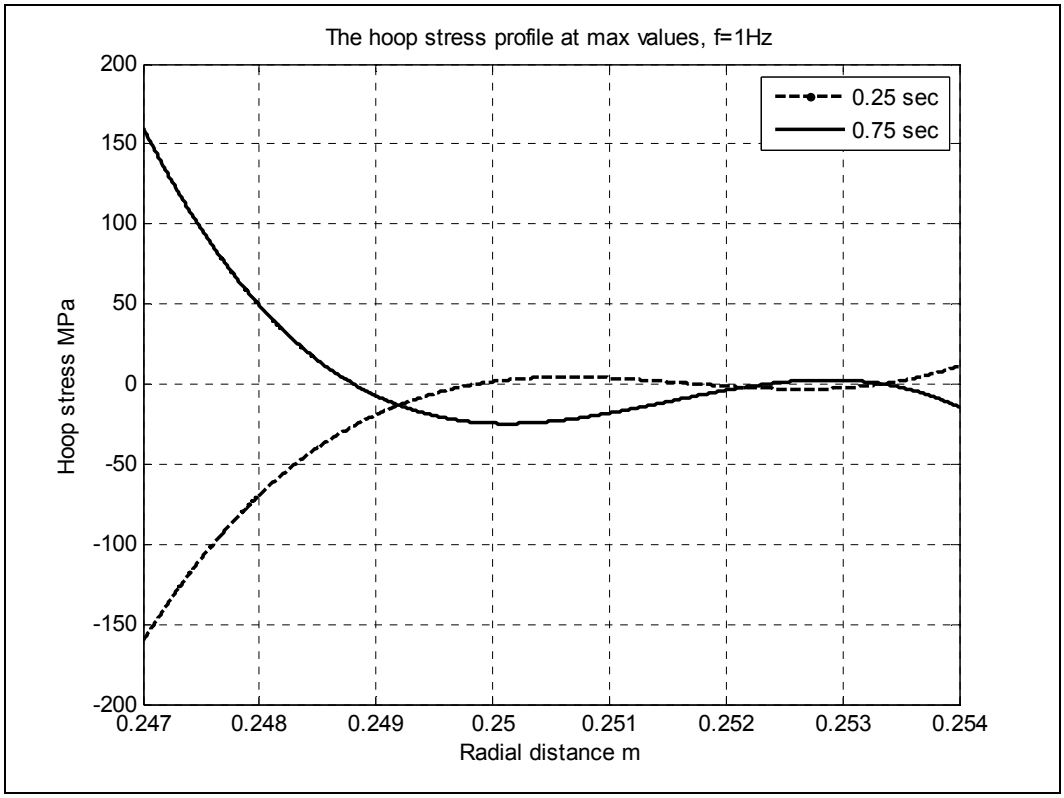

Figure 11. The hoop stress profile distribution through wall thickness of hollow cylinder for instants with extreme values, for f=1 Hz (σ_{comp}= -160 MPa, $\sigma_{tensile}$=160 MPa, $\Delta\sigma_{\theta\theta}$= 320MPa)

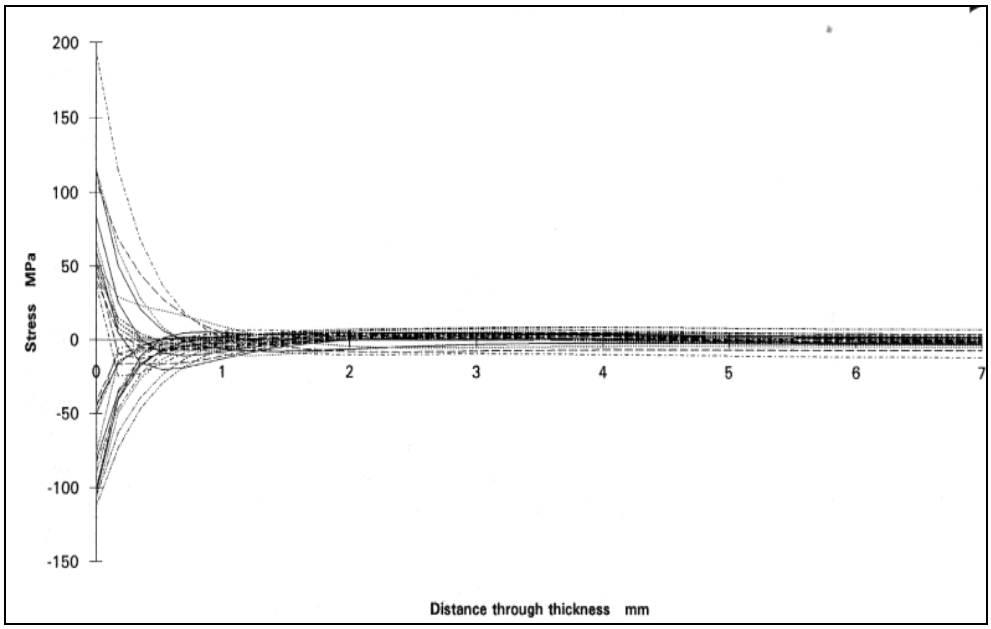

Figure 12. NNC calculations: Axial and hoop stress variation through thickness over time period 20.2 to 20.85 sec for filtered AEA data at position TC01A [23]

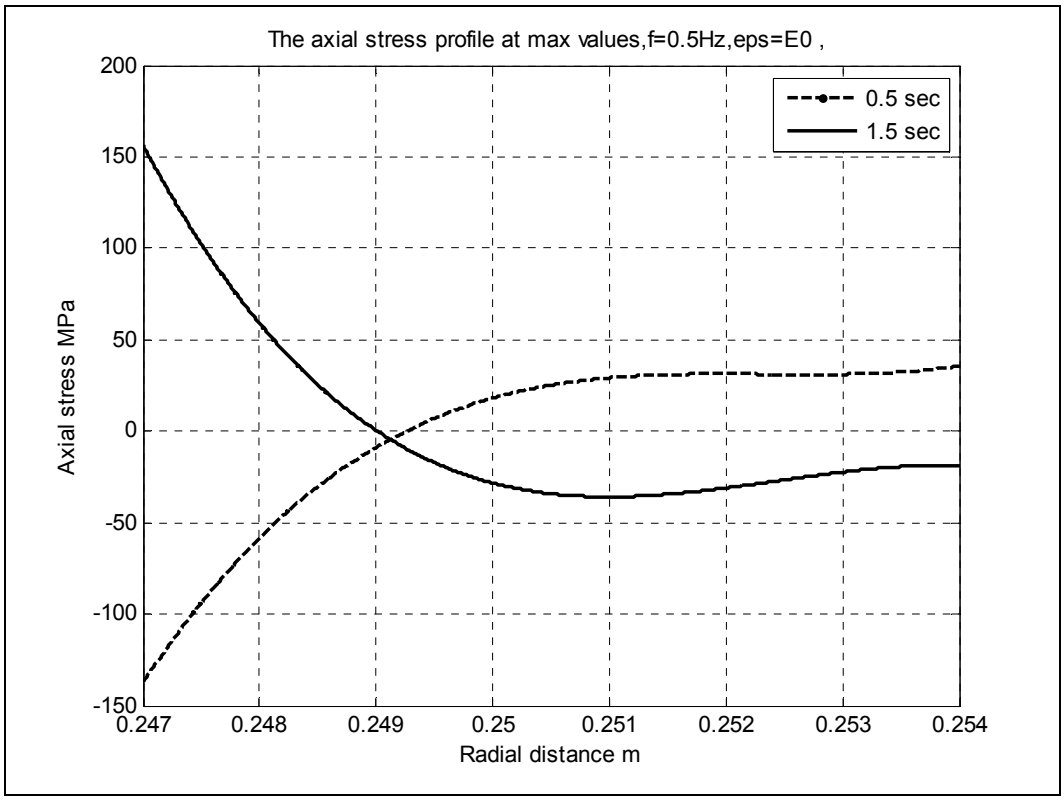

Figure 13. The axial stress profile distributions ($\varepsilon_{zz}=\varepsilon_0$) through wall thickness of hollow cylinder for instants with minimum and maximum values, for f=0.5 Hz (σ_{comp}= -137 MPa, $\sigma_{tensile}$= 156MPa , $\Delta\sigma_{zz}$ =293 MPa)

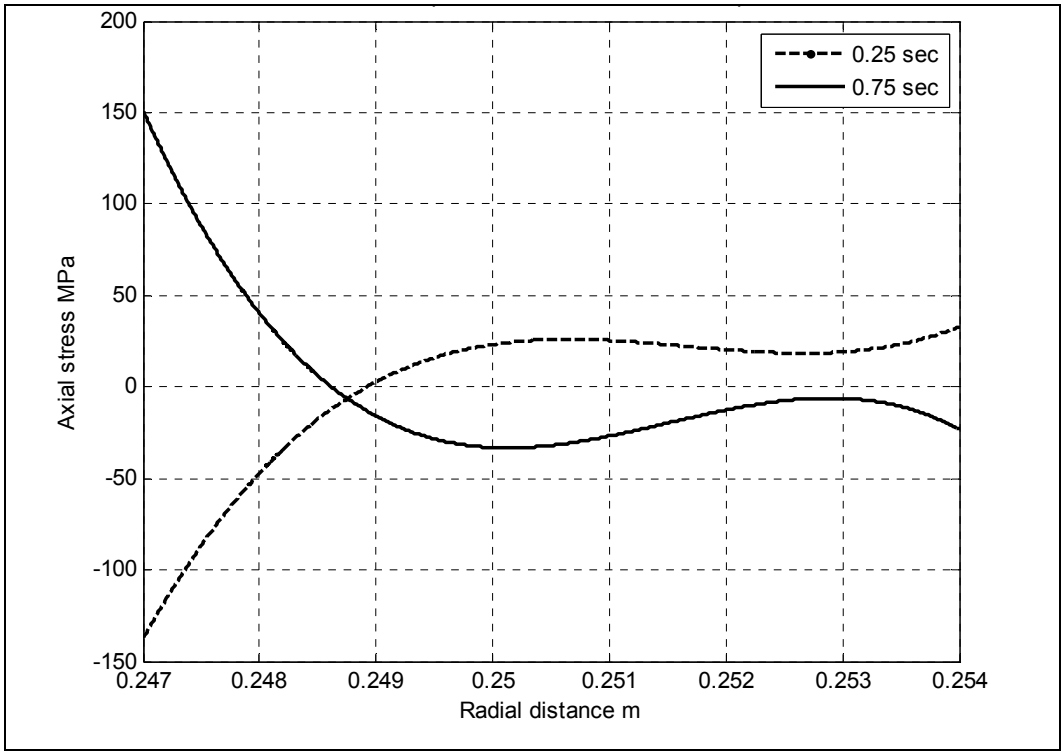

Figure 14. The axial stress profile distribution ($\varepsilon_{zz}=\varepsilon_0$) through wall thickness of hollow cylinder for instants with minimum and maximum values, for f=1 Hz (σ_{comp}= -137MPa, $\sigma_{tensile}$= 151 MPa , $\Delta\sigma_{zz}$ =288 MPa)

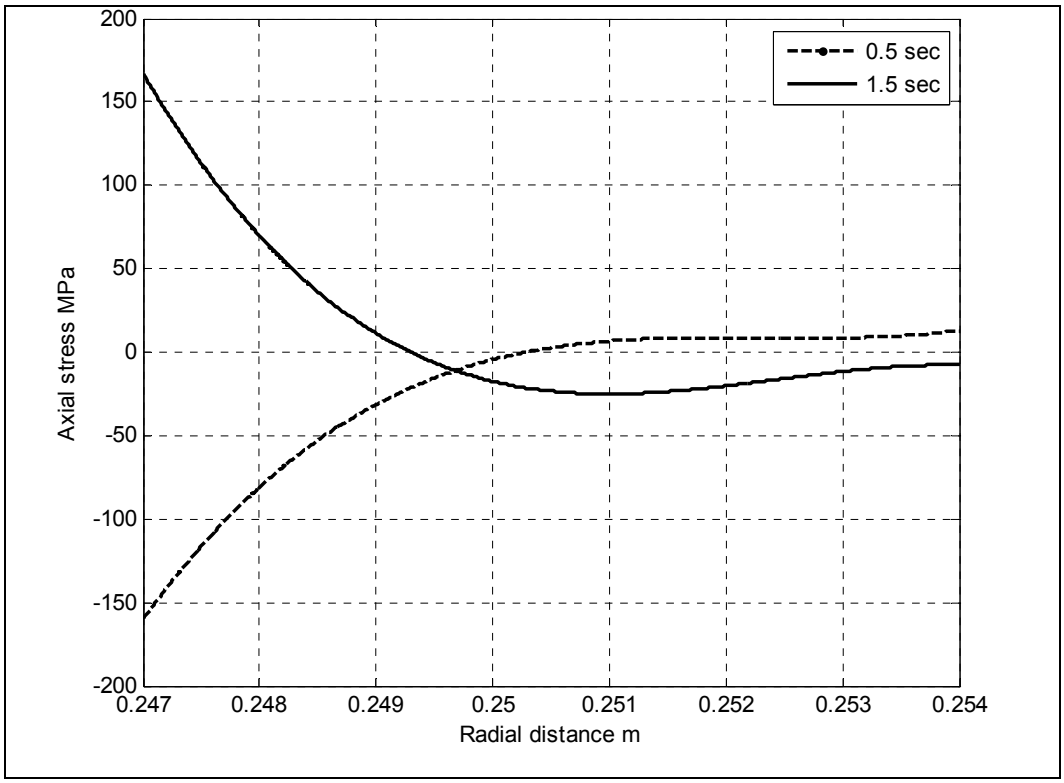

Figure 15. The axial stress profile distributions ($\varepsilon_{zz}=0$) through wall thickness of a hollow cylinder for instants with minimum and maximum values, for f=0.5 Hz (σ_{comp}= -160MPa, $\sigma_{tensile}$= 167MPa, $\Delta\sigma_{zz}$=327 MPa)

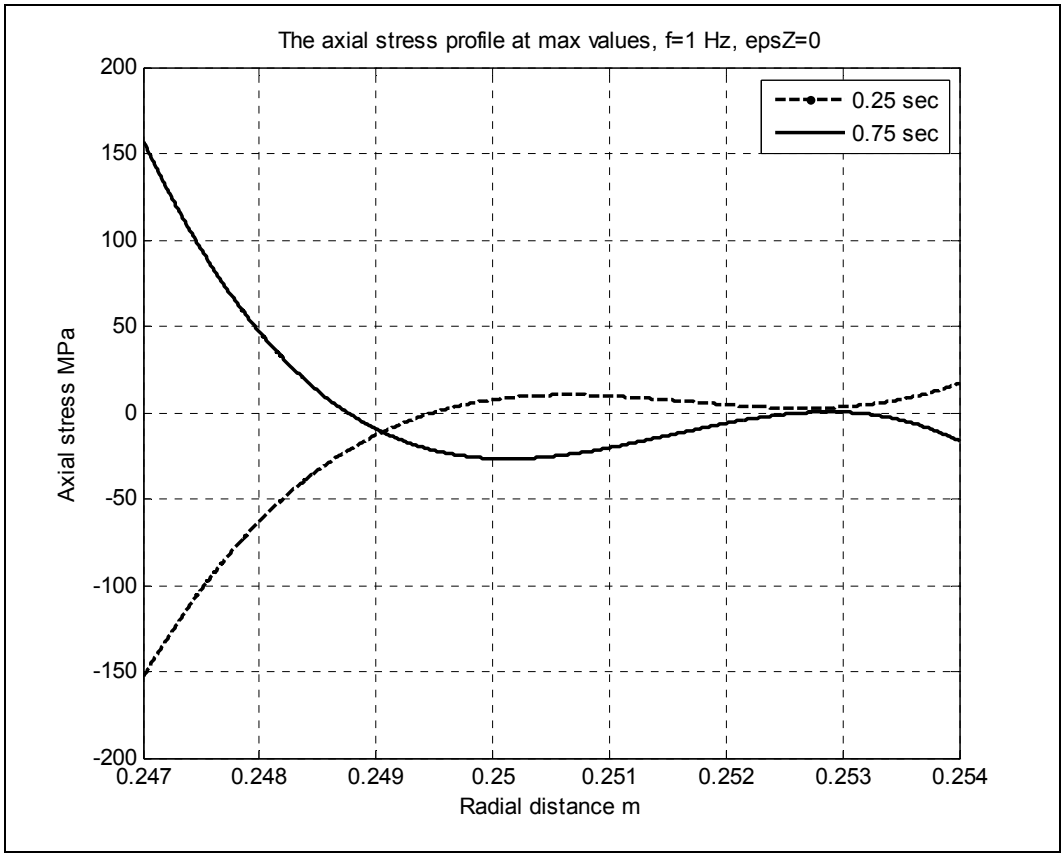

Figure 16. The axial stress profile distributions (ε_{zz}=0) through wall thickness of hollow cylinder for instants with minimum and maximum values, for f=1 Hz (σ_{comp}= -153 MPa, $\sigma_{tensile}$= 157 MPa , $\Delta\sigma_{zz}$ = 310 MPa)

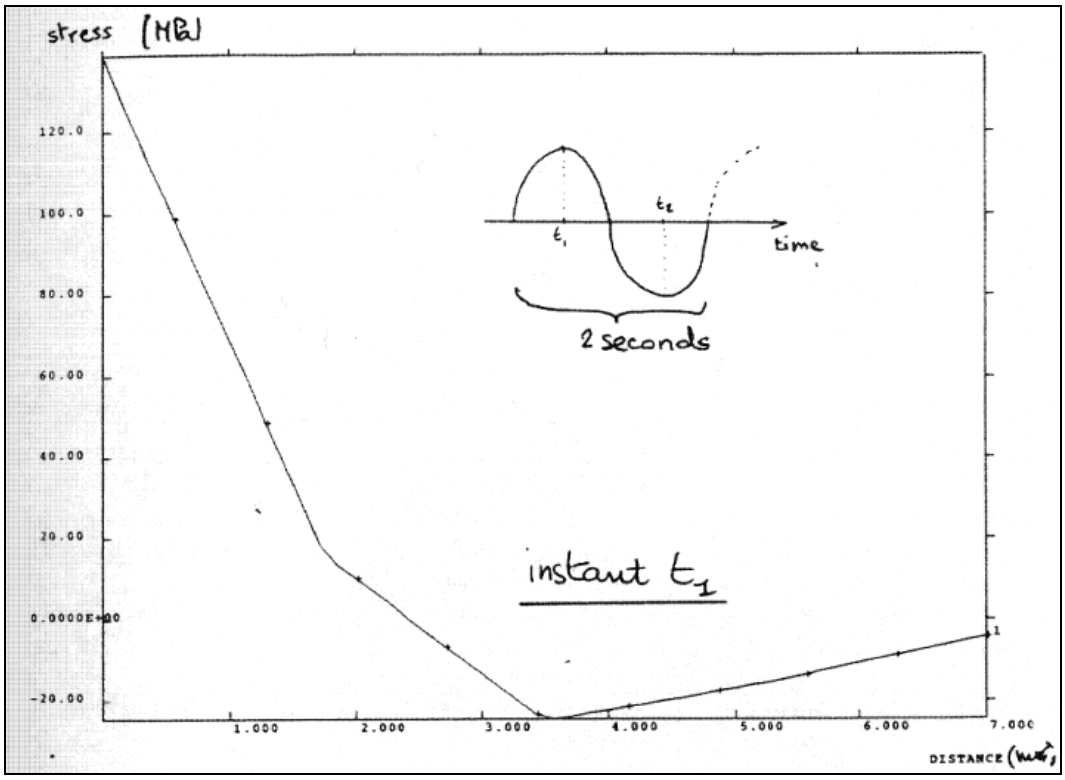

Figure 17 Framatome calculations: Axial stress profile, f=0.5 KHz sinusoidal signal (ε_{zz}=0) [23]

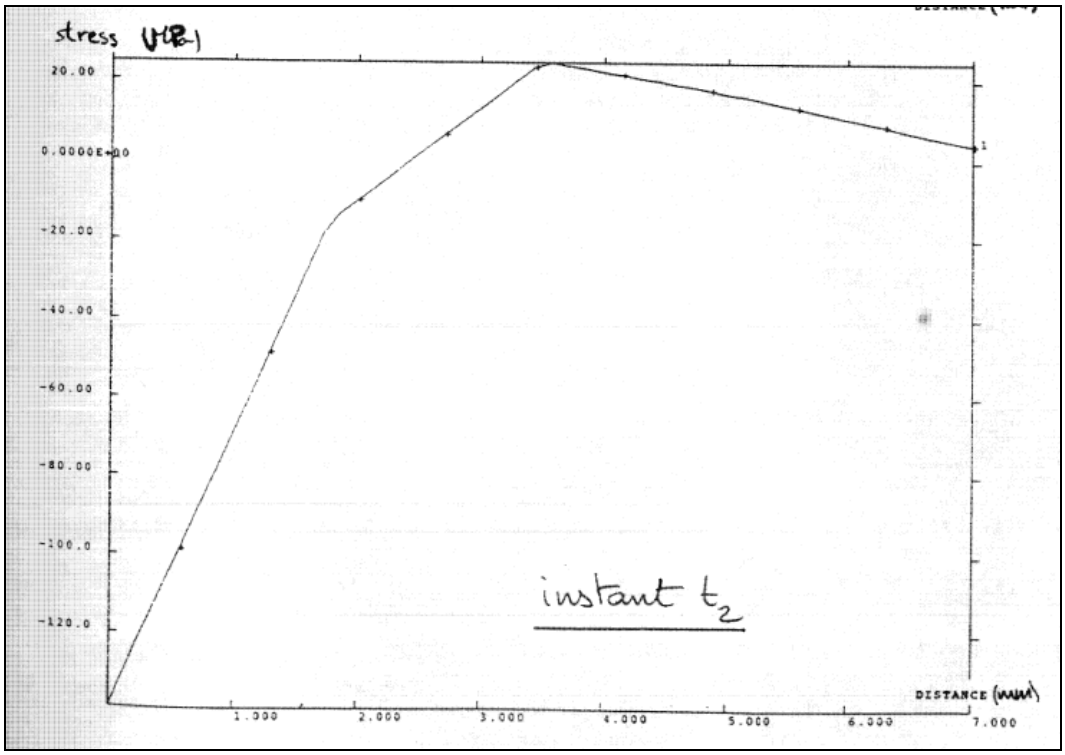

Figure 18 Framatome calculations: Axial stress profile, f=0.5 KHz sinusoidal signal (ε_{zz}=0) [23]

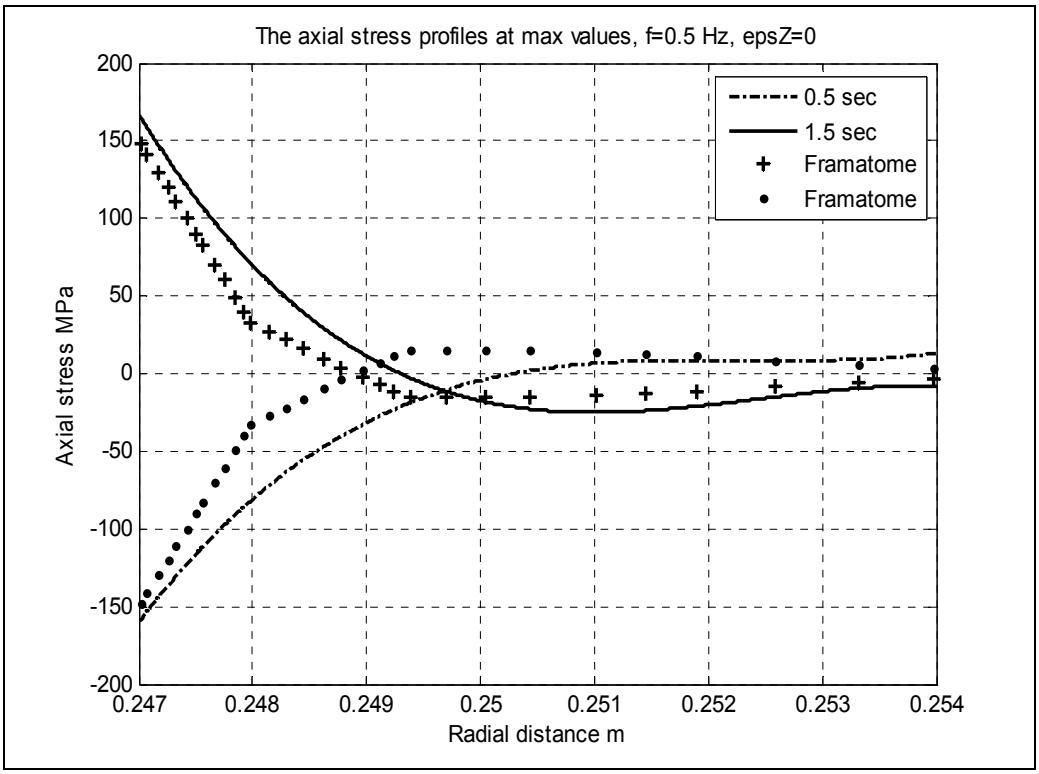

Figure 19. Comparison between predictions from present work and Framatome calculations [23] for axial stress in case f=0.5 Hz and ε_{zz}=0

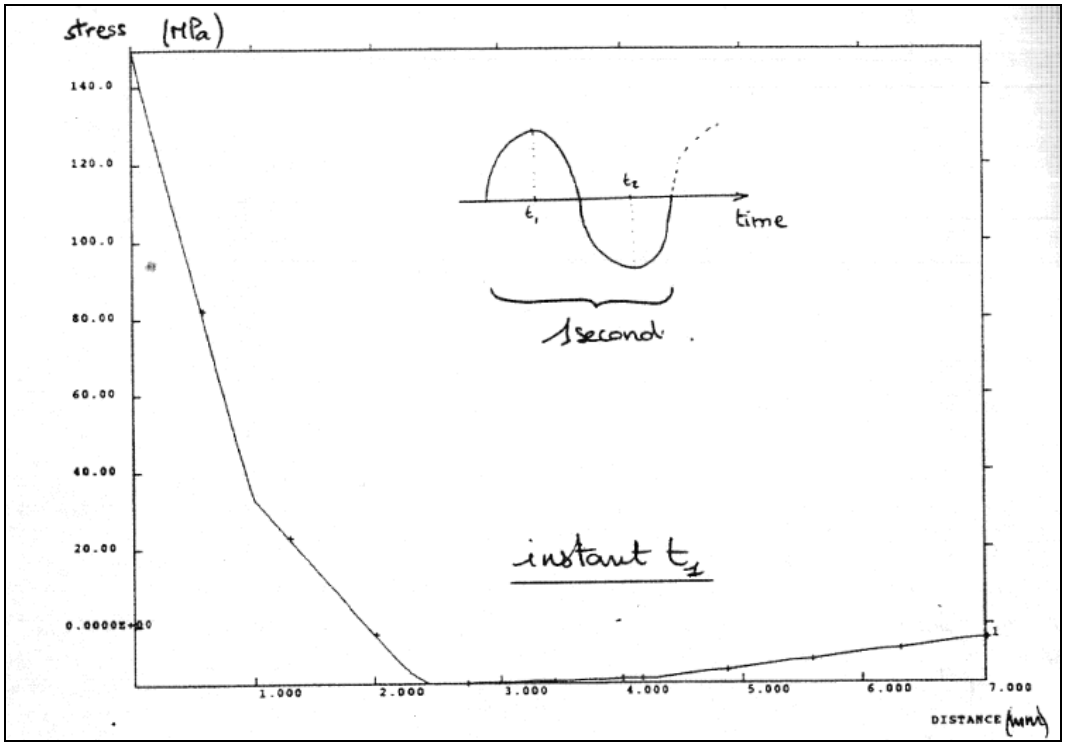

Figure 20 Framatome calculations: Axial stress profile, f=1 Hz sinusoidal signal (ε_{zz}=0) [23]

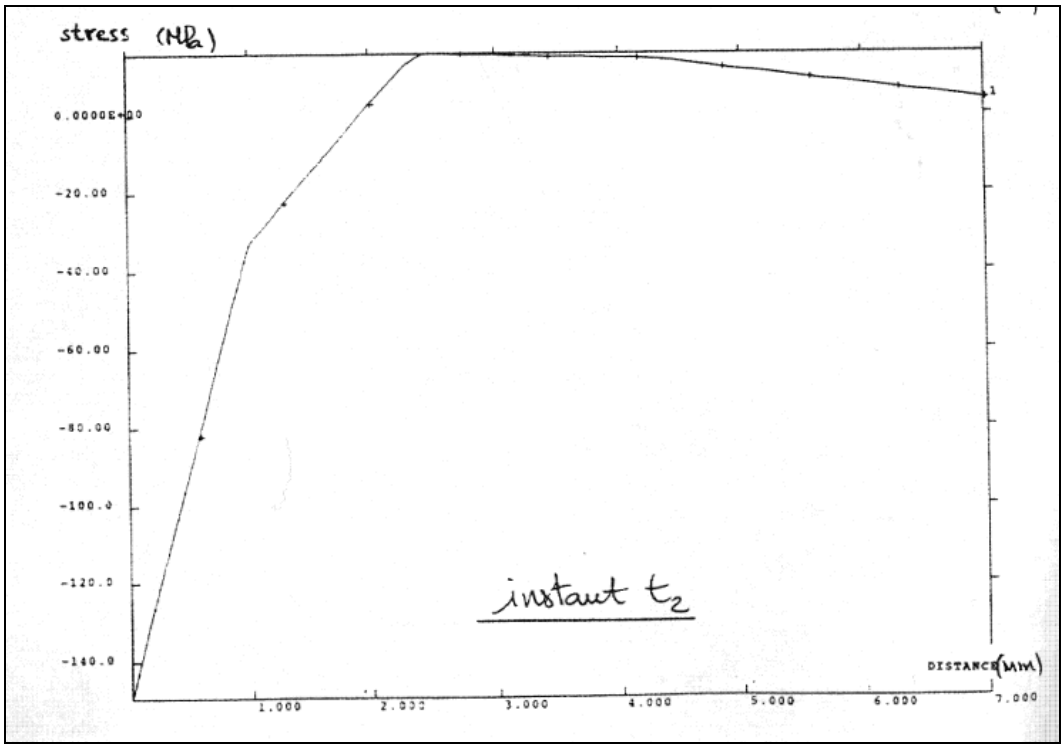

Figure 21 Framatome calculations: Axial stress profile, f=1 Hz sinusoidal signal (ε_{zz}=0)[23]

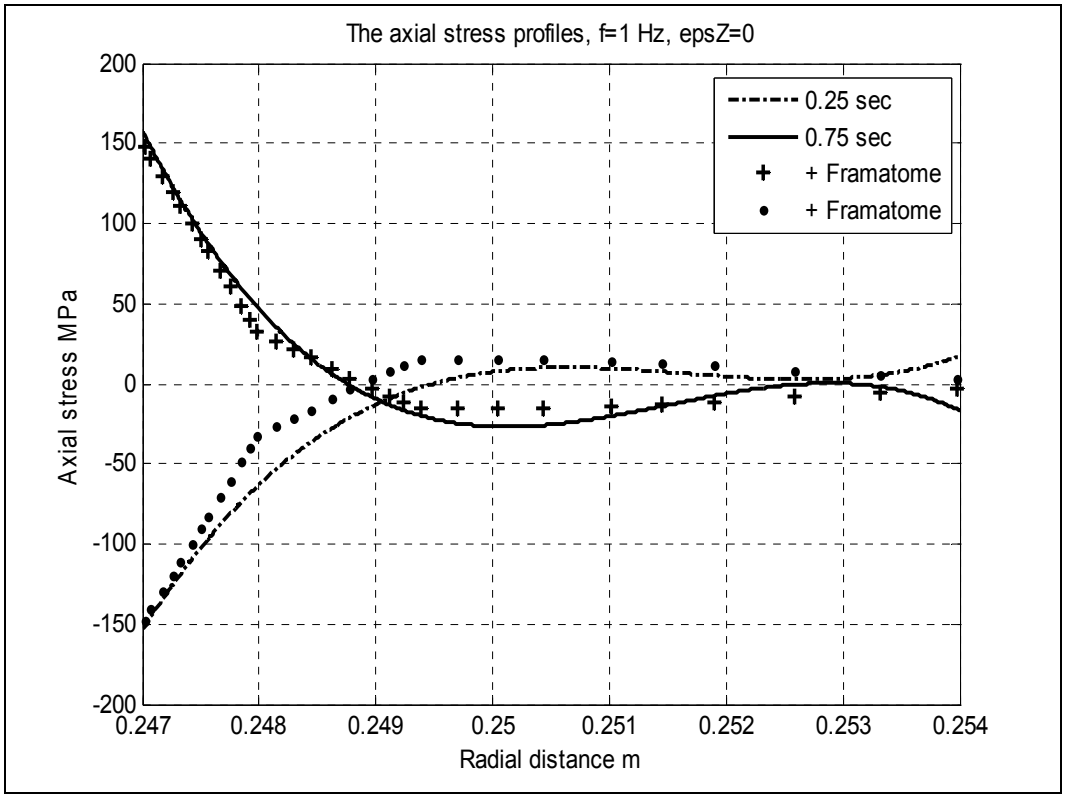

Figure 22 Comparison between predictions from present work and Framatome calculations [23] for axial stress in case f=1 Hz and ε_{zz}=0

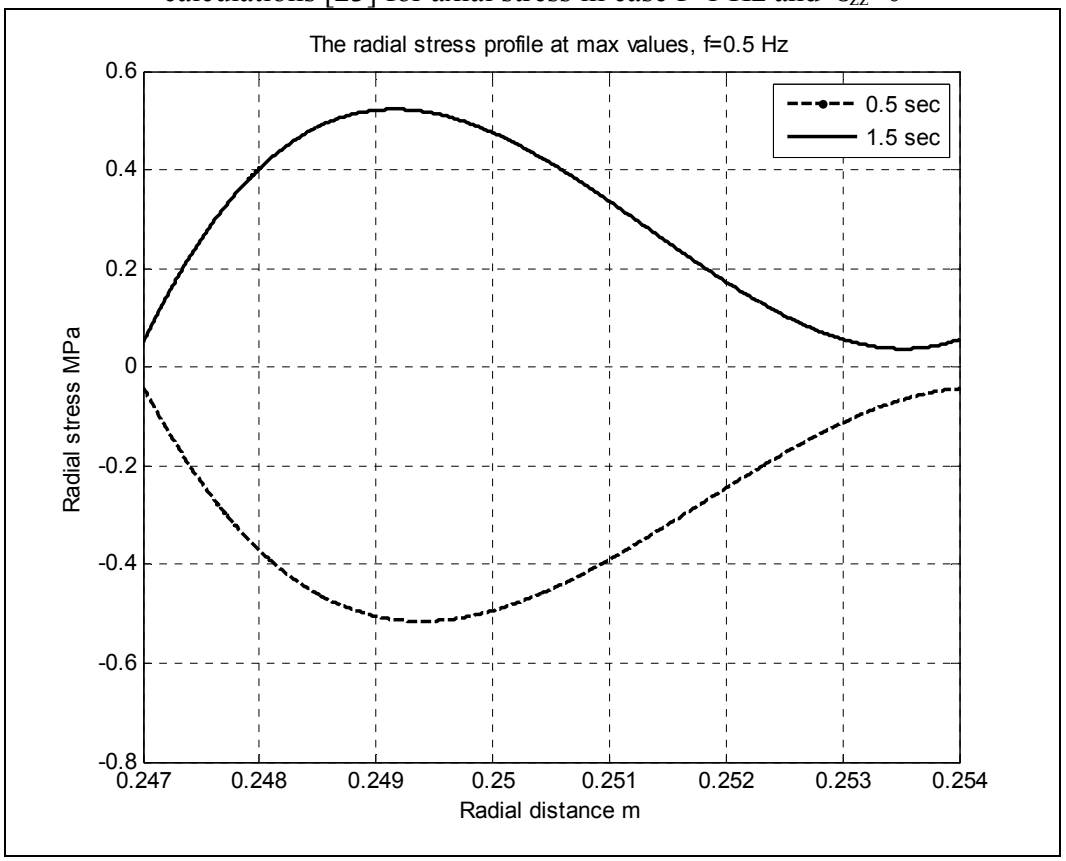

Figure 23. The radial stress profile distributions through wall thickness of hollow cylinder for instants with minimum and maximum values, for f=0.5 Hz (σ_{min}= -0.5MPa, σ_{max}= 0.5MPa, $\Delta\sigma_{rr}$=1 MPa)

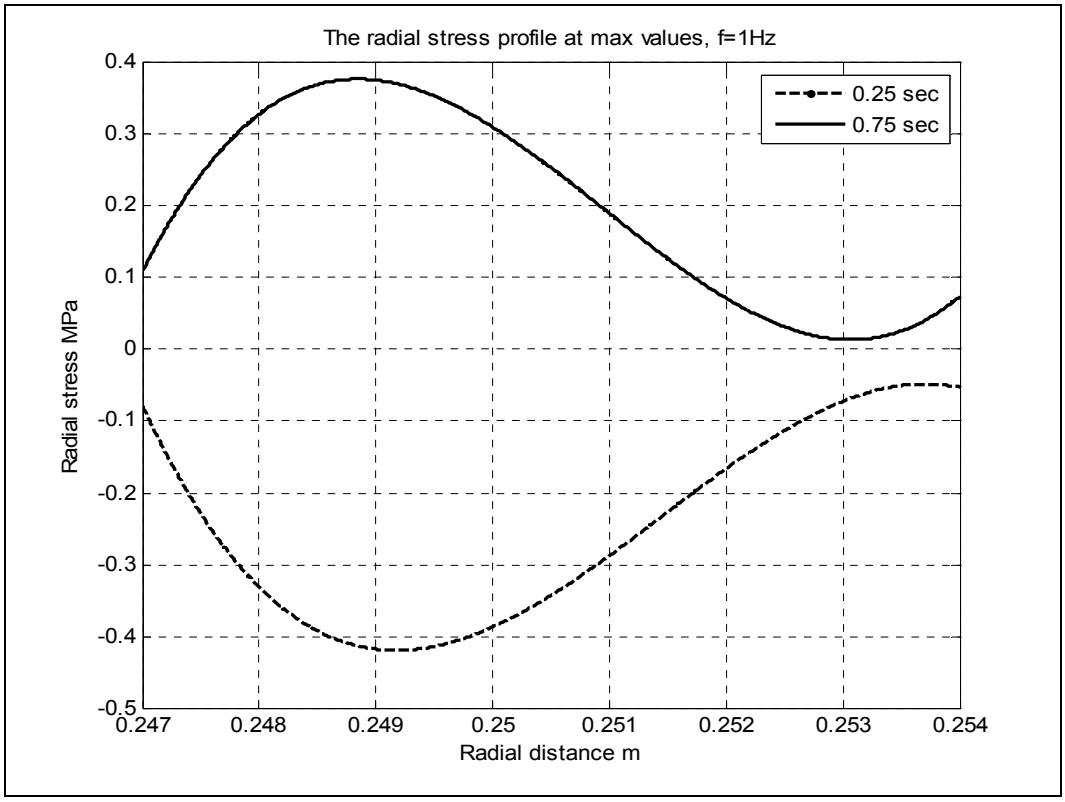

Figure 24. The radial stress profile distributions through wall thickness of hollow cylinder for instants with minimum and maximum values, for f= Hz (σ_{min}= -0.42 MPa, σ_{max}= 0.38MPa, $\Delta\sigma_{rr}$=0.8 MPa)

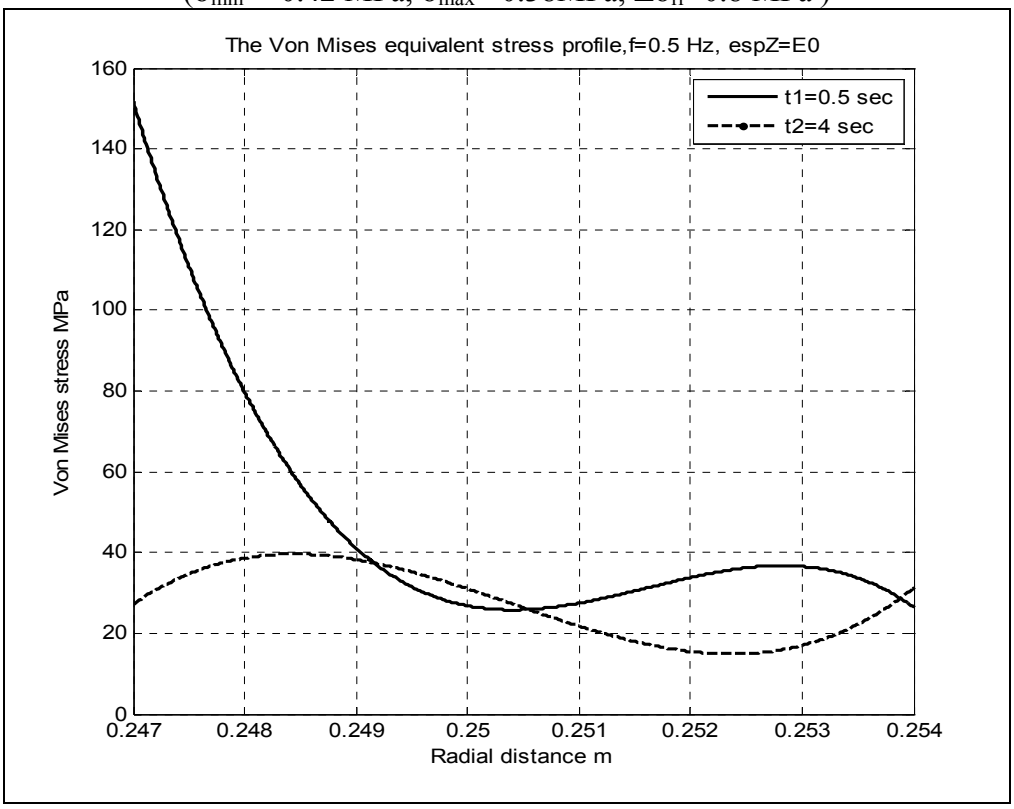

Figure 25. The Von Mises equivalent stress profile distributions (ε_{zz}= ε_0) through wall thickness of hollow cylinder for f=0.5 Hz $\sigma_{V.M.max}$= 152 MPa,)

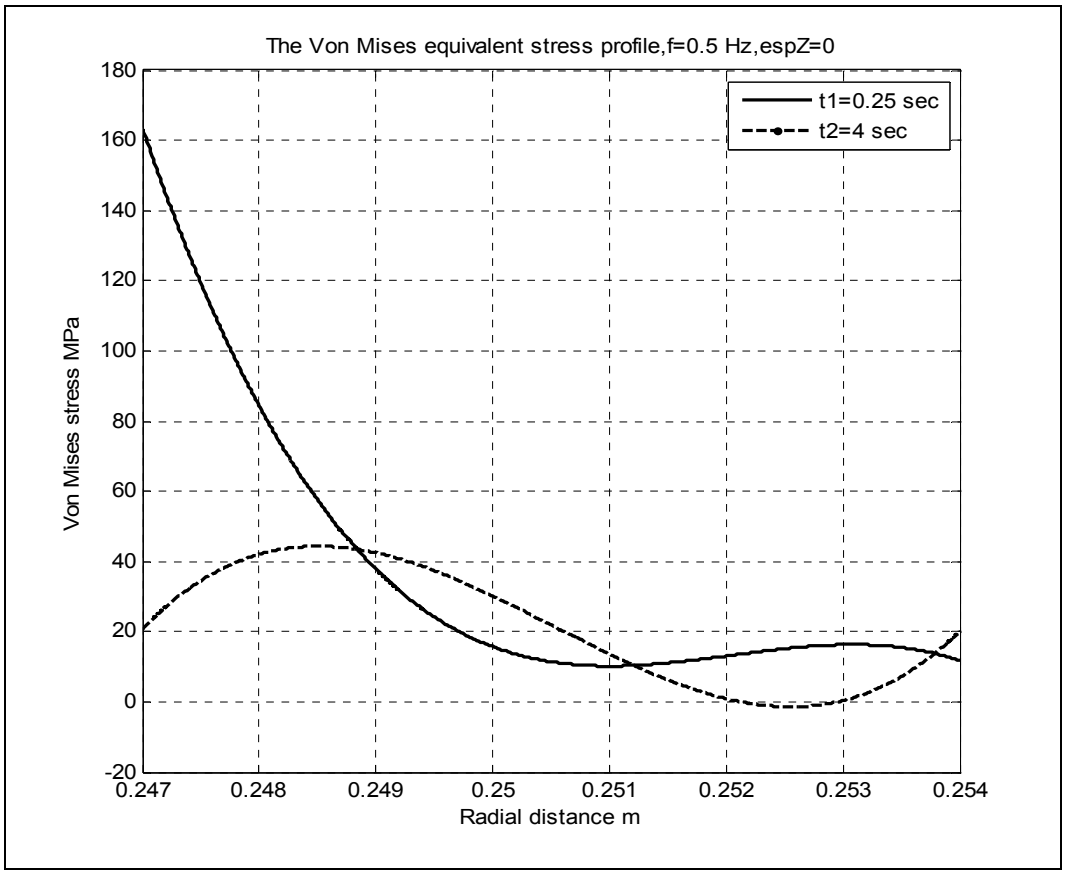

Figure 26. The Von Mises equivalent stress profile distribution (ε_{zz}= 0) through wall thickness of hollow cylinder for f=0.5 Hz, $\sigma_{V.M.max}$= 163 MPa

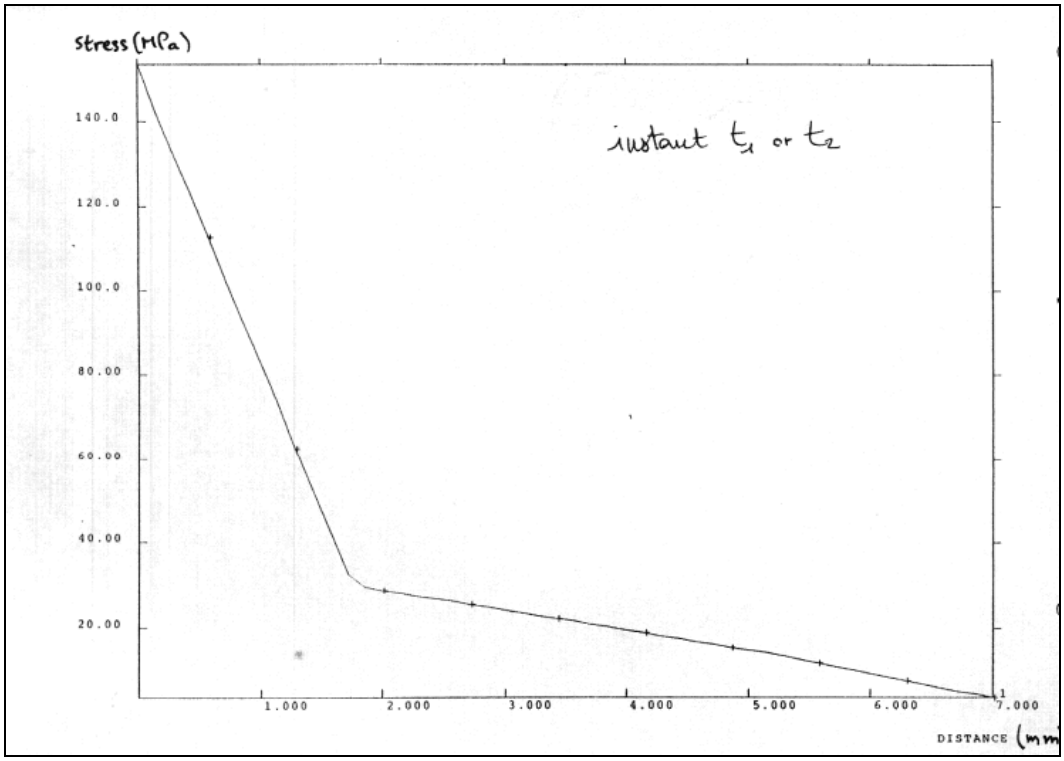

Figure 27 Framatome calculations [23]: Von Mises profile 0.5 Hz sinusoidal signal (ε_{zz}=0)

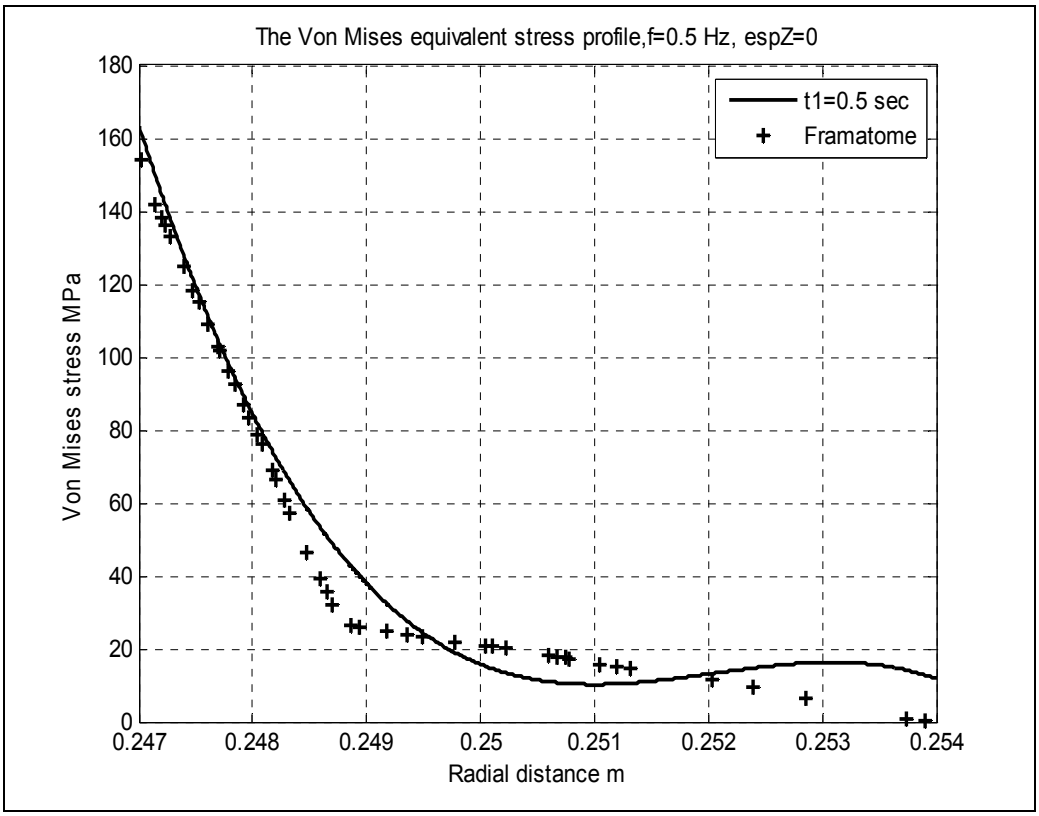

Figure 28 Comparison between predictions from present work and Framatome calculations for Von Mises equivalent stress profile, f=0.5 Hz, ε_{zz}=0

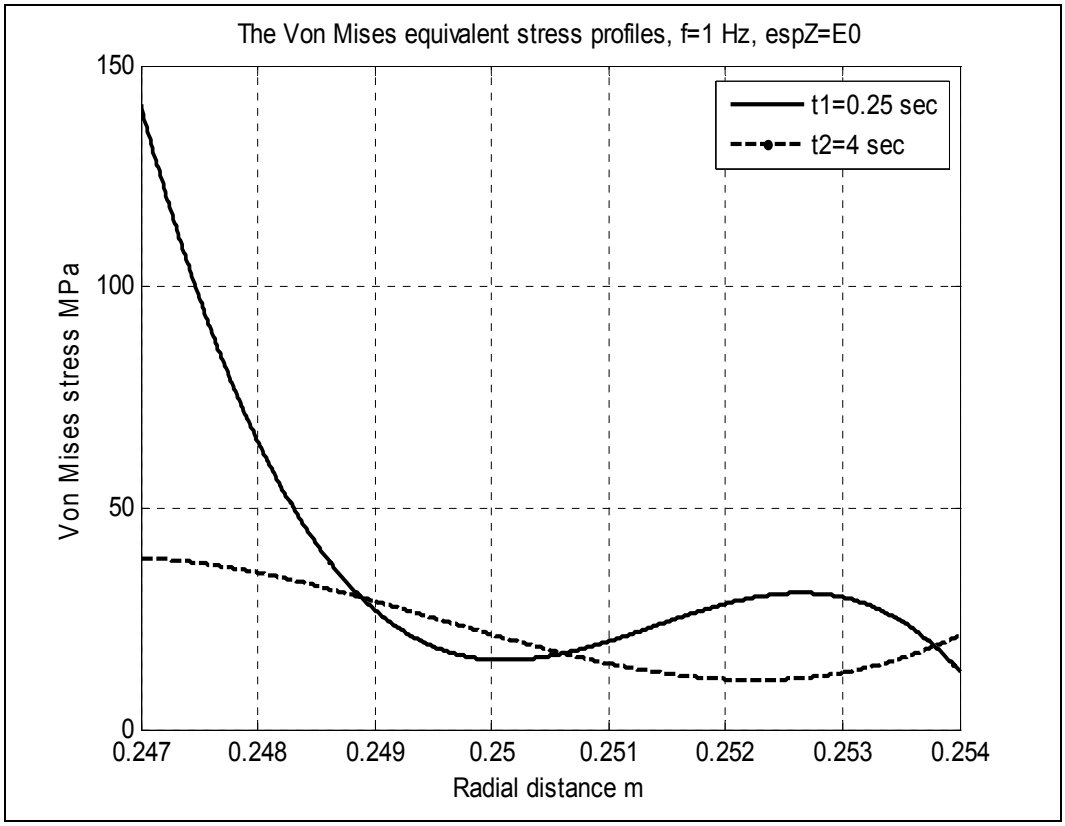

Figure 29. The Von Mises equivalent stress profiles distribution (ε_{zz}= ε_0) through wall thickness of hollow cylinder, f=1 Hz, $\sigma_{V.M.max}$= 141 MPa

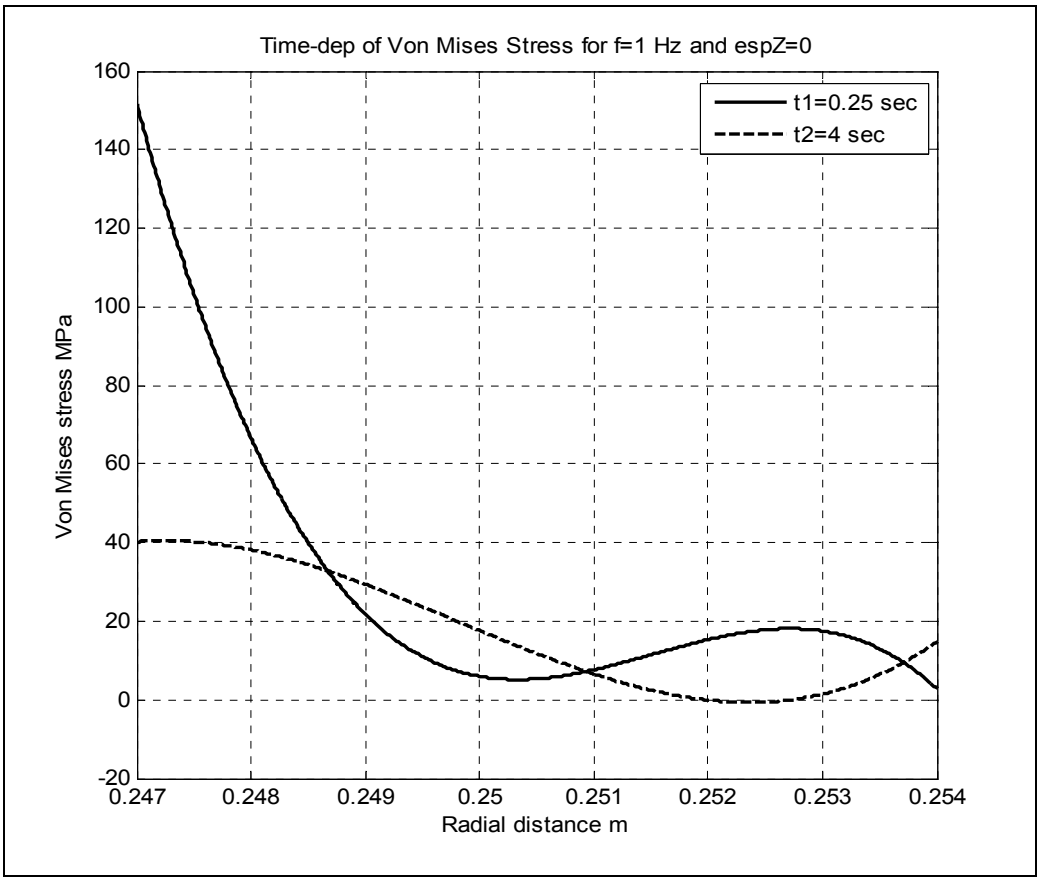

Figure 30. The Von Mises equivalent stress profiles distribution (ε_{zz}= 0) through wall thickness of hollow cylinder for f=1 Hz, $\sigma_{V.M.max}$= 152 MPa

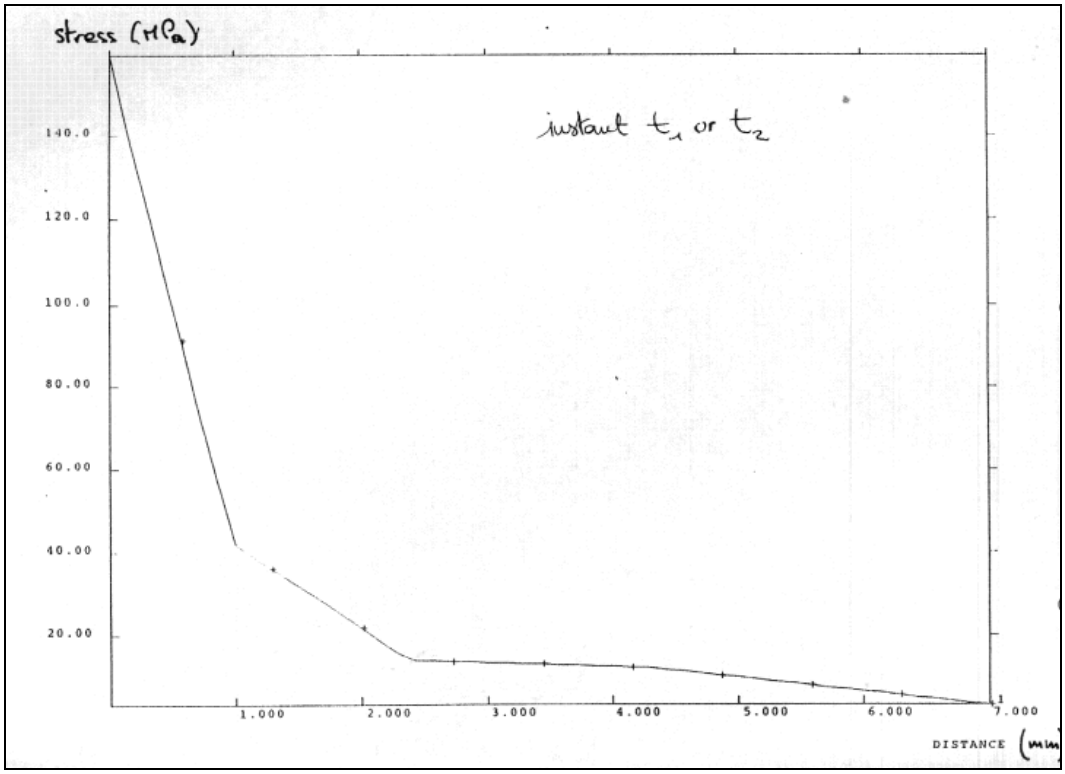

Figure 31 Framatome calculations [23]: Von Mises profile 1 Hz sinusoidal signal (ε_{zz}=0)

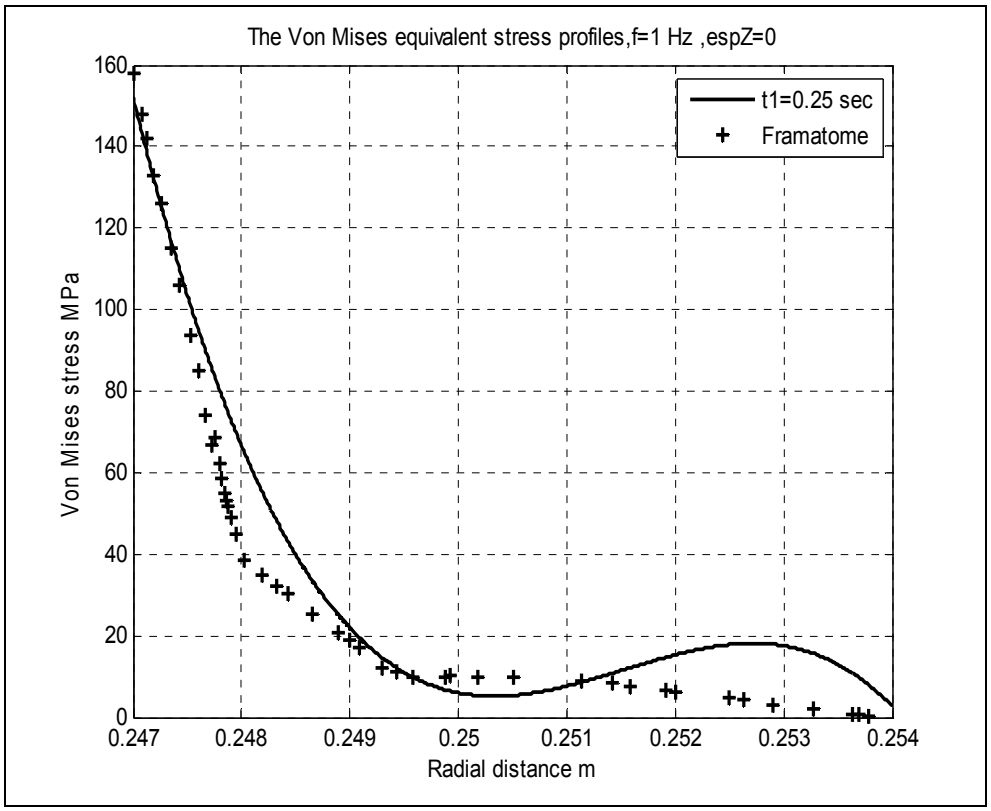

Figure 32. Comparison between profile predictions from present work and Framatome calculations [23] for Von Mises equivalent stress, f=1 Hz, ε_{zz}=0

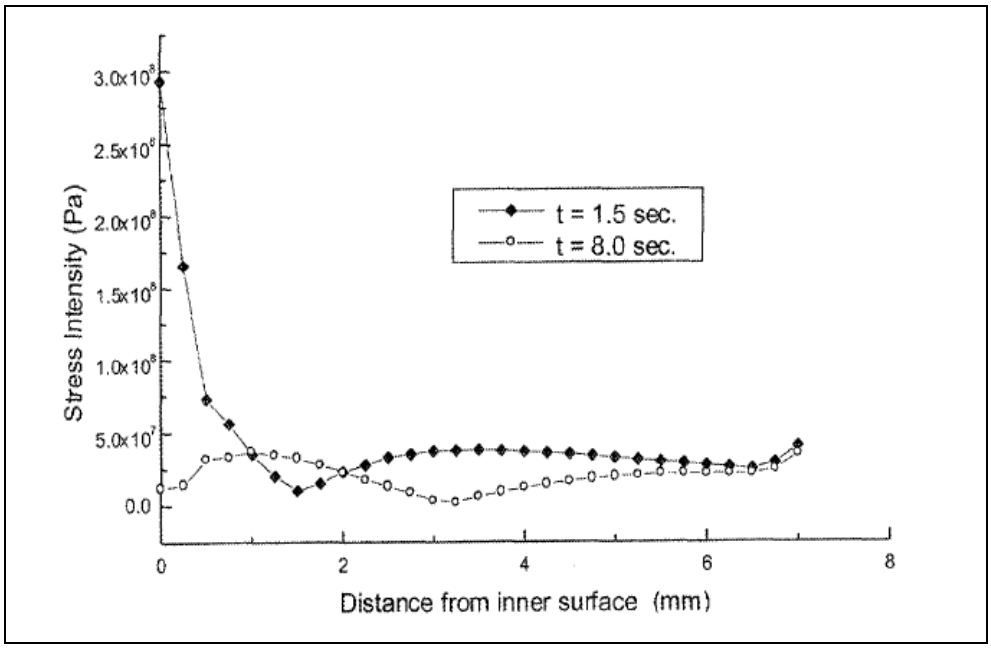

Figure 33 Stress intensity profile (Tresca) along thickness=0.5 Hz [16]

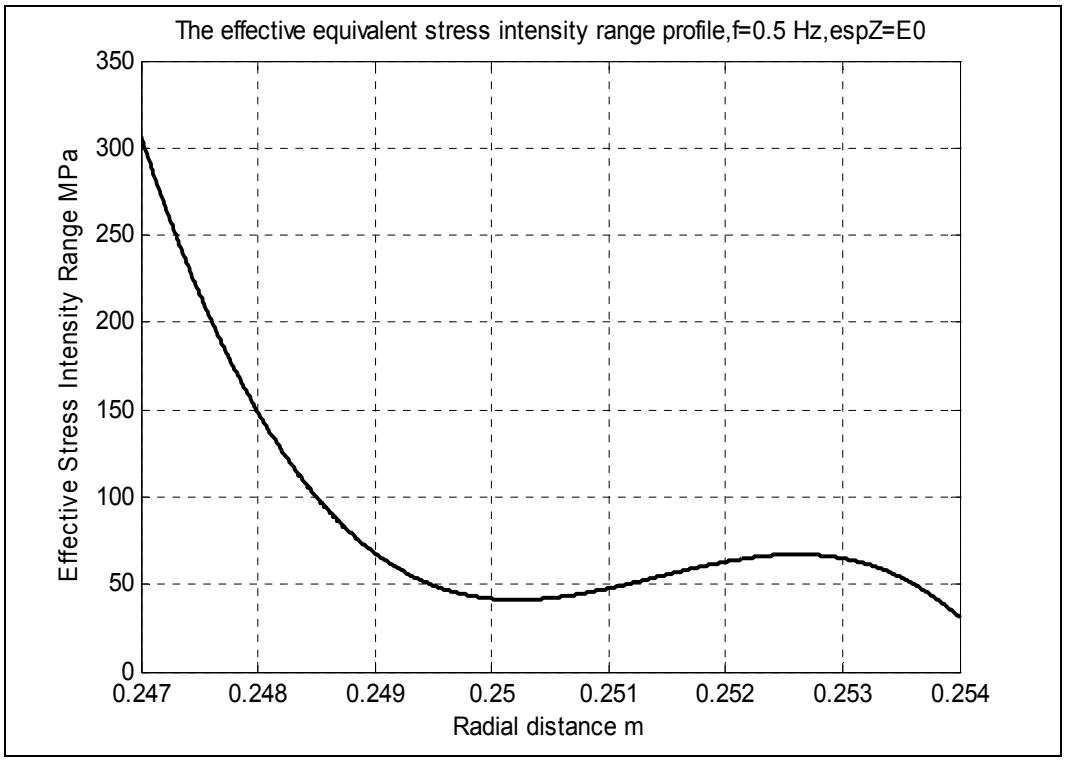

Figure 34. The effective equivalent stress intensity range profile distribution ($\varepsilon_{zz}= \varepsilon_0$) through wall thickness of hollow cylinder for f=0.5 Hz, $\Delta S_{range.max}=$ 307 MPa

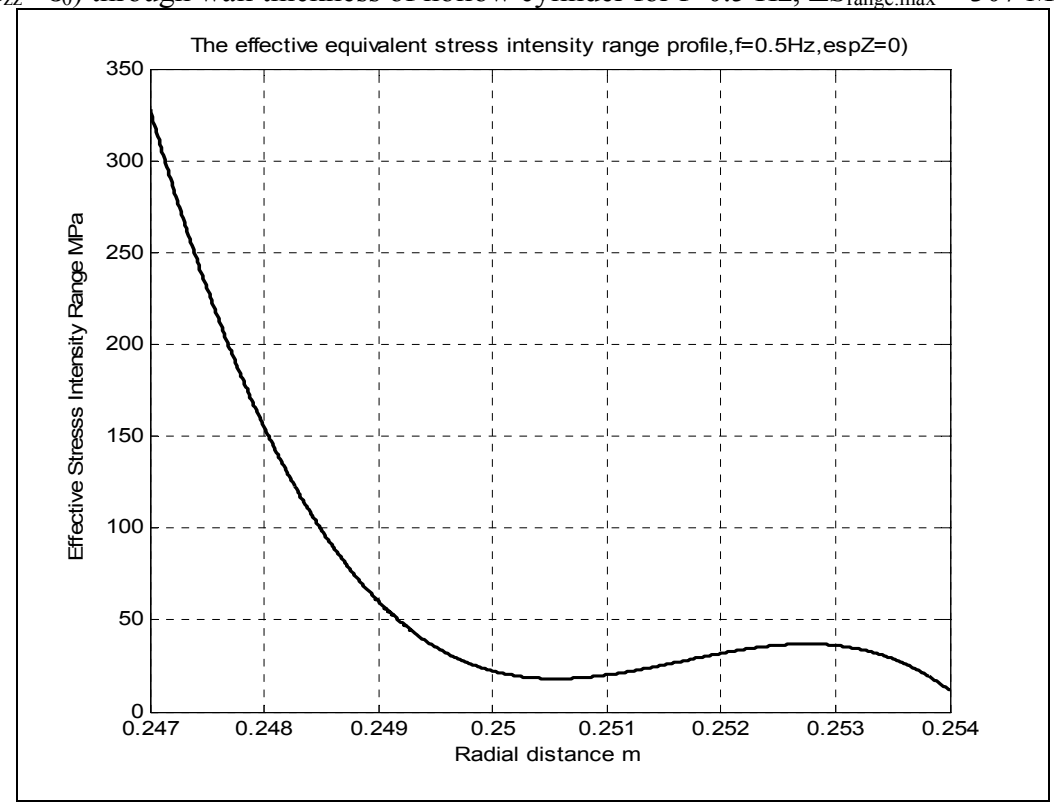

Figure 35. The effective equivalent stress intensity range profile distribution ($\varepsilon_{zz}=0$) through wall thickness of hollow cylinder for f=0.5 Hz, $\Delta S_{range.max}=$ 328 MPa

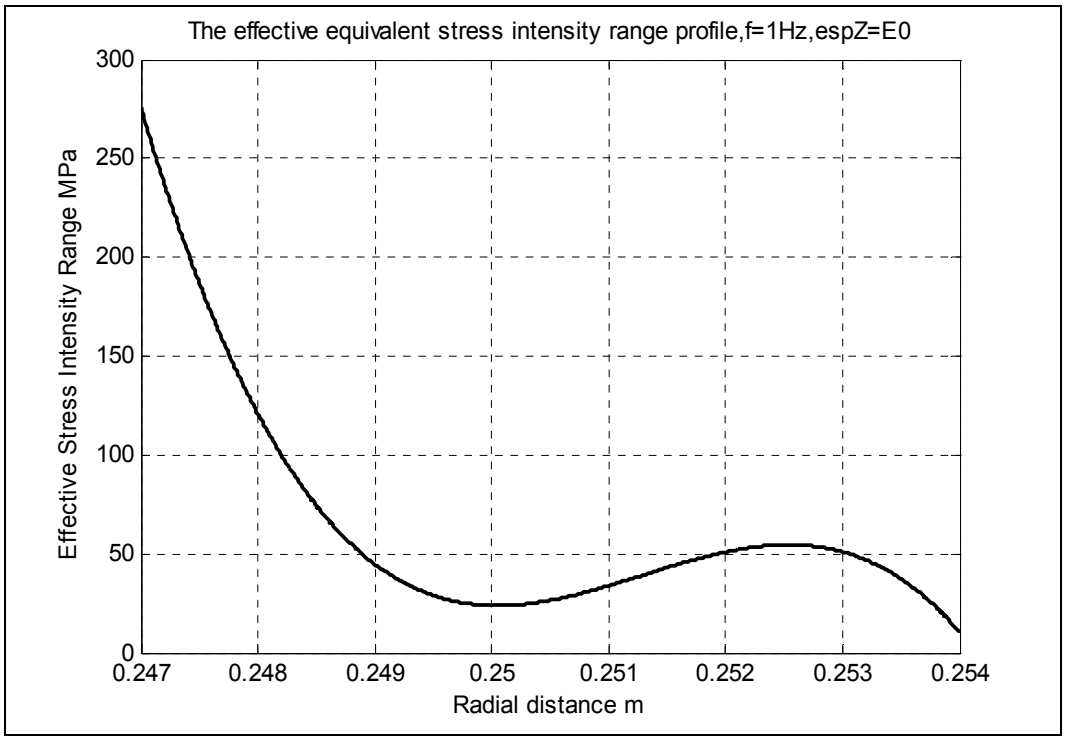

Figure 36. The effective equivalent stress intensity range profile distribution ($\varepsilon_{zz}= \varepsilon_0$) through wall thickness of hollow cylinder for f=1 Hz, $\Delta S_{range.max}=$ 275.7 MPa

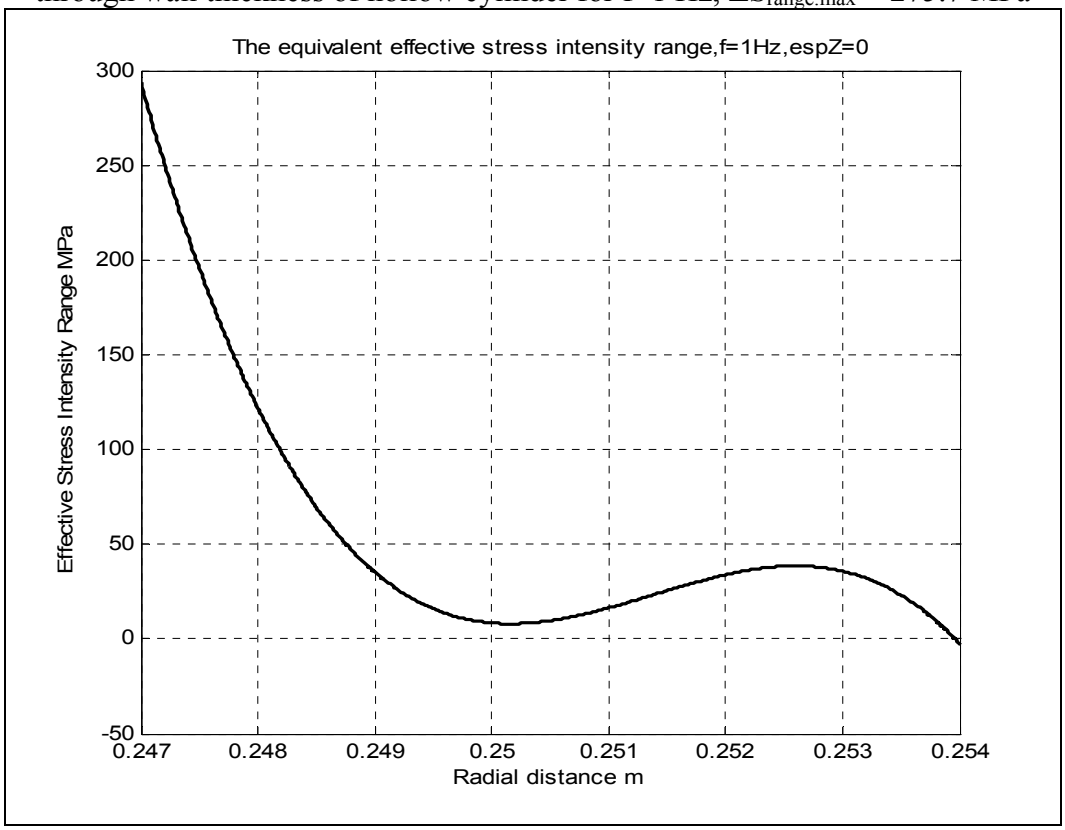

Figure 37. The effective stress intensity range stress profile distribution ($\varepsilon_{zz}= 0$) through wall thickness of hollow cylinder for f=1 Hz, $\Delta S_{range.max}=$ 293.4 MPa

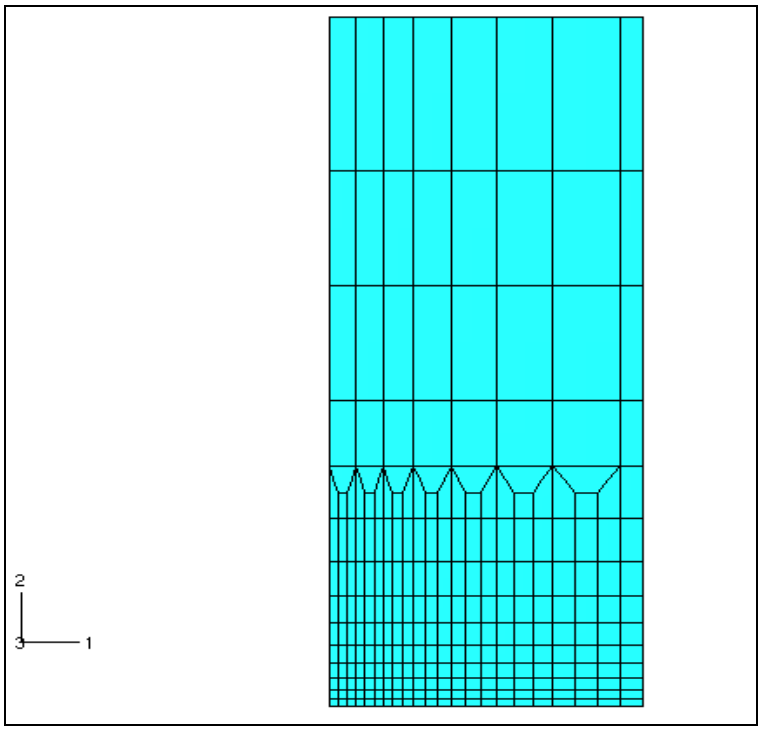

a)

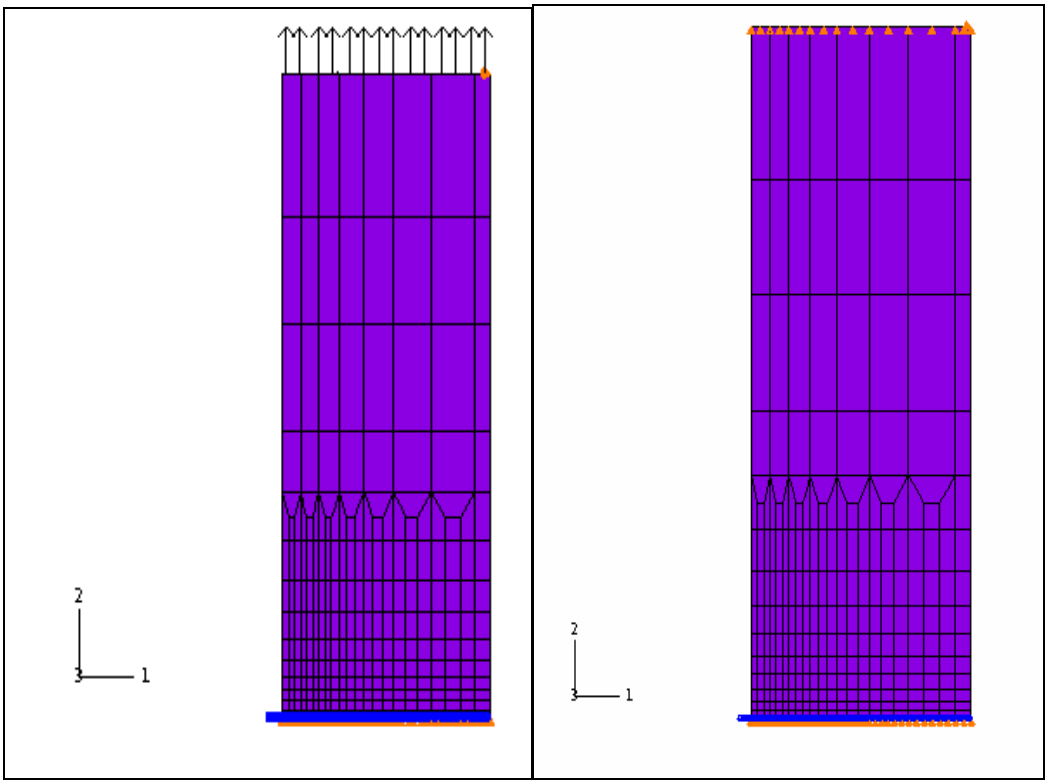

b) c)

Figure 38. a) Abaqus model mesh; b) sample free to expand in the vertical direction ($\varepsilon_{zz}= \varepsilon_0$); c) sample fixed in the vertical direction ($\varepsilon_{zz}= 0$).

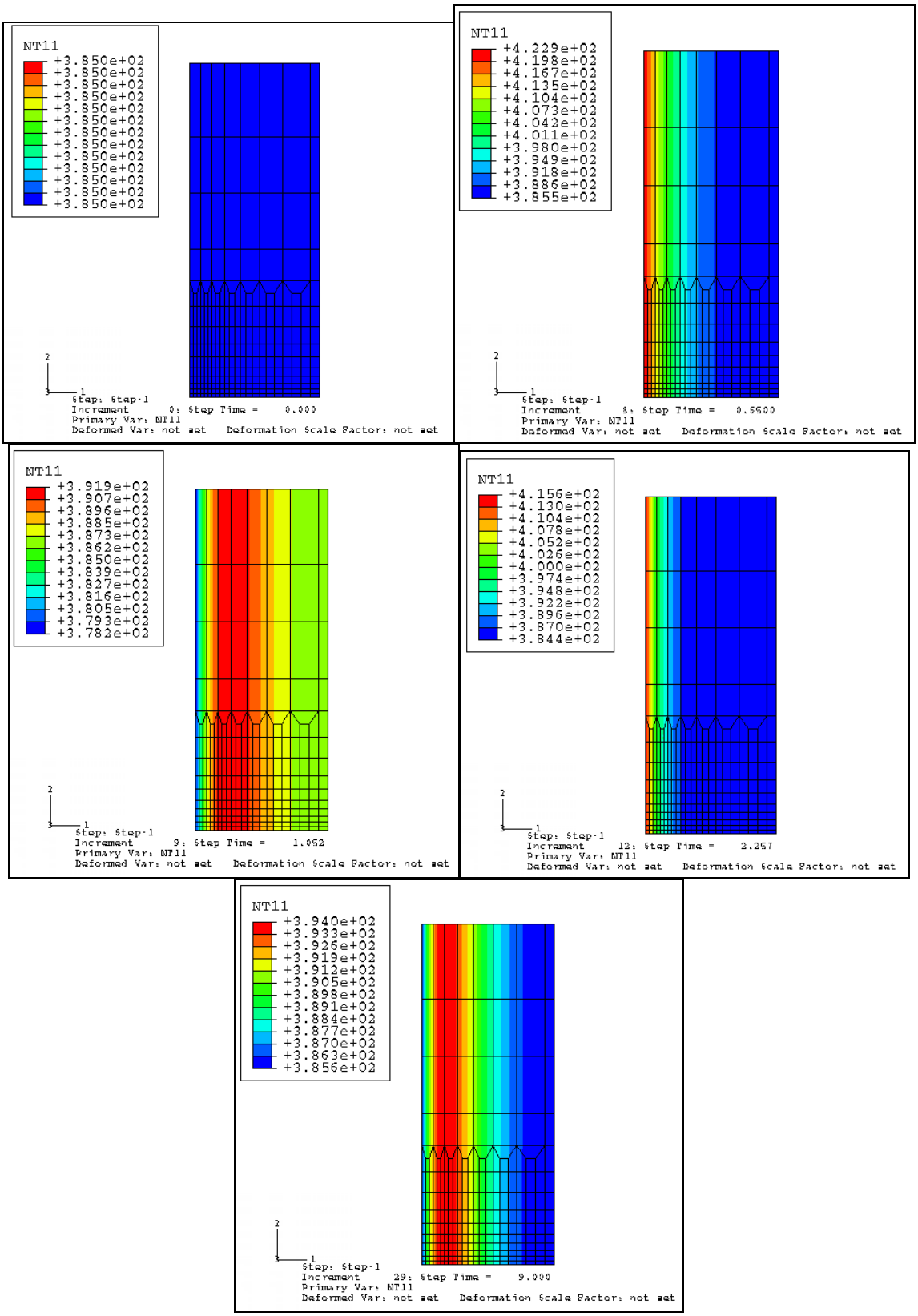

Figure 39. Evolution of the temperature across the wall thickness for v=0.5Hz (t=0 sec; 0.55 sec; 1.052 sec; 2.257 sec; 9 sec).

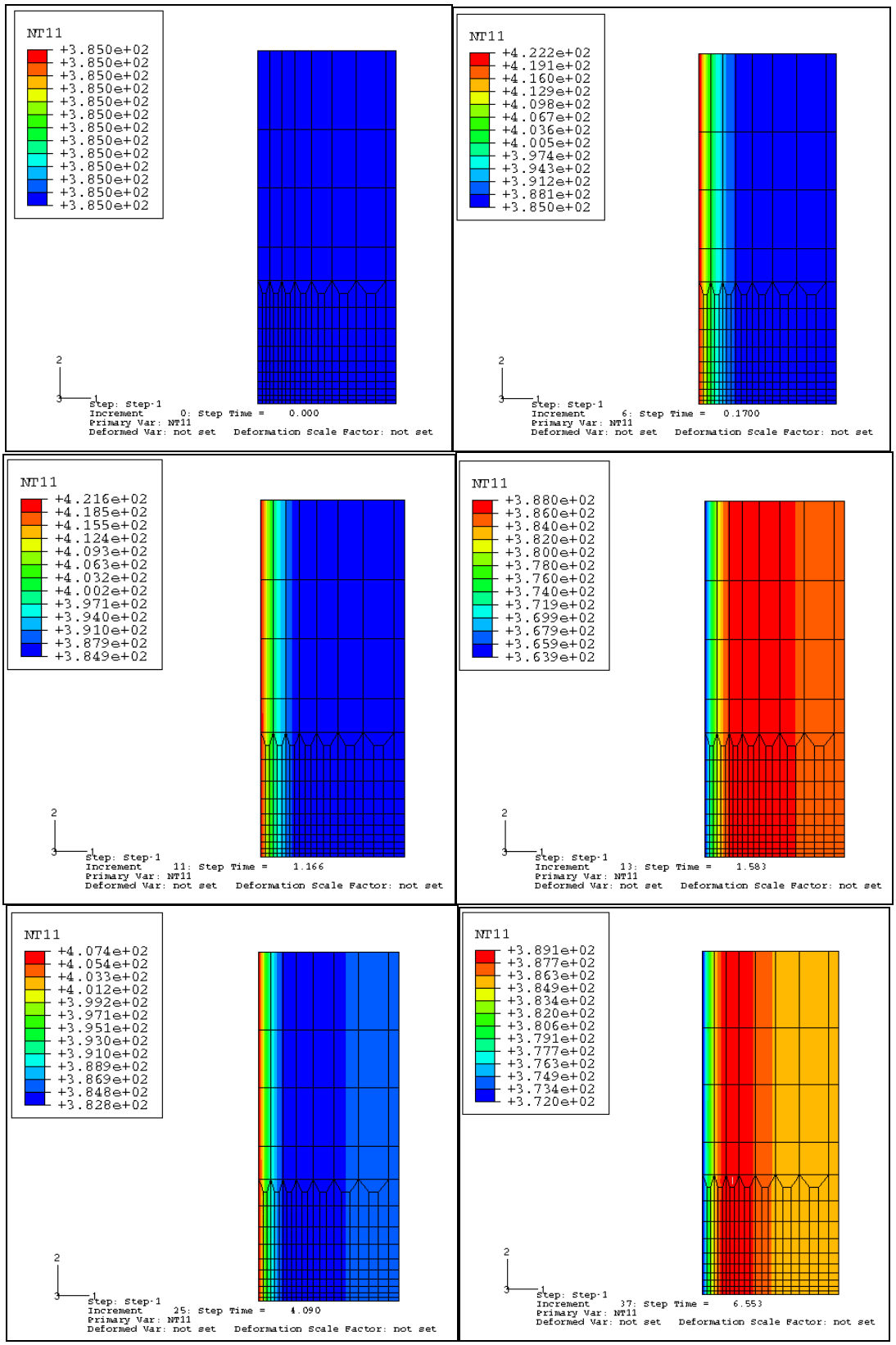

Figure 40. Evolution of the temperature across the wall thickness for v=1Hz (t=0 sec; 0.17 sec; 1.166 sec; 1.583 sec; 4.09 sec; 6.55 sec).

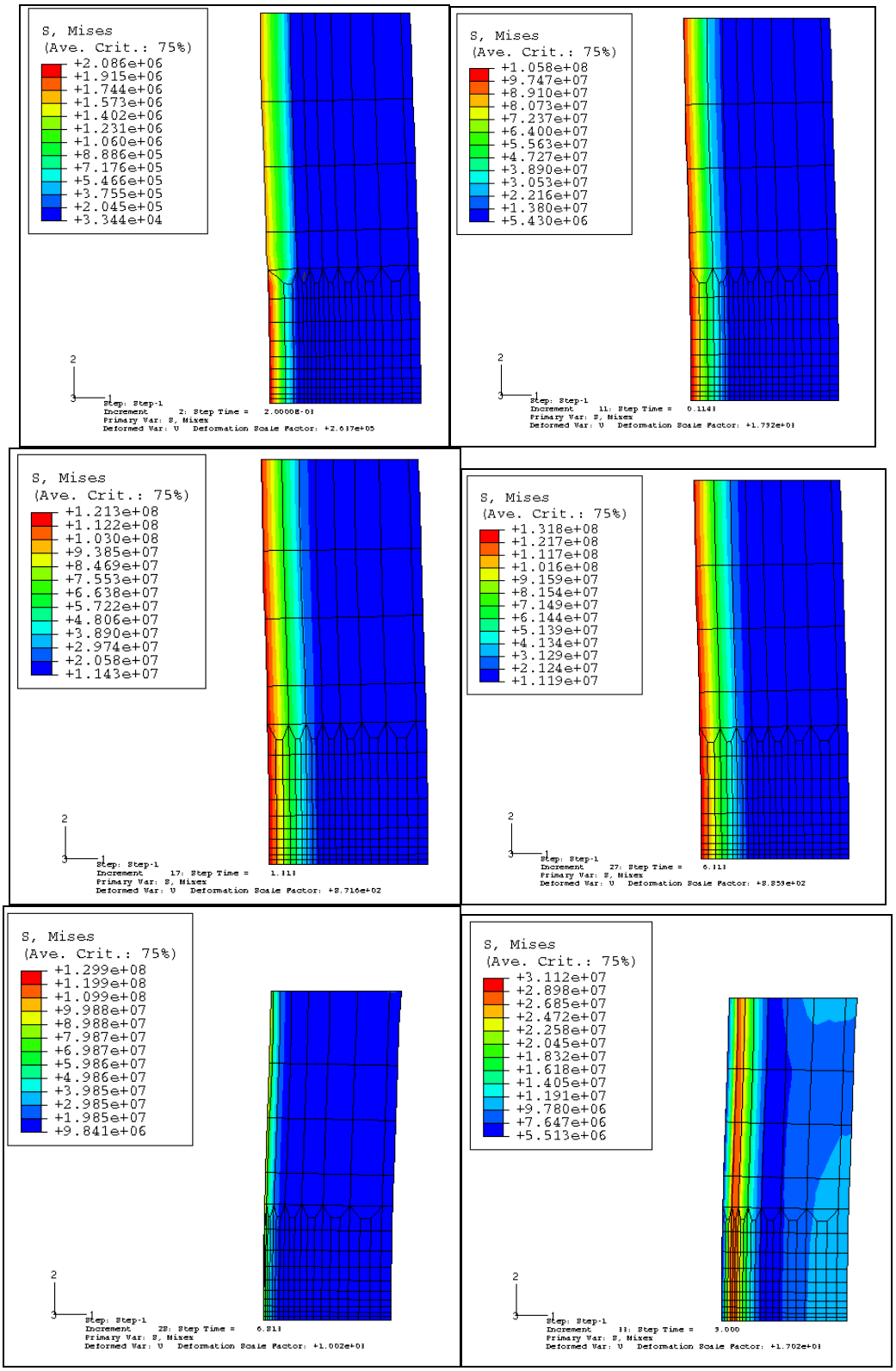

Figure 41. Evolution of the von Mises stress across the wall thickness for v=1Hz and sample free to expand in the axial direction ($\varepsilon_{zz}= \varepsilon_0$) (t=0.002 sec; 0.114 sec; 1.313 sec; 5.313 sec; 6.813 sec; 9 sec)

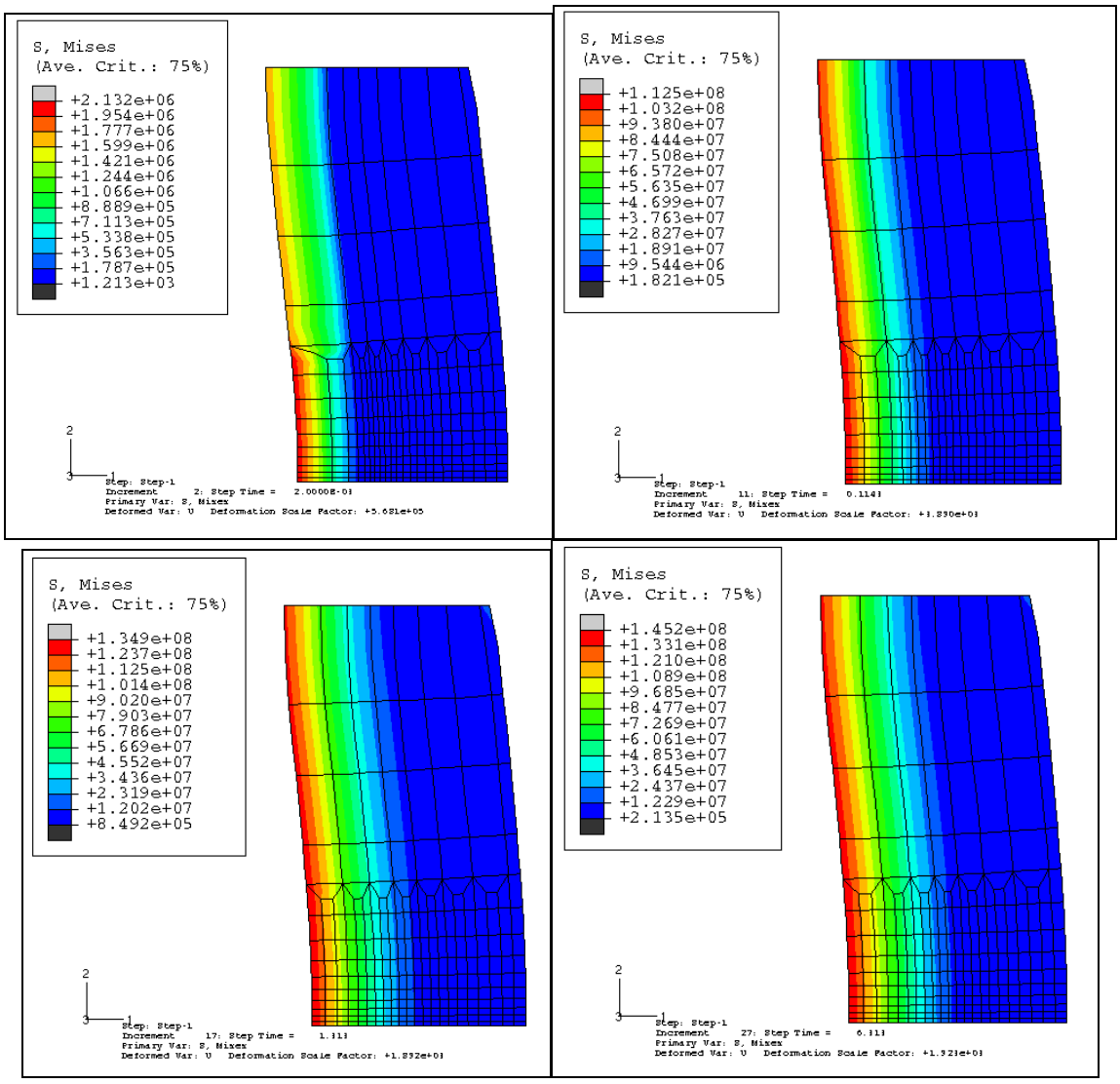

Figure 42. Evolution of the von Mises stress across the wall thickness for v=1Hz sample fixed in the axial direction (ε_{zz}= 0),(t=0.002 sec; 0.114 sec; 1.313 sec; 6.313 sec)

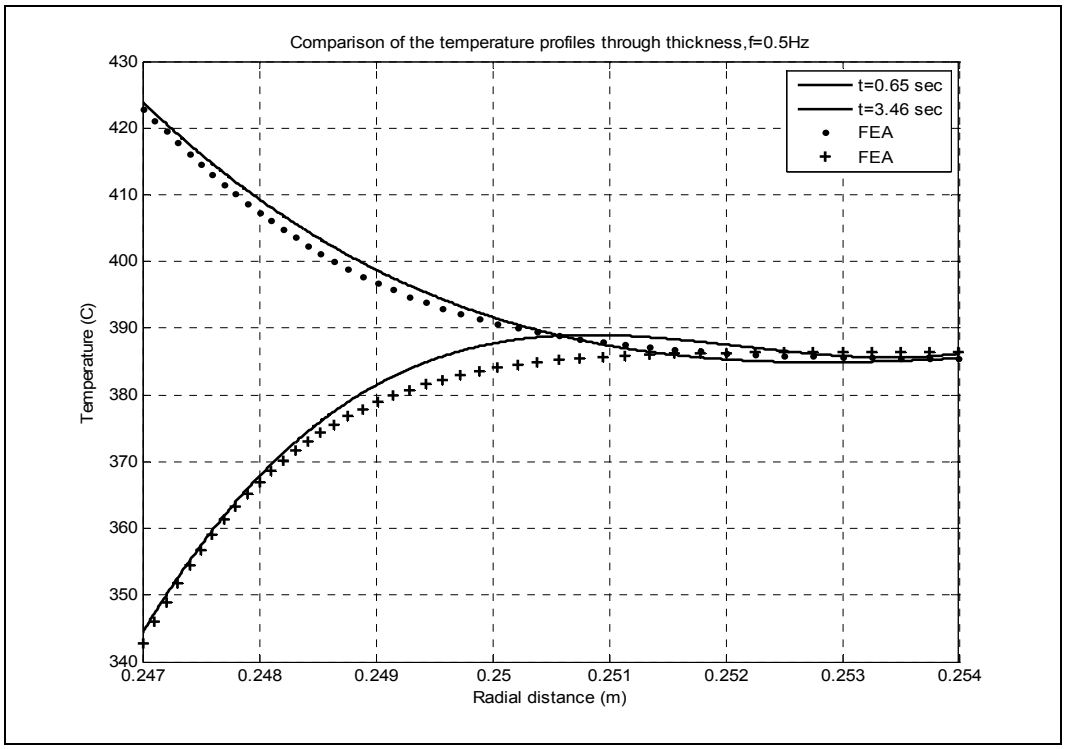

Figure 43. Comparison of temperature profiles predictions: analytical versus FEA, f=0.5 Hz

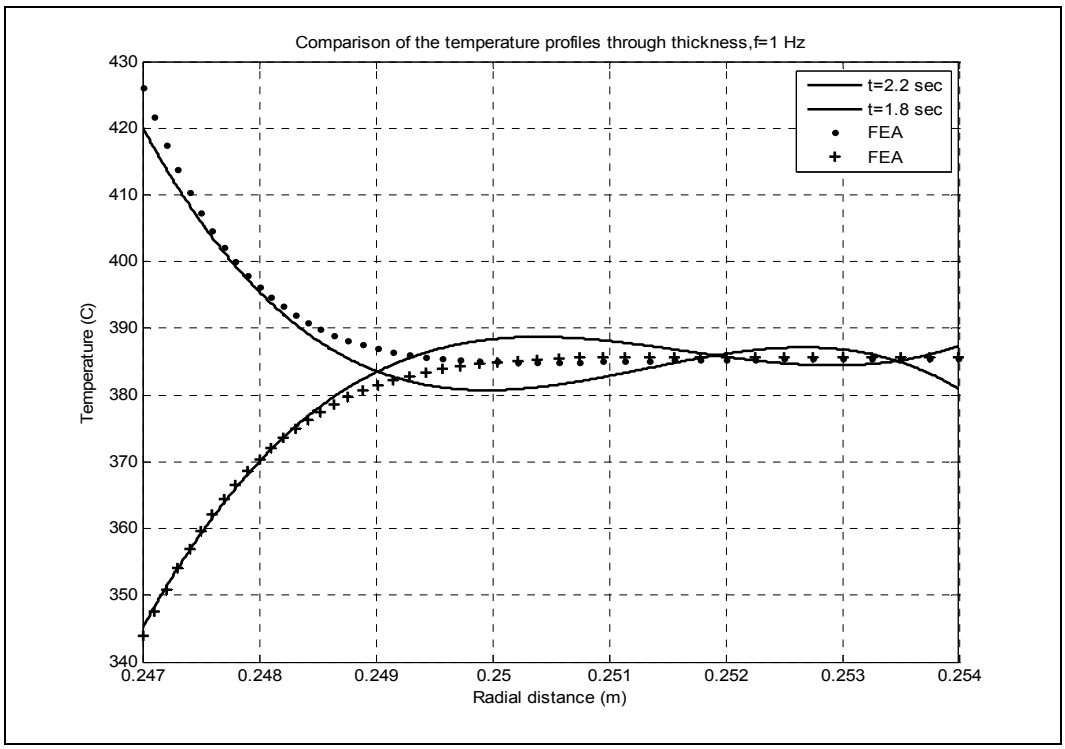

Figure 44. Comparison of temperature profiles predictions: analytical versus FEA, f=1.0 Hz

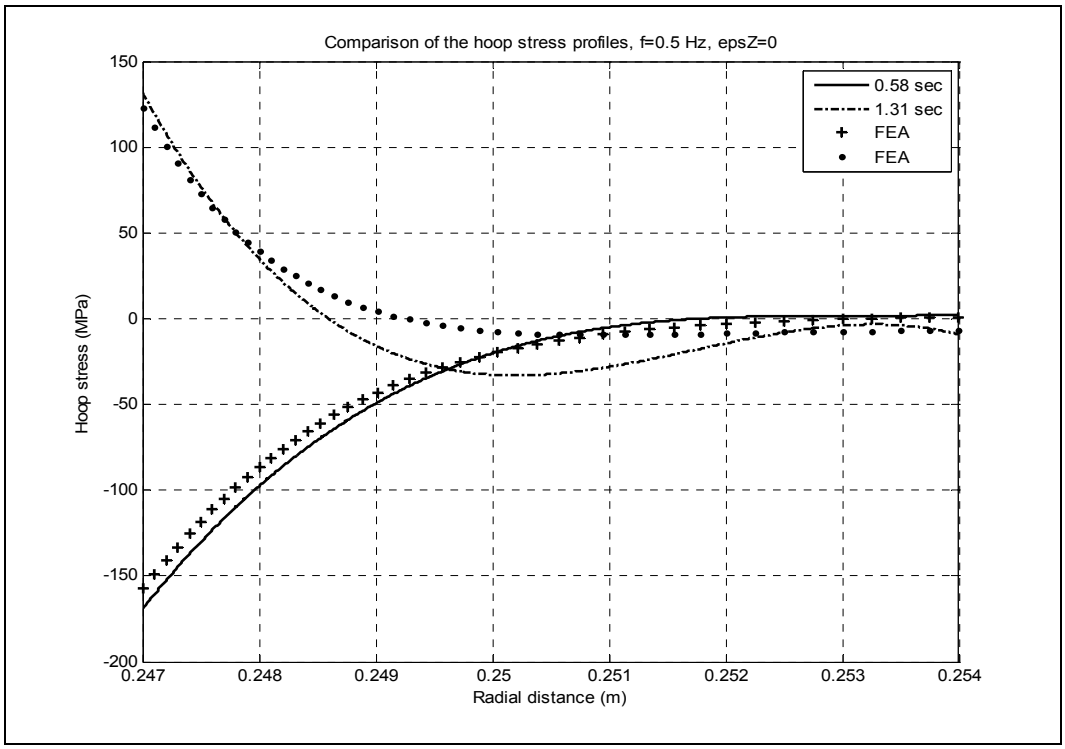

Figure 45. Comparison of the hoop stress profiles: analytical versus FEA, f=0.5 Hz, ε_{zz}=0

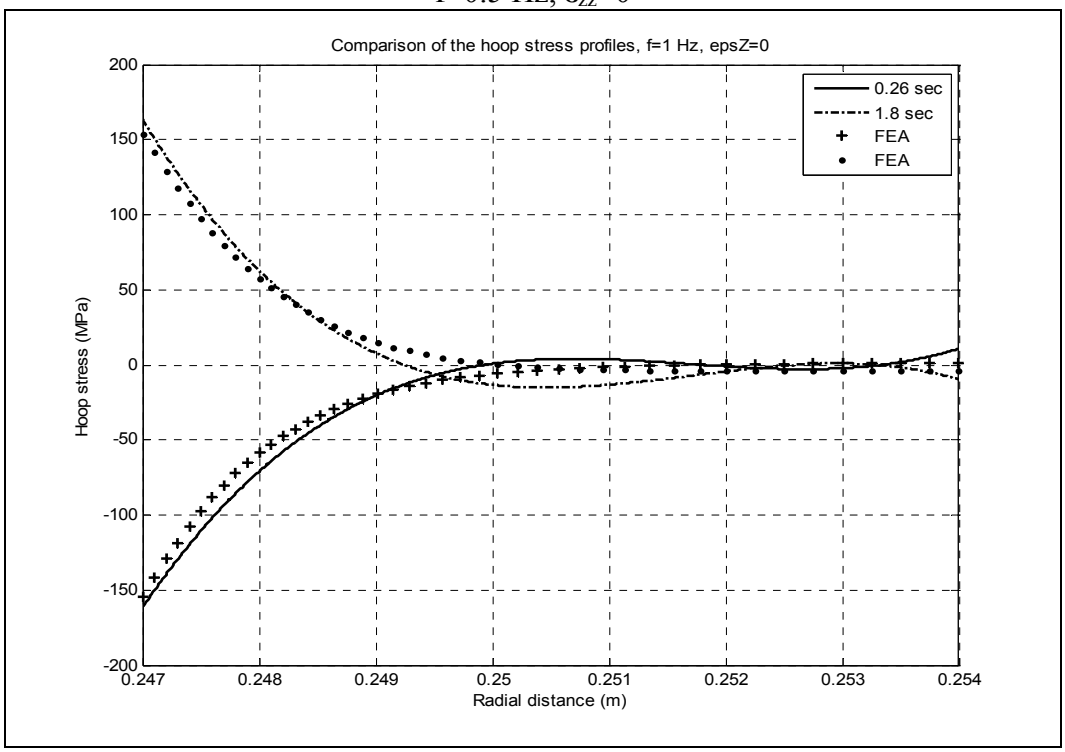

Figure 46. Comparison of the hoop stress profiles: analytical versus FEA, f=1.0 Hz, ε_{zz}=0

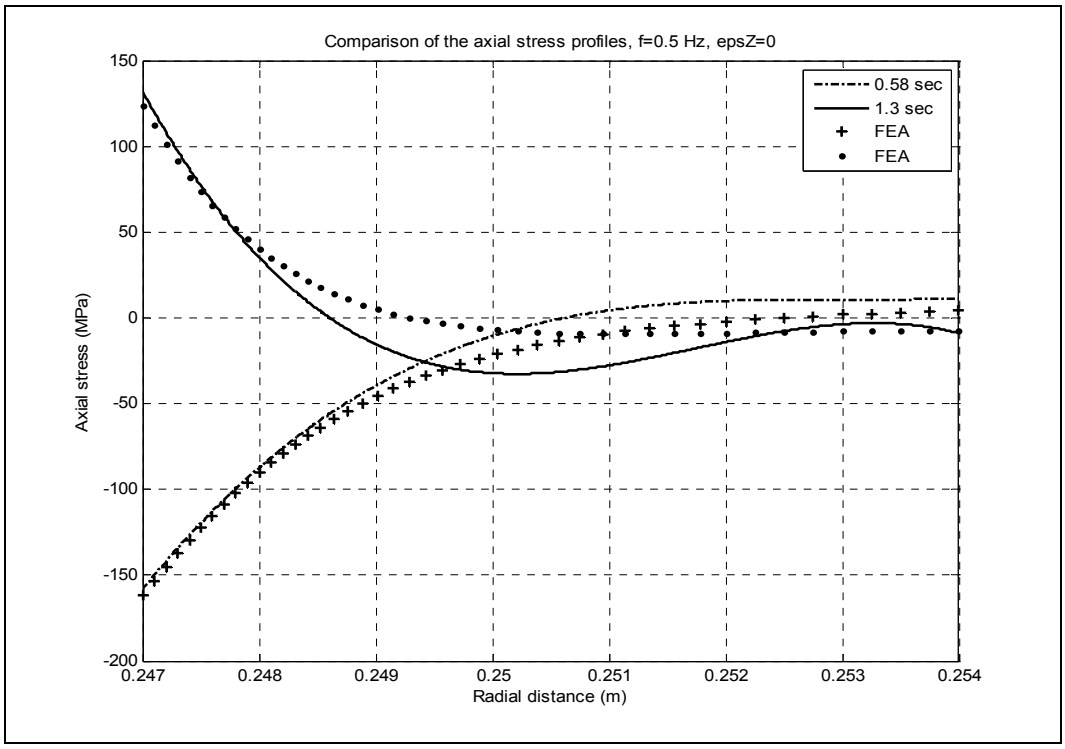

Figure 47. Comparison of the axial stress profiles: analytical versus FEA, f=0.5 Hz, ε_{zz}=0

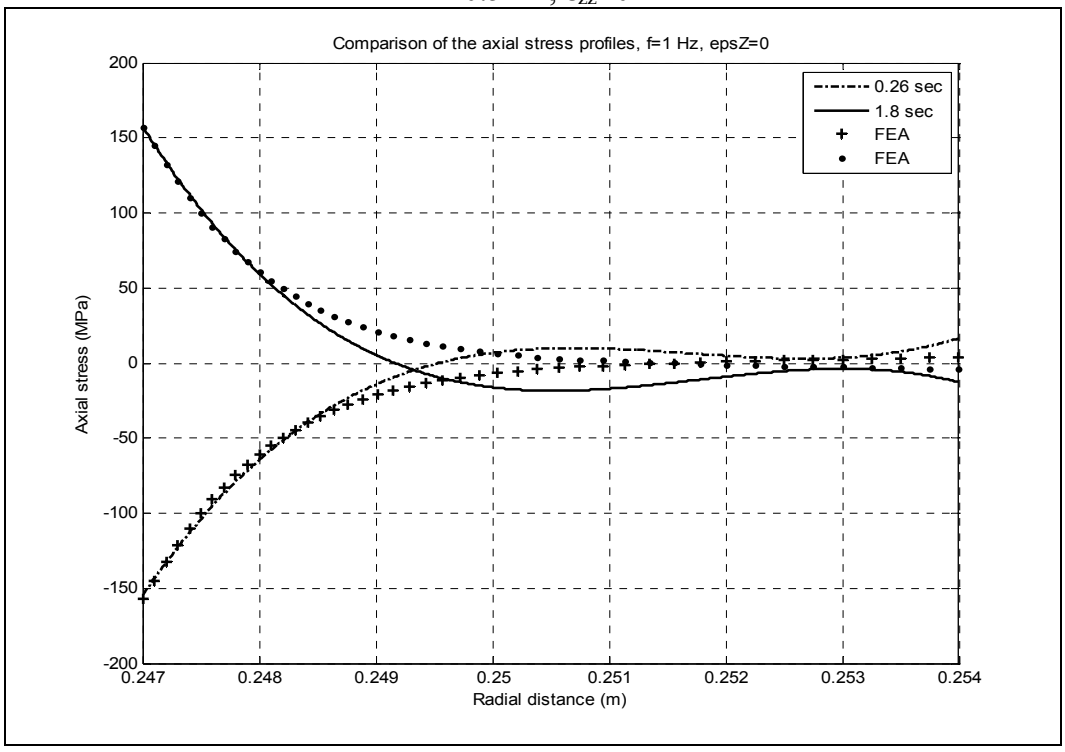

Figure 48. Comparison of the axial stress profiles: analytical versus FEA, f=1.0 Hz, ε_{zz}=0

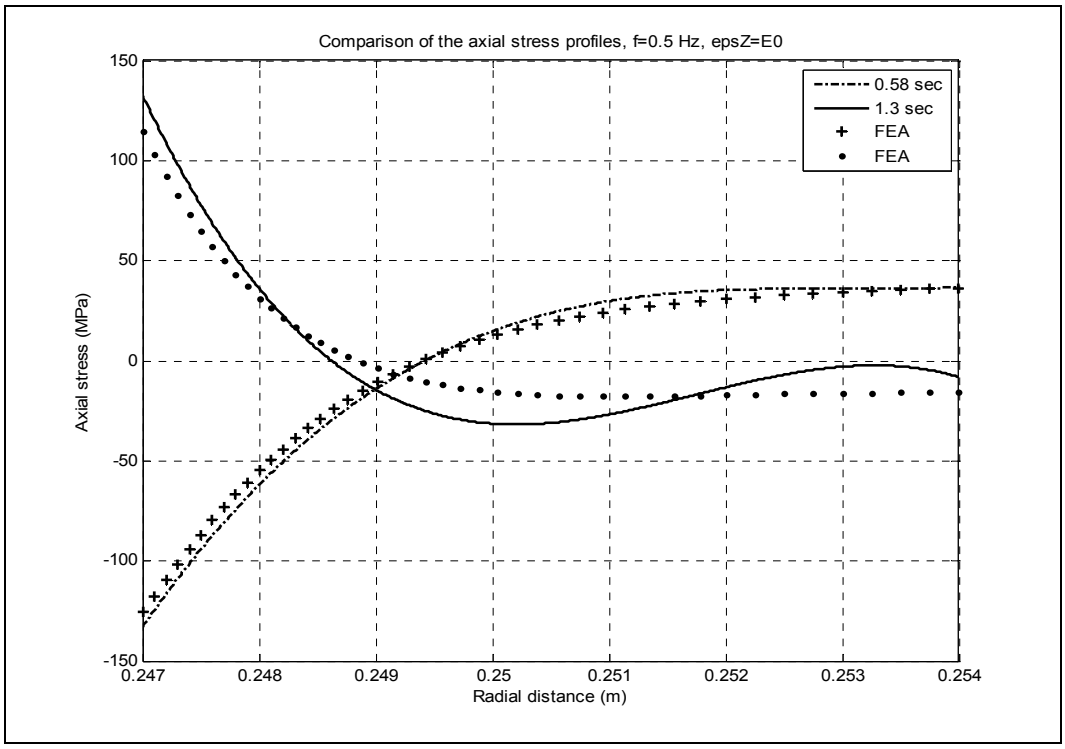

Figure 49. Comparison of the axial stress profiles: analytical versus FEA, f=0.5 Hz, $\varepsilon_{zz}=\varepsilon_0$

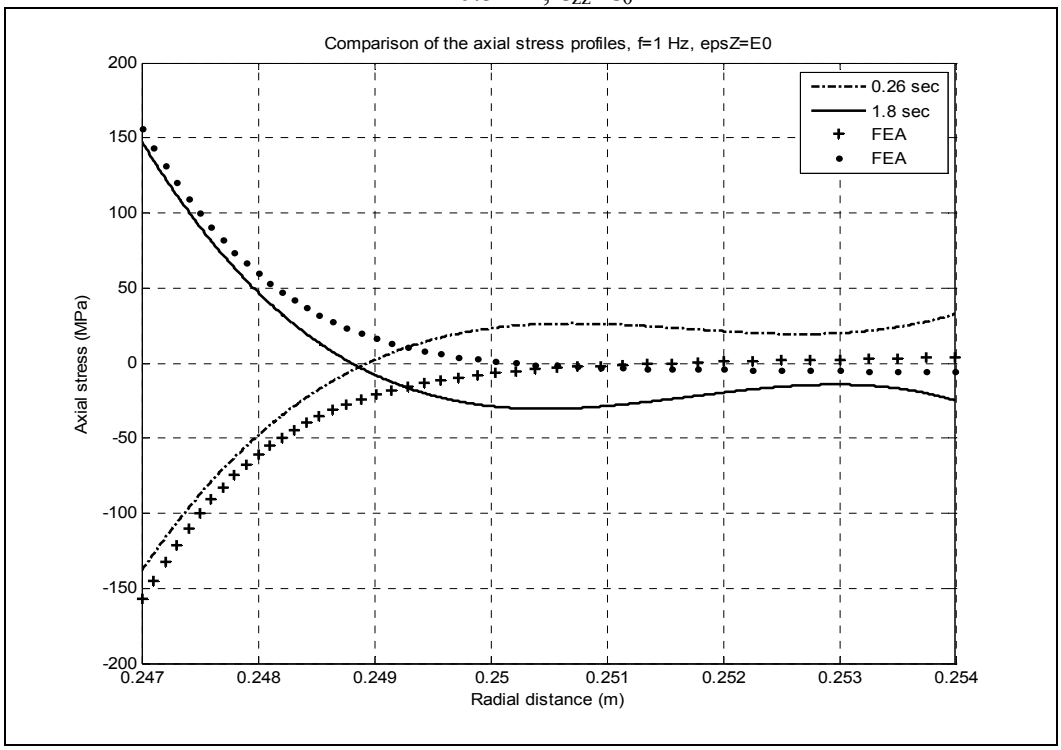

Figure 50 . Comparison of the axial stress profiles: analytical versus FEA, f=1.0 Hz, $\varepsilon_{zz}=\varepsilon_0$

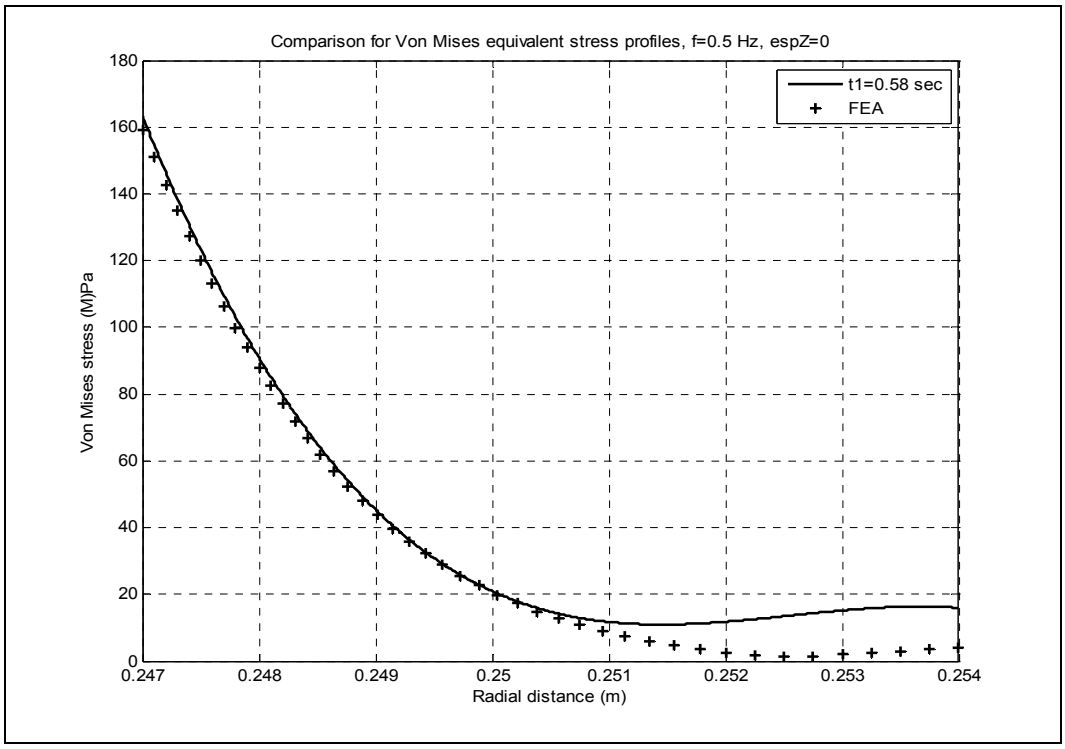

Figure 51. Comparison of the von Mises equivalent stress profiles: analytical versus FEA, f=0.5 Hz, $\varepsilon_{zz} = 0$

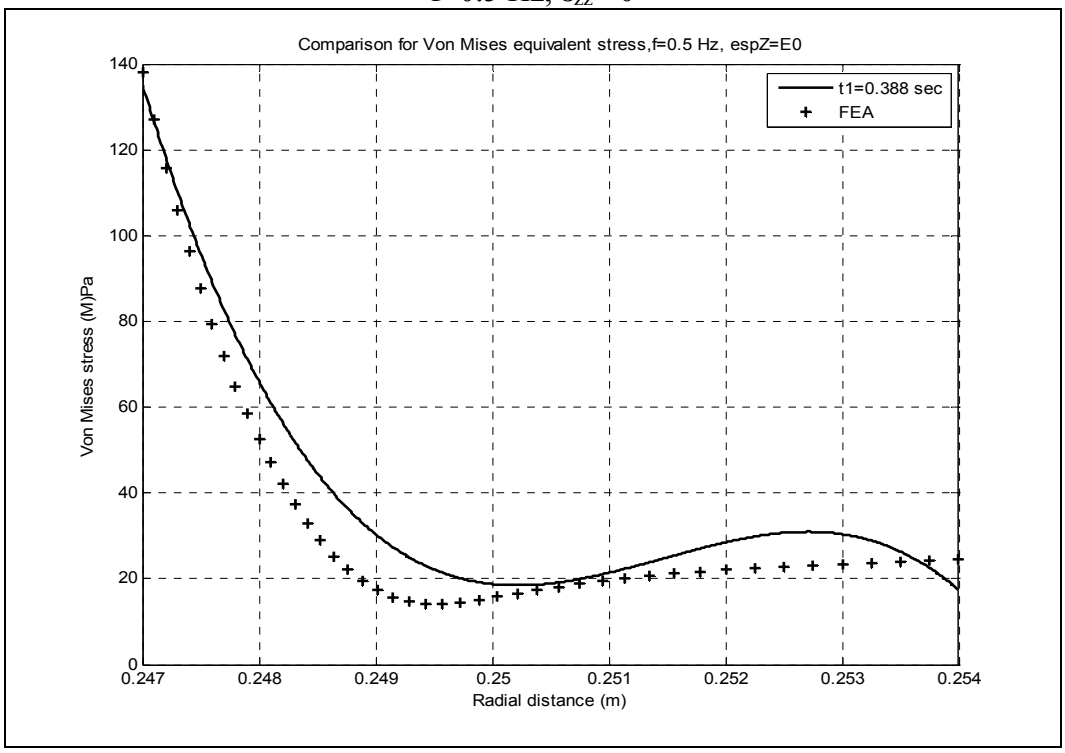

Figure 52. Comparison of the von Mises equivalent stress profiles: analytical versus FEA, f=0.5 Hz, $\varepsilon_{zz} = \varepsilon_0$

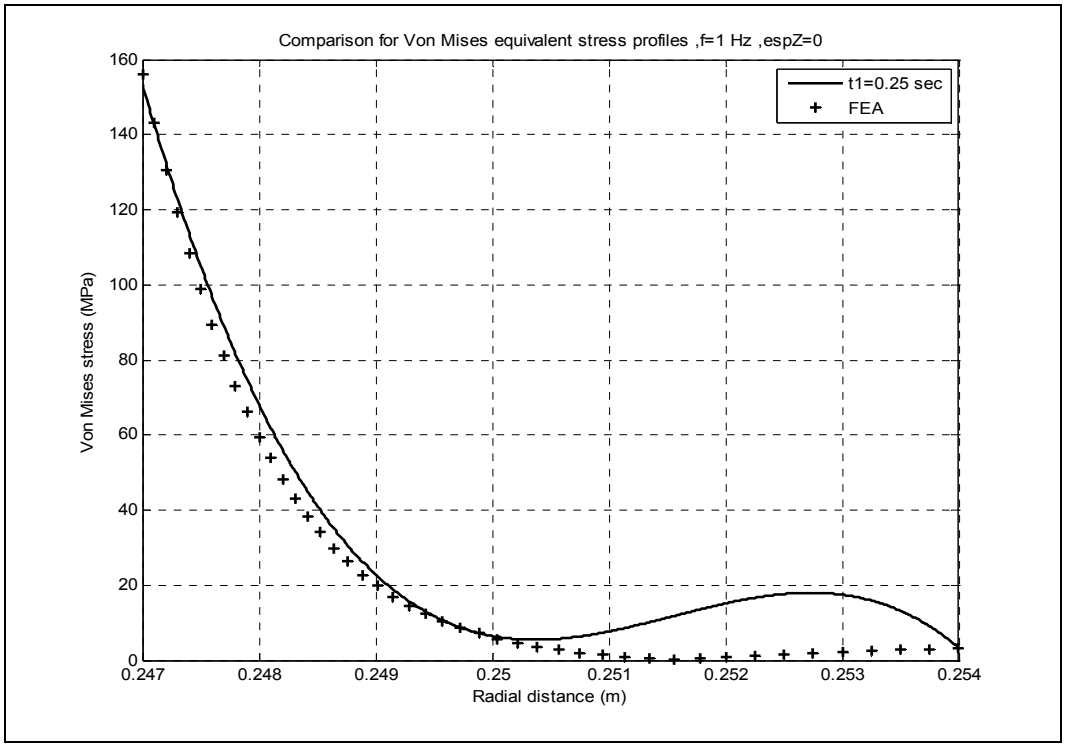

Figure 53. Comparison of the von Mises equivalent stress profiles: analytical versus FEA, f=1.0 Hz, $\varepsilon_{zz}=0$

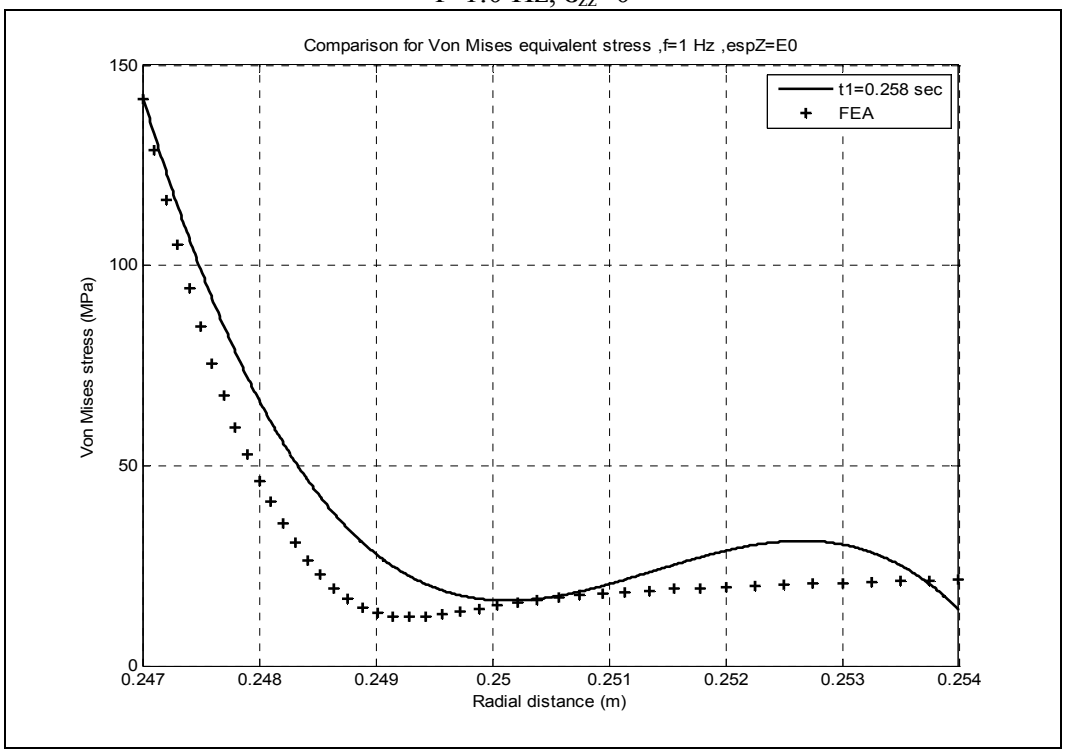

Figure 54. Comparison of the von Mises equivalent stress profiles: analytical versus FEA, f=1.0 Hz, $\varepsilon_{zz}=\varepsilon_0$

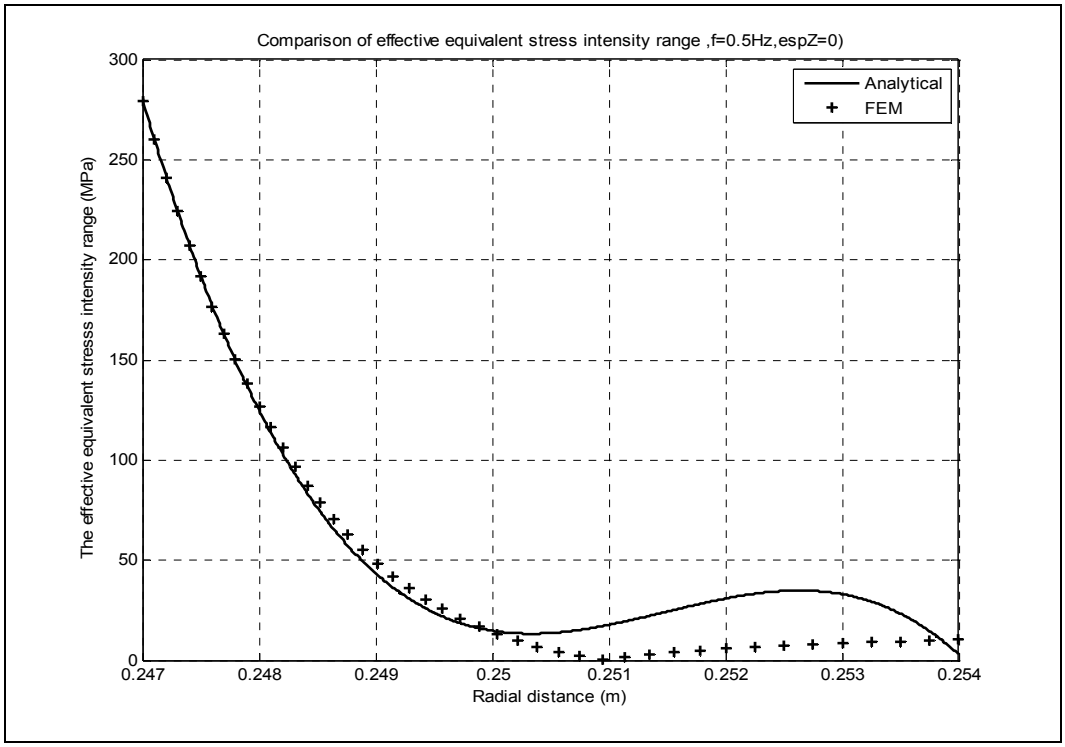

Figure 55. Comparison of the effective equivalent stress intensity range between instants t_1=0.58 sec and t_2=1.3 sec : analytical versus FEA f=0.5 Hz, ε_{zz}=0

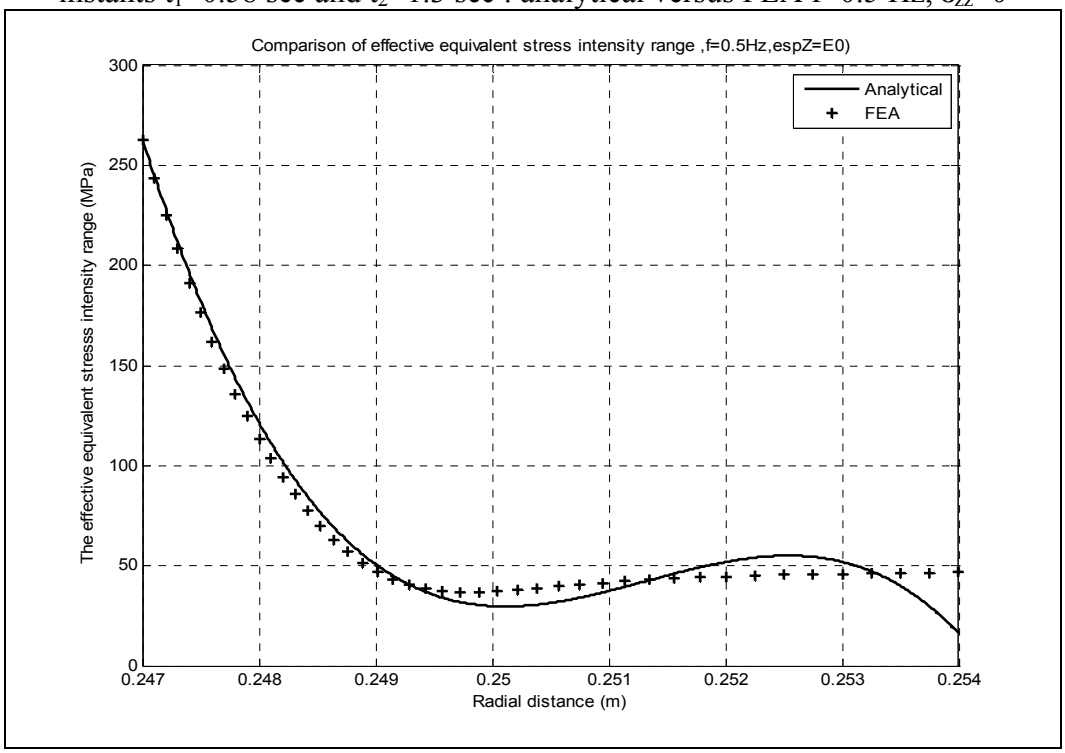

Figure 56. Comparison of the effective equivalent stress intensity range between instants t_1=0.58 sec and t_2=1.3 sec: analytical versus FEA f=0.5 Hz, $\varepsilon_{zz}=\varepsilon_0$

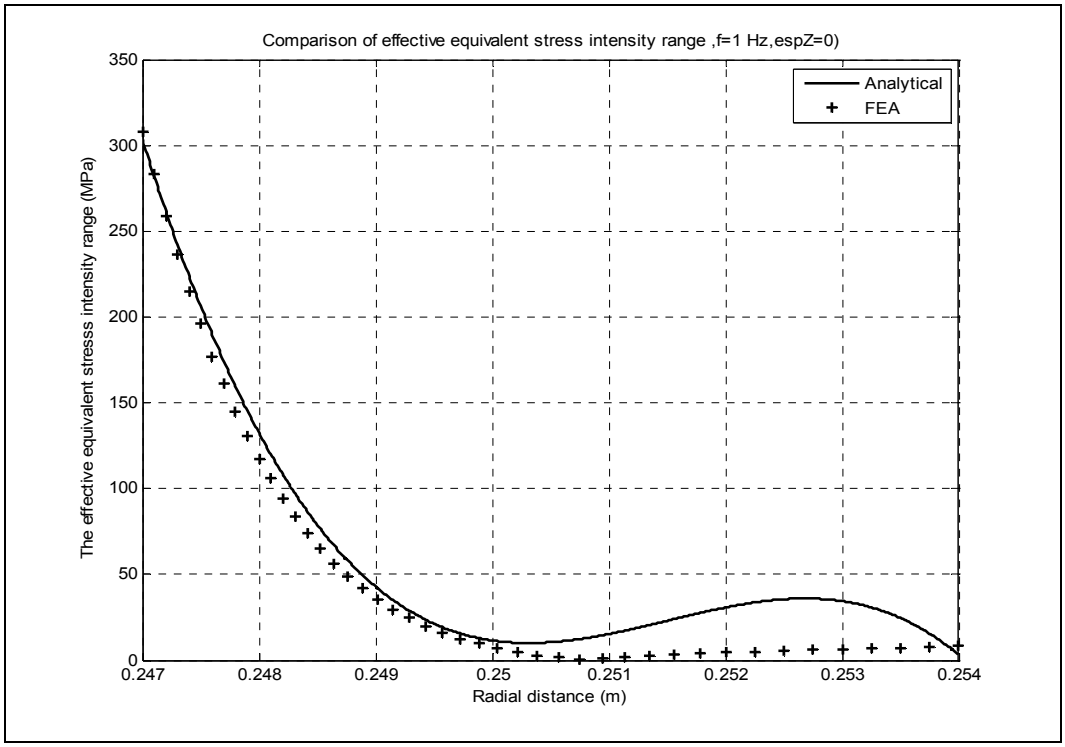

Figure 57. Comparison of the effective equivalent stress intensity range between instants t_1=0.26 sec and t_2=1.8 sec: analytical versus FEA f=1.0 Hz, ε_{zz}=0

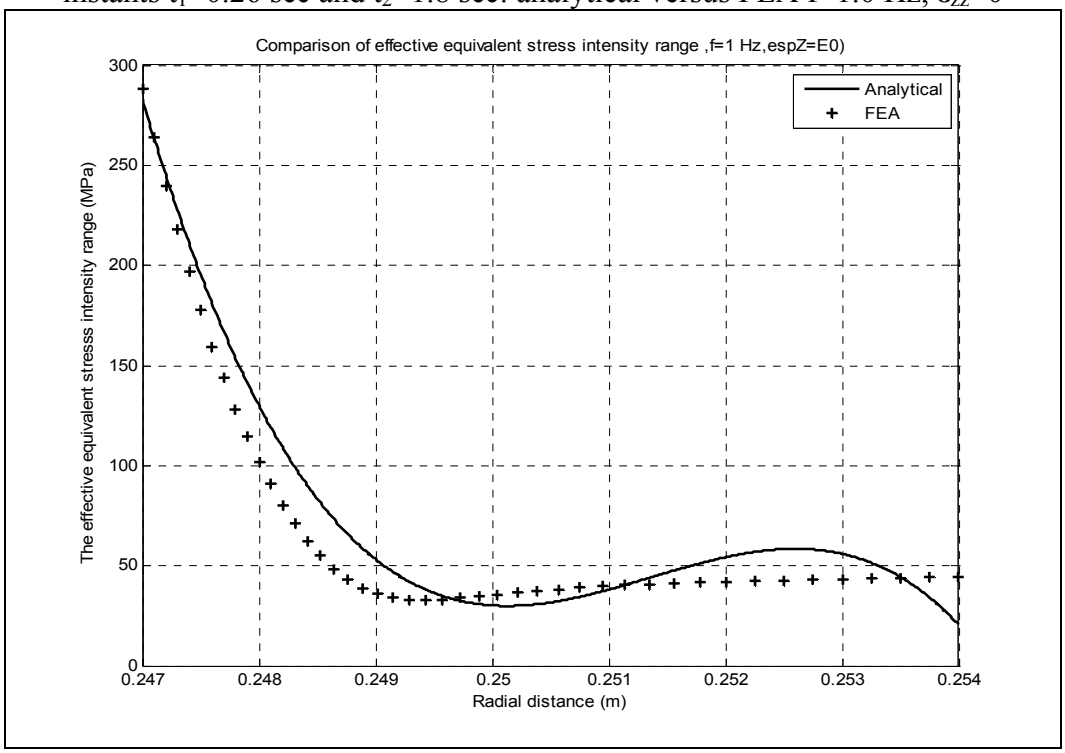

Figure 58. Comparison of the effective equivalent stress intensity range between instants t_1=0.26 sec and t_2=1.8 sec: analytical versus FEA f=1.0 Hz, $\varepsilon_{zz}=\varepsilon_0$

APPENDICES

Appendix 1: Some properties of Bessel functions

The differential equation

$$\frac{d^2 f(z)}{dz^2} + \frac{1}{z} \cdot \frac{df(z)}{dz} + \left(1 - \frac{\upsilon^2}{z^2}\right) \cdot f(z) = 0 \qquad \text{(A1.1)}$$

is a Bessel's differential equation of order υ. The first solution is expressed by

$$J_\upsilon(z) = \sum_{m=0}^{\infty} \frac{(-1)^m}{m!\Gamma(\upsilon + m + 1)} \cdot \left(\frac{z}{2}\right)^{\upsilon+2m} \qquad \text{(A1.2)}$$

and is called a Bessel function of the first kind of order υ, where Γ is the gamma function defined by

$$\Gamma(x) = \int_0^{\infty} e^{-t} \cdot t^{x-1} dt \quad \text{for } x>0 \qquad \text{(A1.3)}$$

The second solution of the Bessel equation which is available for all values of υ is expressed by

$$Y_\upsilon(z) = \frac{J_\upsilon(z) \cdot \cos(\upsilon\pi) - J_{-\upsilon}(z)}{\sin(\upsilon\pi)} \qquad \text{(A1.4)}$$

and is called the Bessel function of the second kind of order υ. If υ is not an integer, $J_\upsilon(z)$ may be used instead of $Y_\upsilon(z)$ as a second solution. Functions $J_\upsilon(z)$ and $J_{-\upsilon}(z)$ are independent solutions of Eq. (A1.1). When υ is an integer n, $J_{-\upsilon}(z)$ is dependent on $J_\upsilon(z)$

$$J_n(z) = (-1)^n J_{-n}(z) \qquad \text{(A1.5)}$$

The complete solution of Eq. (A1.1) is

$$f(z) = A \cdot J_\upsilon(z) + B \cdot Y_\upsilon(z) \quad \text{for all values of } \upsilon \qquad \text{(A1.6)}$$

$$f(z) = A \cdot J_n(z) + B \cdot Y_n(z) \quad \text{for an integer } n \qquad \text{(A1.7)}$$

$$f(z) = A \cdot J_\upsilon(z) + B \cdot J_{-\upsilon}(z) \quad \text{for non-integer } \upsilon \qquad \text{(A1.8)}$$

Some formulas of the Bessel functions are listed as follows

$$\frac{2\upsilon}{z}J_{\upsilon}(z) = J_{\upsilon-1}(z) + J_{\upsilon+1}(z) \tag{A1.9}$$

$$\frac{dJ_{\upsilon})z)}{dz} = \frac{1}{2}\left[J_{\upsilon-1}(z) - J_{\upsilon+1}(z)\right] = J_{\upsilon-1}(z) - \frac{\upsilon}{z}J_{\upsilon}(z) = -J_{\upsilon+1}(z) + \frac{\upsilon}{z}J_{\upsilon}(z) \tag{A1.10}$$

$$\frac{d}{dz}\left[z^{\upsilon}\cdot J_{\upsilon}(a\cdot z)\right] = a\cdot z^{\upsilon}\cdot J_{\upsilon-1}(az) \tag{A1.11}$$

$$\frac{d}{dz}\left[z^{-\upsilon}\cdot J_{\upsilon}(a\cdot z)\right] = -a\cdot z^{-\upsilon}\cdot J_{\upsilon+1}(az) \tag{A1.12}$$

$$J_{n}(z) = (-1)^{n}J_{-n}(z) = (-1)^{n}J_{n}(-z) \tag{A1.13}$$

$$J_{\upsilon+1}(z)\cdot Y_{\upsilon}(z) - J_{\upsilon}(z)\cdot Y_{\upsilon+1}(z) = \frac{2}{\pi z} \tag{A1.14}$$

The above formulas, except for the last, are satisfied by $Y_{\upsilon}(z)$ instead $J_{\upsilon}(z)$.

Appendix 2: Fatigue Evaluation Procedure Based on Elasticity Calculated Stress Results (API 579/2000)

A quantity known as the *"equivalent intensity of combined stress"* or *"stress intensity"* is computed at certain locations on the component or structure of interest. The *stress intensity* at a point is a measure of stress, calculated from stress components utilizing a yield criterion, which can be used for comparison with the mechanical strength properties of the material obtained in tests under uniaxial load.

The "Maximum Distortion Energy Yield Criterion" may be used to establish *stress intensity*. In this case the *stress intensity* is equal to the von Mises equivalent stress:

$$S = \sigma_{vonMises} = \sqrt{\frac{(\sigma_1 - \sigma_2)^2 + (\sigma_2 - \sigma_3)^2 + (\sigma_3 - \sigma_1)^2}{2}} \qquad \text{(A2.1)}$$

Although this yield criterion is more complicated to apply when manual calculations are performed, it is the most common criterion for yield used in finite element analysis, and is generally recognized to give more accurate results than the maximum shear stress yield criterion.

Fatigue Evaluation Procedure Based on Elasticity Calculated Stress Results

A fatigue evaluation should be performed if the component is subject to cyclic operation. The evaluation for fatigue is made on the basis of the number of applied cycles of a stress or strain range at a point in the component. The allowable number of cycles should be adequate for the specified duration of operation to determine the suitability for continued operation. Fatigue curves are typically presented in two forms: fatigue curves that are based on smooth bar test specimens and fatigue curves that are based on the test specimens which include weld details. The stresses and strains produced by any load or thermal condition which does not vary during the cycle need not be considered in a fatigue analysis if the fatigue curves utilized in the evaluation are adjusted for mean stresses and strains.

An *effective total stress intensity amplitude* is used to evaluate the fatigue damage for results obtained from a linear elastic stress analysis. The *effective peak stress intensity amplitude* is defined as one-half the *effective total stress intensity range*, calculated for each cycle described in the loading history. The procedure can be used for the general case where the principal stress directions change during the loading cycle.

The steps required for thermal fatigue crack initiation are described in the following:

Step1. -Determine a load history based on the past operation and future planned operation. The load history should include all significant operating loads and events which the component will be subjected to.

Step 2. – For a location in the component under evaluation, compute the stress components σ_{ij} and the equivalent stress for each point in the load histogram. Use this information to create an effective stress load histogram.

Step 3. – Determine the cyclic stress range based on the effective stress histogram developed in Step 2 using the cycle counting method in ASME E 1049 (rainflow method).

Step 4. Determine the stress tensor at the start and end points for the "kth" cycle in the effective stress histogram counted in Step 3. Using these data, determine the stress range and designate this quantity as $\Delta\,\sigma_{ij}^{k}$.

Step 5. – Compute *an effective stress intensity range* for the "kth" cycle using the "Maximum Distortion Energy Yield Criterion". Using the change in stress components determined in Step 4, compute the ***effective equivalent stress intensity range*** for the cycle:

$$\Delta S_{range}^{k} = \sqrt{\frac{(\Delta\sigma_{11}-\Delta\sigma_{22})^2+(\Delta\sigma_{22}-\Delta\sigma_{33})^2+(\Delta\sigma_{33}-\Delta\sigma_{11})^2+6(\Delta\sigma_{12}^2+\Delta\sigma_{23}^2+\Delta\sigma_{13}^2)}{2}} \qquad \text{(A2.2)}$$

Step 6. – Determine the *effective alternating stress intensity* for the "kth" cycle

$$\Delta S_{alt}^{k} = \frac{1}{2} K_e^k \cdot \Delta S_{range}^{k} \qquad \text{(A2.3)}$$

with

$$K_e^k = 1.0 \qquad for \qquad \Delta S_n^k \le 3S_m \qquad \text{(A2.4)}$$

S_m – allowable stress

$$K_e^k = 1.0 + \frac{1-n}{n(1-m)}\left(\frac{S_n^k}{3S_m}-1\right) \qquad for \qquad 3S_m < \Delta S_n^k < 3mS_m \qquad \text{(A2.5)}$$

$$K_e^k = \frac{1}{n} \qquad for \qquad \Delta S_n^k \le 3mS_m \qquad \text{(A2.6)}$$

where

K_e^k = fatigue knock-down factor for the "kth" cycle (from table with applicability and limitations)

ΔS_n^k = range of primary plus secondary stress intensity for the "kth" cycle

m = material constant
n = material constant

Step 7. – Determine the permissible number of cycles, N^k for the alternating stress intensity computed in Step 6. Fatigue curves are contained in ASME B&PV Code, Section III.

Step 8. – Determine the fatigue damage for the "k^{th}" cycle

$$D_f^k = \frac{1}{N^k} \qquad \text{(A2.7)}$$

Step 9. – Repeat Steps 4 through 8 for all stress ranges identified in the cycle counting process in Step 3.

Step 10. Compute the *accumulated fatigue damage* using the following equation. The component is suitable for continued operation if this equation is satisfied. The permissible damage fraction, D_f, is usually taken as 1.0 unless an alternative value is specified by the Engineer performing the assessment

$$\sum D_f^k \le D_f \qquad \text{(A2.8)}$$

Step 11. – Repeat Steps 2 through 10 for each point in the component subject to a fatigue evaluation.

European Commission

EUR 22802 EN – Joint Research Centre – Institute for Energy
Title: **NEW ANALYTICAL STRESS FORMULAE FOR ARBITRARY TIME DEPENDENT THERMAL LOADS IN PIPES**

Author(s):
V. Radu
E. Paffumi
N. Taylor

Luxembourg: Office for Official Publications of the European Communities
2007 – 80 pp. – 21x 29.7 cm
EUR – Scientific and Technical Research series – ISSN 1018-5593

Abstract
Analytical solutions with several new features have been developed for temperature and elastic thermal stress distributions for a hollow circular cylinder under sinusoidal thermal transient loading at the inner surface.
The approach uses a finite Hankel transform in a general form for any transient thermal loading for a hollow cylinder. Using the properties of Bessel functions, an analytical solution for temperature distribution through wall thickness was derived for a special case of sinusoidal transient thermal loading on inner pipe surface.
The solutions for associated thermal stress components were developed by means of the displacement technique. To the authors' knowledge, this is first time a complete set of such analytical expressions has been openly published.

The mission of the JRC is to provide customer-driven scientific and technical support for the conception, development, implementation and monitoring of EU policies. As a service of the European Commission, the JRC functions as a reference centre of science and technology for the Union. Close to the policy-making process, it serves the common interest of the Member States, while being independent of special interests, whether private or national.